Thermodynamic Properties of Rare Earth Sesquioxides

Yumin Zhang
Supervisor: Prof In-ho Jung
McGill University, Montreal, QC, Canada

Montreal 2016

Acknowledgements

I would like to express my sincere gratitude to my supervisor Prof. In-Ho Jung, who has been giving me all the decisive suggestions and led me to accomplish this research. Without his support, it is undoubtedly that I cannot achieve the success. I would like to thank my friend Guoqiang Lan and his supervisor Prof Jun Song for donating their precious time to support my research.

It is also my pleasure to get to know Dr. Pierre Hudon, who has been supporting our research group for a long time. I would like to thank Pierre to remember everyone's birthday, organize summer getaway vacations and Christmas parties. Because of Pierre, there is always happiness and love in our research group.

My deep thanks also goes to all my friends during my graduate study. I enjoyed the time with all my friends: Xintong Du, Tiantian Ying, Kota Matsuo and Zhimin You. I will not forget the time that we spent together to prepare exams in Prof. Pelton's course.

Last but not least, my father Yuanchao Zhang and grandma Guang Li have been believing in me since the very beginning of my graduate study. I may not grow into the person I am today without their encouragement. They make me confident and determined to chase my goals. I would like to dedicate this thesis to all the people I mentioned here and share my happiness with them.

Yumin Zhang, July – 2016, Montreal

Abstract

In order to develop the thermodynamic database containing rare earth sesquioxides (RE_2O_3), accurate thermodynamic descriptions of all stable and metastable RE_2O_3 phases are required. Rare earth sesquioxides have numerous polymorphs, which are (from low to high temperature) the cubic phase (labelled C), the monoclinic phase (B), the hexagonal phase (A), the high temperature hexagonal phase (H), and the high temperature cubic phase (X). However, the thermodynamic property data available for these different polymorphous are insufficient especially for the phase stable at high temperature region and also for metastable forms.

In this study, all ΔH^o_{298}, S^o_{298}, C_P (or heat content) and phase transition temperature (T_{tr}) data available in the literature were collected and critically evaluated for each rare earth sesquioxide based on the experimental procedures and techniques employed. Relationships between ΔH^o_{298}, S^o_{298}, and T_{tr} against the ionic radii of the entire rare earth sesquioxide series were then established and missing thermodynamic information was predicted. In general, the enthalpy (ΔH°_{tr}) and entropy (ΔS°_{tr}) changes of the C – B, B – A, A – H, and H – X transitions are either scarce or unavailable. For the C – B and B – A transitions, experimental enthalpy data and entropies extracted using the Clausius – Clapeyron relation were collected from the literature and employed together with results obtained from Density Functional Theory (DFT) calculations to estimate the ΔH°_{tr} and ΔS°_{tr}. Based on the observations from the RE_2O_3 liquidus in $RE_2O_3 – Al_2O_3$ binary phase diagrams, a small ΔS°_{tr} value for A – H and H – X transitions was estimated by applying so – called "limiting slope rule" to ensure smooth liquidus slope change between A and H, as well as H and X phases. Regarding the properties of fusion, the similar "limiting slope rule" was employed that a couple of phase diagram data points were taken near the pure RE_2O_3 melting points for ΔH_m and ΔS_m estimations. In these ways, the accurate and consistent Gibbs energies of all stable and metastable RE_2O_3 phases (RE = La, Ce, Pr, Nd, Pm, Sm, Eu, Gd, Tb, Dy, Ho, Er, Tm, Yb and Lu) are prepared. These Gibbs energy data will be ready readily used for the development of a comprehensive thermodynamic database containing rare earth oxides.

Abstract

Afin de développer la base de données thermodynamiques contenant des sesquioxydes de terre rare (RE_2O_3), des descriptions thermodynamique précises pour toutes les phases de RE_2O_3 stable et métastable sont requises. Les sesquioxydes de terres rares ont de nombreuses polymorphes, soit (en ordre de faible à haute température) la phase cubique (appelée C), la phase monoclinique (B), la phase hexagonale (A), la phase hexagonale haute température (H), et la phase cubique haute température (X). Toutefois, les données disponibles concernant les propriétés thermodynamiques pour ces différentes polymorphes sont relativement insuffisantes en particulier pour la région haute température et également pour la forme métastable.

Dans cette étude, les données pour ΔH^o_{298}, S^o_{298}, C_p (ou la capacité thermique) et pour les températures de transition de phase (T_{tr}) disponibles dans la littérature ont été recueillies et évaluées de manière critique pour chaque sesquioxyde de terre rare sur la base des procédures expérimentales et les techniques ci-employées. Les relations entre ΔH^o_{298}, S^o_{298}, et T_{tr} par rapport aux rayons ioniques pour la série entière des sesquioxydes de terre rare ont ensuite été établies et l'information thermodynamique absente a été prédite. En général, les changements en enthalpie (ΔH°_{tr}) et en entropie (ΔS°_{tr}) pour les transitions C – B, B – A, A – H, et H – X sont rares ou inexistants. Pour les transitions C – B et B – A, des données expérimentales pour entropies et enthalpies extraites en utilisant la relation de Clausius-Clapeyron ont été recueillies de la littérature et employées ensemble avec les résultats obtenus à partir de calculs utilisants la théorie de la fonctionnelle de la densité (DFT, de l'anglais *density functional theory*) pour estimer les valeurs de ΔH_{tr} et ΔS_{tr}. Se basant sur les observations provenant du liquidus de RE_2O_3 dans les diagrammes de phases binaires RE_2O_3 - Al_2O_3, une petite valeur de ΔS°_{tr} pour les transitions A – H et H – X a été estimée en appliquant la "règle de pente" pour assurer un changement en douceur de la pente du liquidus entre les phases A et H, ainsi qu'entre les phases H et X. En ce qui concerne les propriétés de fusion, la "règle de pente" a aussi été employée tel qu'un couple de points de données du diagramme de phase ont été prises près des points de fusion de RE_2O_3 purs pour les estimations de ΔS_{tr}. De cette façon, les énergies de Gibbs pour toutes les phases de RE_2O_3 stables et métastables (RE = La, Ce, Pr, Nd, Pm, Sm, Eu, Gd, Tb, Dy, Ho, Er, Tm, Yb et Lu) sont préparées pour l'extension vers des systèmes binaires et à composants multiples.

Table of Contents

Table of Tables

Table of Figures

1. Introduction

RE_2O_3 (rare earth sesquioxides) include the whole series of lanthanide sesquioxides from La_2O_3 to Lu_2O_3 and two rare earth like sesquioxides: Y_2O_3 and Sc_2O_3. The "sesquioxide" simply indicates oxide which has two moles of cations and three moles of oxygen anions in each mole of oxide. RE_2O_3 have a wide range of applications because of their unique physical and chemical properties. One of the most important applications is to use RE_2O_3 as ZrO_2 stabilizers. ZrO_2 is commonly used as heat resistant material on gas engine turbines to protect Ni – based superalloy. The most widely used RE_2O_3 stabilized ZrO_2 system is YSZ (yttrium stabilized zirconia), which is originally developed by NASA in the mid 1970s. Nowadays, a lot of efforts have been poured into researching of more advanced alternative RE_2O_3 – stabilized – ZrO_2 aiming lower thermal conductivity and better durability [1]. Several candidates are Gd_2O_3, Sm_2O_3 and Nd_2O_3 sesquioxides [1]. Rare earth metals and oxides are highly desired in battery, advanced ceramics and military industries. Though rare earth oxides have a wide range of strategic and critical applications, the thermodynamic properties and phase diagrams are still not well determined. For example, neither the Gibbs energies for all stable nor metastable RE_2O_3 are accurately established.

Several years ago, a comprehensive review of thermodynamic properties of RE_2O_3 was performed by Zinkevich [2], who studied standard enthalpy, entropy, C_p and phase stabilities. Basing on his own study, the Gibbs energy data of RE_2O_3 were validated by applying on RE'_2O_3 – RE''_2O_3 phase diagrams. Some of the thermodynamic properties of metastable phases were then deduced from calculated phase diagrams. Some disagreements between assessed results by Zinkevich and experimental data regarding transition temperatures of RE_2O_3 were found. Some of the thermodynamic transition enthalpy and temperature properties of metastable RE_2O_3 were not clearly reported in the work of Zinkevich. Furthermore, the experimental transition enthalpy of A→H transition adopted by Zinkevich was questionably large, which can introduce significantly unreliable estimation of Gibbs energy of A and H phases. Therefore, it is necessary to review all the thermodynamic properties of RE_2O_3 again to produce a more unequivocal and consistent thermodynamic data for entire RE_2O_3 database.

In this study, the completed literature is divided into four parts: (1) phase transition temperatures, (2) standard enthalpies of formation, standard entropies and heat capacity functions, (3) phase transition enthalpies and entropies, and (4) binary $RE'_2O_3 - RE''_2O_3$ phase diagrams. In the first part, the thermal stability and phase transition of each RE_2O_3 were discussed. The best set of transition temperature values for stable and metastable RE_2O_3 phases (five solid polymorphs and one liquid phase) were determined. In the second part, numerous experimental data ΔH°_{298} and S°_{298} were critically assessed and unavailable data were estimated. In the third part, due to limited quantity of experimental data, several methodologies were employed to estimate enthalpy and entropy of transitions. The T_{tr} estimated in conjunction with the studies of transition energies were inserted back to the corresponding T_{tr} sections. In the last part, the constructed thermodynamic database of RE_2O_3 from the previous three parts was employed to the binary $RE'_2O_3 - RE''_2O_3$ phase diagrams for validation purposes of the accuracy of new RE_2O_3 database model.

2. Temperatures of Polymorphs Phase Transitions

Rare earth sesquioxides have different stable crystal structures at room temperature and pressure. The Lanthanide oxides from La_2O_3 to Nd_2O_3, generally called as the light RE_2O_3, are stable as hexagonal structure – A phase; Sm_2O_3 to Gd_2O_3, named as the middle RE_2O_3, are stable in either monoclinic – B or cubic – C phases; Tb_2O_3 to Lu_2O_3, named as the heavy RE_2O_3, are stable in only cubic – C phase. The Pm_2O_3, which positions between the light and middle RE_2O_3, is stable in C phase. Three stable phases C, B and A of RE_2O_3 exist at room temperature. When temperature is raised above 2400K, three room temperature phases transfer to high temperature hexagonal – H and high temperature cubic – X. According to Foex and Traverse [3] in 1960s, these two high temperature phases are just below the melting points but not quenchable to room temperature.

Aldebert and Traverse [4] in 1970s studied the crystal structures of H and X phases using neutron diffraction experiments. In their study, the positions of oxygen atoms in H phase were reasonably determined, but the position of oxygen atoms in X phase are still ambiguous. Therefore, it is difficult to even preform DFT based chemical and physical calculations due to no reliable

crystal structure information of such high temperature phases. Therefore, further study on crystal structures of H and X phases are very necessary.

Ideally, the polymorph transitions of RE_2O_3 occur in the sequence of C→B→A→H→X→L from room temperature to high temperatures. However, some of the transitions become inviable at room pressure especially when ionic radii [5] become smaller from La_2O_3 to Lu_2O_3. According to experimental data, phase transition of the light RE_2O_3 follow the sequence of A→H→X→L, while the other sesquioxides all transform from C phase. The middle RE_2O_3 and Pm_2O_3 obey the ideal transition sequence of C→B→A→H→X→L; and Tb_2O_3 to Dy_2O_3 generally obey the ideal transition without A phase, Ho_2O_3 and Y_2O_3 without A or X phases; Er_2O_3 to Yb_2O_3 transform in the order of C→H→L; Lu_2O_3 and Sc_2O_3 maintain as C structure up to their meltings.

The importance of proper understanding of polymorphic transition urged many investigations starting from Goldschmidt et al., [6] in 1925. In 1961, Warshaw and Roy [7] studied the C→B transition temperatures of selective RE_2O_3 (RE = La – Nd, Sm – Gd, Tb, and Dy) using classical quenching technique with XRD phase analysis. The first comprehensive study of almost entire lanthanide RE_2O_3 involving all the phase transitions until melting was carried out by Foex and Traverse [3] using *in situ* thermal and X – ray analysis. In their study, the measured T_{tr} and T_{fus} were plotted in terms of atomic numbers of the Lanthanide cations to produce a phase transition diagram with provisional phase boundaries. The $T_{tr,C\rightarrow B}$ of Pm_2O_3 was an approximation by Foex and Traverse from their study and result by Weigel and Scherer [8], who studied C, B and A crystal structures of Pm_2O_3. A few years later, Tresvyatkii et al. [9] measured the T_{tr} of some RE_2O_3 (RE = La – Nd, Sm, Gd, Tb – Er, Yb and Y) using DTA and XRD methods. The reversibility of the phase transitions with increasing and decreasing temperature was demonstrated in their work. Coutures and Foex [10] carried out selective binary phase diagram studies of La_2O_3 – RE'_2O_3 systems using TA and XRD methods. They produced the phase diagrams at high temperatures mainly involving H, X and liquid phases. T_{tr} of pure RE_2O_3 can be extracted from these binary phase diagrams as illustrated in Figure 1. Since it was a collaboration between Coutures and Foex [10], excellent agreement with the original work by Foex and Traverse [3] was observed. The most recent comprehensive study of T_{tr} of RE_2O_3, excluding Pm_2O_3 and Eu_2O_3, was performed by Shevthenko and Lopato [11] in 1985 using DTA method in controlled gaseous

environment up to 2873K and TA method in air using solar radiation heating up to 3273K. All the results from these four most comprehensive investigations and some fragmental studies are discussed below, and compared for each phase transition in the following sections 2.1 to 2.6. The best and most reliable set of data were selected in this work and hypothetical transition temperatures for metastable phases were predicted reasonably. Some necessary comparisons between this work and the previous assessment from Zinkevich [2] were also made.

2.1 Temperatures of C→B Phase Transition

The existence of the C→B transition from Pm_2O_3 to Ho_2O_3 is well observed by various authors [3, 9-11]. This transition is yet debatable for Er_2O_3 and Yb_2O_3: for example, in the study by Tresvyatkii et al. [9], mixed or combined phase transitions (1) C→B, B→A→H for Er_2O_3 and (2) C→B→A→H transitions for Yb_2O_3 were observed at single temperatures 2593K and 2653K respectively. Details on the experimental data and assessed values are listed in Table 4 and Figure 2.

Chikalla et al. [12] obtained B polymorph from C – Pm_2O_3 by heating promethium oxalate at 923 – 1023K for 1 week. This is the only experimental study for Pm_2O_3 available in literature. Zinkevich [2] proposed 457K as the transition temperature, which were estimated from the T_{tr} from Sm_2O_3 to Gd_2O_3. It should be noted that the C→B transition temperatures proposed by Zinkevich from Sm_2O_3 to Gd_2O_3 were also lower than the experimental values [7, 13-15] . In this study, results from Chikalla et al. on Pm_2O_3 is accepted because of strong experimental evidences. The $T_{tr,C→B}$ of Pm_2O_3 in this study is 973K, which is the middle value of the experimental findings (923 – 1023K) of Chikalla et al.

The transitions of Sm_2O_3, Eu_2O_3 and Gd_2O_3 were measured using heat treatment and XRD analysis [7, 13, 15]. Roth and Schneider [13] reported the annealing of C form of Sm_2O_3 at several temperatures up to 1173K for 1 – 2 weeks did not produce B form, but heating at 1273K for a few hours readily formed B phase, which indicated the transition temperature is between 1173K and 1273K. Later Warshaw and Roy [7] found the formation of the B form Sm_2O_3 at 1153K after 20 hours annealing, which is more or less consistent with Roth and Schneider. In the present study,

the result from Warshaw and Roy is accepted because of excellent alignment with $T_{tr,C\rightarrow B}$ of neighboring sesquioxides Eu_2O_3, Gd_2O_3 and Pm_2O_3 in Figure 2.

For Eu_2O_3, Curtis and Tharp [15] reported C→B transition at about 1323K, but it was not reversibly reproducible. They suggested that C form was either metastable or had extremely slow transition mechanism during the reversion process. Roth and Schneider [13] later preformed the same experiment of Curtis but did not find transformation even after 100 hours annealing at 1323K. Roth and Schneider suggested 1348K as transition temperature. The result of Roth and Schneider was later well supported by Warshaw and Roy [7], who found a small amount of B form when heating C sample at 1378K for 30 hours. In the literature, the transition temperature of Eu_2O_3 by Roth and Schneider is widely accepted and employed by both Fitzgibbon et al. [16] and Lyutsareva et al. [17] for the calculation of ΔH_{tr}°. In the present study, 1348K is also accepted as the C→B transition temperature of Eu_2O_3.

Roth and Schneider [13] observed the C→B transition of Gd_2O_3 at 1523K after several days of annealing. Warshaw and Roy [7] reported the C→B transition at 1508K after 20 hours annealing. A slightly higher transition temperature 1561K was reported by Kolitsch [18]. Considering the consistency of the results of Kolitsch with the whole middle RE_2O_3, 1561K is accepted as the C→B transition temperature of Gd_2O_3.

Zinkevich [2] estimated the C→B transition temperatures of Sm_2O_3, Eu_2O_3 and Gd_2O_3 from the optimized binary phase diagrams of $Y_2O_3 – Sm_2O_3$, $Y_2O_3 – Eu_2O_3$ and $Y_2O_3 – Gd_2O_3$ as shown in Figure 3. But the temperatures are much lower than the real experimental data explained above.

Warshaw and Roy [7] reported C→B transition for Tb_2O_3 to be around 2113K . However, Warshaw's experiments might suffer from slow kinetics of phase transition, which caused unusual high temperature. Results discovered by Foex and Traverse [3] suggested $T_{tr,C\rightarrow B}$ located between 1679 and 1829K. 1823K can be extracted from the T_{tr} – Ionic radii phase diagram by Foex and Traverse. Zinkevich [2] obtained 1823K from the analysis of the relationship between temperature and pressure of phase transition from the study of Hoekstra [19] and recommended 1823K for C→B transition. In the present study, 1823K is accepted for C→B transition temperature for Tb_2O_3.

DTA and TA data for C→B transition of Dy_2O_3 were reported by several authors [3, 9-11]. Tresvyatkii et al. [9], Foex and Traverse [3] reported exactly same T_{tr}=2223K, and a slightly higher value 2353K was reported by Shevthenko and Lopato [11]. The transition temperature of 2140K from the binary La_2O_3 – Dy_2O_3 phase diagram of Coutures and Foex [10] could be roughly extrapolated, but this value could be unreliable due to lack of data in Dy_2O_3 rich region. On the present study, the average temperature 2238K of Foex and Traverse, Tresvyatkii et al., Shevthenko and Lapoto is accepted.

Ho_2O_3 is the last RE_2O_3 which has stable C→B transition at 1 atm. Transition temperatures measured by [3, 9-11] using TA and DTA methods are in good agreement and the average 2460K is taken in this study.

Regarding the phase transitions of Er_2O_3, many authors [3, 10, 11] agreed that the C→B transition was no longer existed. However, Tresvyatkii et al. [9] reported transitions of C→B and B→A→H occurred concurrently at 2593K. In this study, C→H transition is accepted for Er_2O_3 instead of the mixed transition suggested by Tresvyatkii et al. To ensure the slight instability of B phase against H phase, $T_{tr,C\rightarrow B}$ for Er_2O_3 was intentionally raised slightly higher to 2600K rather than 2593K for C→H transition temperature. Details of C→H transition will be found in 2.6.1.

Metastable transition temperature of C→B of RE_2O_3 (RE = Tm – Lu, Y, Sc) should be estimated in order to develop the full thermodynamic database. *Figure 2* shows the variation of C→B transition temperature with ionic radii of RE_2O_3 cations. As can be seen in *Figure 2*, the experimental C→B transition temperatures of Dy_2O_3 to Sm_2O_3 is linearly shaped with ionic radii of RE^{3+}. This linear trend is extrapolated and extended to heavy RE_2O_3 (Tm_2O_3 – Lu_2O_3) and Sc_2O_3. Y_2O_3 was specially treated because the value calculated from the linear relationship was lower than assessed $T_{tr,\,C\rightarrow H}$ (as seen in Table 9). During estimation, it is necessary to ensure the metastable $T_{tr,\,C\rightarrow B}$ is higher than stable transitions $T_{tr,\,C\rightarrow H}$ and $T_{tr,\,C\rightarrow L}$. Otherwise, for example, the linearly extrapolated $T_{tr,C\rightarrow B}$ for Y_2O_3 could produce C→B→H transition instead of C→H transition. The average value 2756K calculated from $T_{tr,\,C\rightarrow B}$ of Er_2O_3 and Tm_2O_3 was accepted for $T_{tr,\,C\rightarrow B}$ of Y_2O_3 in this study.

The metastable $T_{tr,C\rightarrow B}$ of light RE_2O_3 (RE = La – Nd, stable phase transition starts from A phase) were calculated using optimized ΔH°_{tr} and ΔS°_{tr} of C to B transition. The details of the optimization process of ΔH°_{tr} and ΔS°_{tr} will be discussed in section 6.2.1. It should be noted that the optimized metastable $T_{tr,C\rightarrow B}$ of light RE_2O_3 show the continuous linear relationship between T_{tr} and ionic radii, as can be seen in Figure 2.

2.2 Temperatures of B→A Phase Transition

The B→A transition was confirmed to exist from Pm_2O_3 to Eu_2O_3 by many researchers [3, 8-11]. However, inconsistency in the literature was observed starting from Gd_2O_3 where mixed transitions occurred [9, 11]. The details of experimental, estimated and assessed values can be found in Table 5 and Figure 3.

The A form of Pm_2O_3 was obtained by Weigel and Scherer [8] after heating $Pm(OH)_3$ above 1873K in air or argon environment for several hours. A similar value $T_{tr,B\rightarrow A}$ 2013K for Pm_2O_3 was also reported by Chikalla et al. [12] using DTA technique. Differently, Zinkevich [2] recommended 936K, a much lower temperature than both experimental data [8, 12]. The result of Chikalla et al. showed consistent with the general B→A transition trend of adjacent sesquioxides, therefore is accepted in this study.

The experimental $T_{tr,B\rightarrow A}$ of Sm_2O_3 were reported by many researchers [3, 9-11] using TA and DTA techniques. Excellent agreements were found in three studies [3, 9, 11] except the work by Coutures and Foex [10]. In fact, the result of Coutures was extracted presumably from the binary La_2O_3 – Sm_2O_3 phase diagram. Therefore, the average value 2170K calculated using three studies [3, 9, 11] is accepted in this study.

The only experimental result 2323K for Eu_2O_3 is reported by Foex and Traverse [3]. This value is consistent with T_{tr} of adjacent sesquioxides as can be seen in Figure 3, therefore this temperature is accepted in this work.

The B→A transition of Gd_2O_3 was investigated by numerous researchers [3, 9-11, 20] using TA, DTA and electric conductivity methods. The two results by Foex and Traverse [3], and Coutures and Foex [10] using TA technique showed fair agreements, but lower than the results by Tresvyatkii et al. [9], Shevthenko and Lopato [11] from DTA method. The two DTA results were exactly the same in value of 2443K and in good agreement with Barkhatov et al. [20] using ECM (electric conductivity measurements) method. It should be noted that Tresvyatkii et al. discovered B→A and A→H transitions occurred in a temperature range 2443 – 2473K, and Shevthenko and Lopato determined two possible transitions B→A and B→H coexisted at a single temperature 2443K. These results indicate that the stability range of A phase is probably too small to detect. According to the phase diagram of La_2O_3 – Gd_2O_3 system by Coutures and Foex who determined B→A transition in the binary system from 70 at.% Gd_2O_3 to pure Gd_2O_3, $T_{tr,B\rightarrow A}$ of pure Gd_2O_3 is 2383K. In this study, 2383K from Coutures and Foex is taken for B→A transition of Gd_2O_3.

For Tb_2O_3, Dy_2O_3 and Ho_2O_3, B→H transition was observed by Foex and Traverse [3], A phase was not found. This is also supported by the study of Coutures and Foex [10], where the inexistency of A phase was confirmed according to their La_2O_3 – Dy_2O_3 and La_2O_3 – Ho_2O_3 phase diagrams.

On the other hand, Tresvyatkii et al., [9], Shevthenko and Lopato [11] reported the possible existence of A phase in Tb_2O_3, Dy_2O_3 and Ho_2O_3 using DTA. For Tb_2O_3, inseparable transition B→A and A→H were found by Tresvyatkii et al. at 2448K. Shevthenko and Lopato discovered B→A at 2433K, A→H and B→H simultaneously at 2448K. The similar phase transitions were also observed for Dy_2O_3 in the studies of Shevthenko and Lopato, and Tresvyatkii et al., where both works reported the same T_{tr}=2463K for B→A and A→H transitions. For Ho_2O_3, a mixture of C→B, B→A and A→H phase transitions were discovered by Tresvyatkii et al. in temperature range 2463 – 2563K. The complex phase transitions reported by Tresvyatkii et al., Shevthenko and Lopato are probably due to slow kinetics of phase transition. In this study, A phase is considered as metastable in Tb_2O_3, Dy_2O_3 and Ho_2O_3. For Tb_2O_3 – Lu_2O_3 and Sc_2O_3, temperatures of metastable B→A transition were calculated by extrapolating from the linear dependence of $T_{tr,B\rightarrow A}$ with respect to ionic radii between Gd_2O_3 at (0.938Å, 238K) and an assumed coordination (0.84Å, 2800K). In this way, the instability of metastable B→A transition and stability of B→H of these RE_2O_3 are

secured. For La_2O_3 – Nd_2O_3, the B→A transition is not observed because A form is stable down to room temperature. For the sake of simplicity, the hypothetical transition temperatures of B→A for La_2O_3 – Nd_2O_3 were estimated from the DFT results of ΔH_{tr}° of B→A by Wu et al. [119] with the assumed ΔS_{tr}° at 0.05J/mol·K using Equation 5. That is $T_{tr,B\rightarrow A}=(\Delta H_{tr}/\Delta S_{tr})$.

2.3 Temperatures of A→H Phase Transition

The A→H transition was generally well-studied from La_2O_3 to Nd_2O_3. Some confusions were reported in the works of Tresvyatkii et al. [9], Shevthenko and Lopato [11] for Gd_2O_3 – Ho_2O_3. All the experimental data, estimated and assessed values are listed in Table 6 and plotted in Figure 4.

"A" phase is the stable phase for La_2O_3 – Nd_2O_3 at room temperature. The A→H transition, was well investigated by many researchers [3, 9-11] using TA and DTA methods. Most of the data are in excellent agreement. Therefore, the averages obtained from experimental measurements for La_2O_3 – Nd_2O_3 were accepted in this study. For Pm_2O_3 and Eu_2O_3, the only experimental data were reported by Chikalla et al.[12], Foex and Traverse [3] respectively, and they were accepted in this work.

Several experimental data for Sm_2O_3 were reported [3, 9-11] using TA and DTA methods. Some variations were observed. The results of Coutures and Foex [10] was accepted in this study because their results were based on La_2O_3 – Sm_2O_3 phase diagram.

For Gd_2O_3, mixed transitions of B→A and A→H were reported at values 2458K and 2473K by Tresvyatkii et al. [9], Shevthenko and Lopato [11], respectively (as seen in Table 6). Other investigations by Foex and Traverse [3], Coutures and Foex [10], Barkhatov et al. [20] agreed on discrete B→A and A→H transitions even though the temperature differences between the two transitions were as small as 22 – 45K. Because of substantial evidences found [3, 10, 20], the two results of mixed transitions [9] [11] were regarded as T_{tr} of A→H transition. In this study, the average value 2447K of all available is accepted because variations of values were small.

For the heavy RE_2O_3, starting from Tb_2O_3, unstable A→H transition is observed. Complex transitions, involving metastable A were reported for Tb_2O_3, Dy_2O_3 and Ho_2O_3 by Tresvyatkii et al. [9], Shevthenko and Lopato [11] who found "B→A A→H" and "A→H B→H" transitions respectively. Stable B→H transition occurs for Tb_2O_3 – Ho_2O_3, and stable C→H transition occurs for Y_2O_3, Er_2O_3 – Yb_2O_3. The metastable $T_{tr,A\rightarrow H}$ for these heavy RE_2O_3, Y_2O_3 and Sc_2O_3 were estimated based on experimental temperatures of combined transitions B→H, C→H, C→L and their corresponding transition ΔH_{tr}° and ΔS_{tr}°. Generally, the longer the combined transition, the more assumptions were involved. For example, the Lu_2O_3 and Sc_2O_3, which have C→L transition, are the most difficult cases because the most estimations were involved: $T_{tr,H\rightarrow X}$ and $T_{tr,X\text{-}L}$ determined from ionic dependent temperature trend, and the calculated ΔH_{tr}° and ΔS_{tr}° of discrete phase transformations among C, B, A, X and L. The details will be introduced in section 6.2.3 on ΔH_{tr}° and ΔS_{tr}° of A→H transition. $T_{tr,A\rightarrow H}$ calculated from combined transitions for Y_2O_3, Sc_2O_3 and Tb_2O_3 – Lu_2O_3 showed large fluctuations, however, the magnitudes of these estimated values are less critical as long as properties of the stable combined transitions are closely aligned to experimental results (eq. $\Delta H_{tr,C\rightarrow H}^{\circ}$ and $T_{tr,C\rightarrow H}$). The accepted $T_{tr,A\rightarrow H}$ of La_2O_3 – Gd_2O_3 in this study showed larger fluctuation than the results from Zinkevich [2]. This smooth linear temperature – ionic radii relationship might be a result of manual adjustment.

2.4 Temperatures of H→X Phase Transition

Experimental data for the H→X transition of La_2O_3 – Dy_2O_3 were investigated [3, 9-12] using TA and DTA techniques. RE_2O_3 after Dy_2O_3 melt directly from H phase and therefore their $T_{tr,H\rightarrow X}$ must be properly estimated. Experimental and assessed data are listed in Table 7 and plotted in Figure 5.

Several experimental data were reported for La_2O_3 and Pr_2O_3 [3, 9-11]. The results of La_2O_3 are in excellent agreement except those from Tresvyatkii et al. [9], where results were 60 – 70K lower than other data. In this study, the average value of the experimental transition temperatures excluding the result of Tresvyatkii et al. is taken for the $T_{tr,H\rightarrow X}$ of La_2O_3. In the case of Pr_2O_3, the average of all available data is accepted for the $T_{tr,H\rightarrow X}$. Exact same transition temperature of 2443K was reported by Tresvyatkii et al., Shevthenko and Lopato [11] for Ce_2O_3,

which is accepted in this study. For Nd_2O_3, the results of Foex and Traverse [3], and Shevthenko and Lopato [11] are collectively below those of Coutures and Foex [10] and Tresvyatkii et al., by 30 – 40K. In this study, the later [9, 10] were chosen because of the well-established H→X transition in the binary La_2O_3 – Nd_2O_3 phase diagram by Coutures and Foex.

The transitions of Pm_2O_3 and Eu_2O_3 were investigated by Chikalla et al., [12] Foex and Traverse [3] respectively. The transition temperatures were all fairly aligned with the trend established by available data of the other adjacent RE_2O_3 as seen in Figure 5. Therefore, their experimental data are accepted in this study.

The transition temperature of Sm_2O_3 were reported from 2498K to 2553K by several research groups [3, 9-11]. The average value 2526K is accepted in this study because of generally small discrepancies among all data. It should be noted that the average is supported by the data 2520K from binary La_2O_3 – Sm_2O_3 phase diagram of Coutures and Foex [10].

Regarding Gd_2O_3, Foex and Traverse [3], and Tresvyatkii et al., [9] agreed lower $T_{tr,H\rightarrow X}$ (2613 – 2622K) while Coutures and Foex [10], Shevthenko and Lopato [11] concurrently reported higher values (2641 – 2643K). Because of well determined H→X transition in the La_2O_3 – Gd_2O_3 phase diagram by Coutures and Foex, present study accepts higher transition temperatures [10, 11].

Mixed H→X→L transition was observed by Tresvyatkii et al., [9] for Tb_2O_3 and Dy_2O_3 at 2613 – 2643K and 2633K, respectively. On the other hand, discrete H→X transitions of Tb_2O_3 and Dy_2O_3 were confirmed by Coutures and Foex [10], Shevthenko and Lopato [11], which are accepted in this study.

Heavy RE_2O_3 with smaller ionic radii than the one of Dy_2O_3 melt directly from H phase. Therefore, the $T_{tr,H\rightarrow X}$ of Y_2O_3 and Ho_2O_3 – Lu_2O_3 were estimated from the linear relationship established from transition temperature – ionic radii of La_2O_3 – Dy_2O_3 discussed above. Since the ionic radius of Sc_2O_3 is much smaller than Lu_2O_3, the simple estimation from this linear relationship was not adequately accurate. As the matter of fact, when $T_{tr,H\rightarrow X}$ was estimated using

the linear relationship, the resultant $\Delta H^{\circ}_{tr,C\rightarrow L}$ was too large, so the calculated $\Delta H^{\circ}_{tr,C\rightarrow L}$ exceeded experimental enthalpy of fusion of Sc_2O_3 reported by Shpil'rain et al., [21]. Therefore, $T_{tr,H\rightarrow X}$ of Sc_2O_3 was calculated using properly estimated $\Delta H^{\circ}_{tr,H\rightarrow X}$ and $\Delta S^{\circ}_{tr,H\rightarrow X}$, which will be explained in details in section 6.2.3.

2.5 Temperatures of X→L Phase Transition

The last discrete transition X→L was confirmed to exist in the range La_2O_3 – Dy_2O_3 by various researchers [3, 9-11, 22-27] using TA, DTA and direct melting in crucible methods. Experimental values, hypothetical and assessed results are listed in Table 8 and plotted in Figure 6.

Numerous experimental data [3, 9-11, 23, 27] were reported for the two light RE_2O_3 members La_2O_3 and Pr_2O_3. The experimental data for La_2O_3 are all 2581±3K. The data of Pr_2O_3 spread between 2533 and 2573K, but it is hard to reject any data because all data were obtained using similar experimental procedures. Therefore, the average values were accepted in this study. Exact the same result 2513K were obtained by Tresvyatkii et al [9] , Shevthenko and Lopato [11] for Ce_2O_3, which is accepted in this work. Excellent agreement for the transition of Nd_2O_3 is found in the results of Foex and Traverse [3] and Mizuno et al.,[26], while other studies [9-11, 22] show a larger scattering. Result by Mizuno et al. was further supported by their Nd_2O_3 liquidus data of the Nd_2O_3 – Al_2O_3 phase diagram [26], which was accurately reproduced by the assessment of Wu and Pelton [28]. Therefore, an average temperature 2574K from the two studies by Foex and Traverse, and Mizuno et al. is accepted in this study for Nd_2O_3.

The only result for Pm_2O_3 was reported by Chikalla et al., [12], and showed great consistency with its adjacent RE_2O_3 as shown in Figure 6. Therefore, this result is accepted in this study. The transition temperatures [3, 9-11, 24] are all within 2597±16K. As the reliabilities of all the reported values for Sm_2O_3 are considered as acceptable, the average 2597K is employed in this study. Experimental melting data for Eu_2O_3 was limited to two values reported by Foex and Traverse [3] 2598K, and Mizuno et al., [25] 2633K using TA technique. The average value 2616K is accepted for Eu_2O_3 in this study. Melting temperature of Gd_2O_3 were somewhat scattered from

2665K to 2718K noted in Table 8. Exact the same value 2683K was discovered by both Shevthenko and Lopato [11], and Mizuno et al., which is nearly the average value of all available data. Therefore, 2683K is accepted in this work for Gd_2O_3.

The melting of Tb_2O_3 from X phase was reported at 2673K in all the investigations [3, 9, 11], which is accepted in this work. For Dy_2O_3, Tresvyatkii et al., [9] and Mizuno et al., [29] reported the melting at 2633 and 2643K respectively, which are lower than 2674±1K by Foex and Traverse, Coutures and Foex, and Shevthenko and Lopato [3, 10, 11]. Considering abundant liquidus data in the La_2O_3 – Dy_2O_3 phase diagram reported by Coutures and Foex, the 2674K is accepted in this work.

For the heavy RE_2O_3 with smaller ionic radii than one of Dy_2O_3, their meltings occur directly from H or C phase instead of X. Therefore, the metastable $T_{tr,X\rightarrow L}$ for Y_2O_3 and Ho_2O_3 – Yb_2O_3, were calculated using the evaluated $\Delta H^{\circ}_{tr,X\rightarrow L}$ and $\Delta S^{\circ}_{tr,X\rightarrow L}$. The details will be discussed in section 6.2.3. For Lu_2O_3 and Sc_2O_3, C phase was retained until melting. The $T_{tr,X\rightarrow L}$ for Lu_2O_3 was estimated using a linear relationship of $T_{tr,X\rightarrow L}$ with respect to ionic radii of RE^{3+} for all the assessed and calculated data from La_2O_3 to Yb_2O_3. The simple linear relationship of $T_{tr,X\rightarrow L}$ was not applied successfully to Sc_2O_3. The $T_{tr,X\rightarrow L}$ for Sc_2O_3 was estimated using calculated ΔH°_{tr} and ΔS°_{tr} of Sc_2O_3, which will be discussed in section 6.2.3.

2.6 Temperatures of C→H, B→H, H→L and C→L Phase Transition

Although the standard transition sequence of RE_2O_3 is C→B→A→H→X→L, other stable transitions of C→H, B→H, H→L and C→L occur in heavy RE_2O_3, Y_2O_3 and Sc_2O_3.

2.6.1 C→H Phase Transition

The stable phase transition of C→H was observed for heavy RE_2O_3 in the range of Er_2O_3 to Yb_2O_3 and Y_2O_3 by several researchers [9, 11, 30-32]. The experimental data and assessed values in this study are plotted in Figure 7 and listed in Table 9.

The transition of Y_2O_3 reported by Shevthenko and Lopato [11] is 2663K, which is higher than the results of Navrotsky [31] at 2581K, Tresvyatkii et al., [9] at 2623K, and Shpil'rain et al., [32] at 2600K. The $T_{tr,C\rightarrow H}$ by Shpil'rain et al has been widely accepted in literature and show excellent agreement with Navrotsky and Tresvyatkii's DTA results. It should be noted that 2600K was also accepted by Zinkevich [2], while Grobner et al., [30] used 2660K in their assessment of Y – O binary system. Because of supportive evidences from various researchers, 2600K was accepted for C→H of Y_2O_3 in this work.

The C→H transition of Er_2O_3, Tm_2O_3 and Yb_2O_3 were determined by many researchers [3, 9-11, 33], and results show large scattering. In the present study, the transitions determined by Shevthenko and Lopato [11] using DTA technique are accepted because they show precise linear relationship between T_{tr} and ionic radii in Er_2O_3 – Yb_2O_3 range.

2.6.2 B→H Phase Transition

The B→H transition was observed for RE_2O_3 in the range Tb_2O_3 – Ho_2O_3 by several researchers [3, 9-11] using TA and DTA methods. Experimental and assessed transition temperatures were plotted in Figure 8 and listed in Table 10.

Tresvyatkii et al., [9], Shevthenko and Lopato [11] reported mixed transitions involving H phase for Gd_2O_3, but this seems due to slow kinetics. Similar confusing result was reported for Er_2O_3 by Tresvyatkii et al. For Tb_2O_3, Dy_2O_3 and Ho_2O_3, Foex and Traverse [3], Coutures and Foex [10] observed combined B→H transition using TA technique, while Tresvyatkii et al., Shevthenko and Lopato reported a mixture of multiple transitions involving H phase. Therefore, the results by the groups of Foex [3] and Coutures [10], which are in excellent agreement, are accepted in this study. A precise linear relationship between T_{tr} and ionic radii of RE^{3+} is established, as seen in Figure 8.

2.6.3 H→L Phase Transition

The H→L transition is confirmed to occur from Y_2O_3 –Yb_2O_3 by many researchers [3, 9-11, 30-32] using TA, DTA, drop calorimetry and electric conductivity measurements. Experimental results and assessed values were presented in Table 11 and plotted in Figure 9.

For Y_2O_3, the melting temperatures from many investigations [3, 9, 11, 32] are between 2683 and 2713K, while the result of Navrotsky [31] is 2655K, which is much lower than the others. In this work, 2703K from Shpil'rain et al., [32] is accepted for the melting of Y_2O_3. The melting of Ho_2O_3 [3, 9-11] was measured by TA and DTA techniques. In this study, the average value 2686K is accepted because of comparable reliability of the data. For the meltings of Er_2O_3 and Yb_2O_3, the results of Tresvyatkii et al., [9] show a lower value, therefore excluded in averages for Er_2O_3 and Yb_2O_3. For Tm_2O_3, the experimental data were limited to two values reported by Foex and Traverse [3], Shevthenko and Lopato [11]. Therefore, the average of these two works [3, 11]was accepted as recommendation in this work.

2.6.4 C→L Phase Transition

Lu_2O_3 and Sc_2O_3 retain in C structure until their meltings. Shevthenko and Lopato [11] reported the melting at 2783K for Lu_2O_3 and Shpil'rain et al., [32] reported 2782±20K for Sc_2O_3.

2.7 Overall View of Phase Transitions

The overall stable phase transformations optimized in this study are shown in Figure 10. Each point represents the selected value after rigorous assessment of all available experimental results in the literature. To present the phase transition clearly, solid lines are used to connect the same phase transition type, and dotted lines show the changes in the phase transition type between adjacent RE_2O_3. In general, the temperature of the same type of phase transition is increasing with decreasing ionic radii of RE^{3+} (that is, increasing atomic number). In particular, the slope of C→B and B→A transitions with ionic radii are steepest than other transitions.

3. Standard Enthalpy of Formation

The enthalpies of formation of lanthanide sesquioxides (excluding Sc_2O_3 and Y_2O_3) have been critically assessed by Cordfunke and Konings [34] in 2001 by critically evaluating all available literature data until 2000. In this work, original experimental data of all RE_2O_3, including Sc_2O_3 and Y_2O_3 were collected and critically evaluated again. The best consistent set of ΔH_{298}° was obtained after critical and systematic assessment of available experimental data and rigorous adjustment for consistency with the phase transition. Some of the ΔH_{298}° data earlier than 1950 were not discussed in this work because of inaccuracy due to obsolete experimental techniques and low purity rare earth metals employed, as pointed out by Cordfunke and Konings [32]. The high quality rare earth metals were not available until Dr. Spedding was able to produce them using ion exchange method [35] in the late 1940s. More information about studies prior to 1950 can be found in the study of Cordfunke and Konings.

Generally, the ΔH_{298}° of RE_2O_3 are measured using solution calorimetry and combustion calorimetry. The reaction procedures of the aqueous solution calorimetry are illustrated from Reaction 1 – 4 [32], the dissolution enthalpies from Reaction 1 and Reaction 2 are collected from literature, while the enthalpies of decomposition of H_2O into elemental products in HCl solution with different concentrations were carefully calculated by Cordfunke and Konings [36]. Since the H_2O decomposition enthalpies are extensively studied through history, the values reported by Cordfunke and Konings [36] are used directly without modifications.

Reaction 1 ($\Delta H_{r,1}^{\circ}$): $2RE + 6HCl = 2RECl_3 + 3H_2$

Reaction 2 ($\Delta H_{r,2}^{\circ}$): $RE_2O_3 + 6HCl = 2RECl_3 + 3H_2O$

Reaction 3 ($\Delta H_{r,3}^{\circ}$): $3H_2O(sol) = 1.5O_2 + 3H_2$

Reaction 4 ($\Delta H_{r,4}^{\circ}$): $2RE + 1.5O_2 = RE_2O_3$

Equation 1 ΔH_f° RE_2O_3 = $\Delta H_{r,4}^{\circ}$ = ($\Delta H_{r,1}^{\circ}$– $\Delta H_{r,2}^{\circ}$) + $\Delta H_{r,3}^{\circ}$.

For combustion calorimetry, ΔH_{298}° is measured directly by reacting pure metal and oxygen. The combustion reaction is illustrated below:

(ΔH_{298}°): $2RE + 1.5O_2 = RE_2O_3$

The present study used the similar analysis technique for the evaluation of ΔH°_{298} of RE_2O_3 as Cordfunke and Konings [34] did. In the most of cases, the differences between the optimized data in this study and the assessed data by Cordfunke and Konings on lanthanide sesquioxides are smaller than few kJ/mol except Ce_2O_3. In addition, in this study, the ΔH°_{298} of Sc_2O_3, Y_2O_3 and Gd_2O_3 (C form) were optimized which were not available in the study by Cordfunke and Konings. It should be noted that Zinkevich [2] adopted the assessed values of Cordfunke and Konings without any modification. The detailed discussions about the evaluation of the enthalpy in this study are below.

3.1 Standard Enthalpy of Formation of Sc_2O_3 and Y_2O_3

3.1.1 The ΔH°_{298} of C – Sc_2O_3

The ΔH°_{298} of C – Sc_2O_3 was determined by Mah [37] using combustion calorimetry. Huber used combustion calorimetry in his first study [38] with Holley in 1962 and both solution and combustion techniques in the second study [39] with Fitzgibbon in 1963. The results reported by both research groups [37-39] were listed in Table 12. Mah analyzed the starting metal and final product of combustion experiment and confirmed the non – metallic impurities in the starting metallic sample and crucible materials in the product, which caused uncertainty in enthalpy data. Huber and Holley also reported the usage of relatively impure Sc metal and contamination of product by non – Sc_2O_3. In Huber's second study with Fitzgibbon, the impurities of initial metal sample and final product were corrected for combustion experiment, while the result from solution calorimetry was composed without known states of impurities. Therefore, combustion result from Huber and Fitzgibbon is accepted in this study. It should be also noted that after the experiment of Huber and Fitzgibbon, Mah conducted a trail combustion experiment again using sample supplied by Huber and a Sc_2O_3 crucible, a similar result to Huber and Fitzgibbon was obtained [36]. Furthermore, Huber's second combustion value was also accepted in the assessment by Leonidov et al., [40] of thermodynamic properties of Sc_2O_3.

3.1.2 The ΔH°_{298} of C – Y_2O_3

The ΔH°_{298} of C – Y_2O_3 was determined by Huber and Holley [41], Lavut and Chelovskaya [42] using combustion calorimetry technique. Wang et al., [43] and Morss et al., [44] measured the enthalpy of Y metal and Y_2O_3 in 1M HCl aqueous solution, respectively. All the available experimental data and selected values were presented in Table 12.

Huber and Holley [41] made correction for the impurities in starting material Y and product Y_2O_3 to get ΔH°_{298}. Lavut and Chelovskaya [42] discussed the combustion reaction in the study by Huber and Holley was incomplete by judging the color of the final oxides (light tan color due to deficiency of oxygen). They carefully reinvestigated using combustion calorimetry and obtained -1919.4±2.8kJ/mol [42], which was about 14kJ/mol more negative than the result of Huber and Holley.

Wang et al., [43] measured the dissolution enthalpy of Y metal in 1M HCl solution and estimated ΔH°_{298} of Y_2O_3. Morss et al., [44] determined the ΔH°_{298} of Y_2O_3 by combining their dissolution enthalpy of Y_2O_3 oxide in 1M HCl and Wang's experimental result for Y. The starting materials used in the studies of Morss and Wang were higher in purity than those of Huber and Lavut [41, 42]. It is noted final result ΔH°_{298} from Morss et al., is more negative than both combustion values [41, 42] by 10 – 30 kJ/mol, but very close to the estimation in the study of Wang et al., as shown in Table 12. Considering the high purity materials used by Morss et al., and Wang et al., the combined result reported by Morss et al. is selected in this study.

3.2 Standard Enthalpy of Formation for Light RE_2O_3

3.2.1 The ΔH°_{298} of A – La_2O_3

The ΔH°_{298} of A – La_2O_3 was measured by Huber and Holley [45] using combustion calorimetry, Fitzgibbon and Holley [46] and Gvelesiani and Yashvili [47] using solution calorimetry. All the experimental results were listed in Table 13.

Prior to the study of Huber and Holley [45], the measurements from literature had large discrepancies mainly due to the usage of impure La metal, therefore those measurements were not

considered in this study. Fitzgibbon and Holley [46], Gvelesiani and Yashvili [47] measured the dissolution enthalpy of La and La_2O_3 in aqueous solution calorimeter. However, Cordfunke and Konings [34] reported that the enthalpies of La metal dissolution in both studies have issues of incomplete dissolution. Therefore, the result of La from Merli et al., [48] and the result of La_2O_3 from Fitzgibbon and Holley, and Gvelesiani and Yashvili were combined to obtain ΔH_{298}° of La_2O_3 in this study. That is the average of revised values.

3.2.2 The ΔH_{298}° of A – Ce_2O_3

ΔH_{298}° of Ce_2O_3 was measured by combining the combustion heat of Ce_2O_3 to CeO_2 and Ce to CeO_2 because burning Ce metal always resulted in CeO_2 instead of Ce_2O_3 [49]. The reaction scheme of the combustion calorimetry for Ce_2O_3 was shown below [50]:

Reaction 5 ($\Delta H_{r,1}^{\circ}$): $Ce_2O_3 + \frac{1}{2}\ O_2 = 2CeO_2$

Reaction 6 ($\Delta H_{r,2}^{\circ}$): $Ce + \ O_2 = CeO_2$

Reaction 7($\Delta H_{r,3}^{\circ}$): $2Ce + \frac{3}{2}O_2 = \ Ce_2O_3$

ΔH_{298}° Ce_2O_3 = $\Delta H_{r,3}^{\circ}$ = $-\ (\Delta H_{r,1}^{\circ} - \Delta H_{r,2}^{\circ})$

All the results of Ce_2O_3 were listed in Table 13. Heats of Reaction 5 were measured by Kuznetsov et al., [49], Mah [50], Baker and Holley [51]. They further combined their results of Reaction 5 with the result of Reaction 6 by Huber and Holley [52] to obtain ΔH_{298}° of Ce_2O_3. The relatively large differences between the three results may be due to carbon and hydrogen impurities [53] or slight oxidation in the starting Ce_2O_3 materials [34, 51].

Recently, Huntelaar et al., [53] using solution calorimetry and Putnam et al., [54] using transposed temperature drop calorimetry measured the ΔH_{298}° of Ce_2O_3. Huntelaar et al., performed five measurements on dissolution enthalpy of Ce_2O_3 in 0.25M HCl and combined with the dissolution enthalpy of Ce from Spedding and Miller [55] to get ΔH_{298}°. Some CeO_2 debris were found after their experiments, but correction was made accordingly on the final ΔH_{298}°. Putnam et al., [52] used the same preparation and characterization methods to the one of Huntelaar

et al. That is, both studies used the same high purity Ce_2O_3 samples for experiments. In this study, the average -1809.45±3.3KJ/mol of these two studies [53, 54] is accepted for ΔH_{298}° of Ce_2O_3.

3.2.3 The ΔH_{298}° of A – Pr_2O_3

The limited ΔH_{298}° of Pr_2O_3 were reported by Stubblefield et al., [56] and Fitzgibbon et al., [57] using solution calorimetry. All the available experimental data and the recommended values were shown in Table 13.

In the study of Stubblefield et al., [56], the heat of Pr_2O_3 dissolution in 6M HNO_3 was measured and combined with Pr metal dissolution enthalpy in 1.2M HCl measured by Spedding and Flynn [58] to obtain the final ΔH_{298}°. Later in 1969, Stubblefield [59] conducted more measurements using adiabatic solution calorimeter of enthalpy of dissolving rare earth metals in acidic solutions with various concentrations (6M HNO_3, 1M HCl and 6M HCl). It is found that the dissolution enthalpy of Pr metal in 6M HNO_3 [59] was around 300kJ/mol more negative than the result of Spedding and Flynn in 1.2M HCl. Fitzgibbon explained in his study that dissolution of Pr metal in HNO_3 solution might not be desirable because the hydrogen produced during reaction could reduce the acid. Fitzgibbon conducted extensive measurements on dissolution of Pr and Pr_2O_3 in different acidic solutions, including 2M HCl, 2M HNO_3 and 6M HNO_3. The result of rigorous study by Fitzgibbon et al., [57] is accepted in this work.

3.2.4 The ΔH_{298}° of A – Nd_2O_3

Since Nd_2O_3 is one of the widely used rare earth sesquioxides, experimental ΔH_{298}° were reported as early as 1900s. After 1950, data with acceptable accuracy were reported by Huber and Holley [60] and Spedding et al., [61] using combustion calorimetry, and Fitzgibbon et al., [62], Yashvili and Gvelesiani [63], Morss and Haar [64] and Monaenkova et al., [65] using solution calorimetry. All the experimental and selected values are shown in Table 13.

For combustion experiments by Huber and Holley [60], the starting materials were carefully characterized and the completeness of the combustion experiment was nearly 100%.

Extra oxygen was found in the final products after experiments, but corrected for the final ΔH°_{298}. In comparison with the work by Huber and Holley, the result obtained using combustion method from Spedding et al., [61] was more positive and considered as less reliable due to incompleteness of the combustion and mass loss of the crucible.

Regarding the results from solution calorimetry, Fitzgibbon et al., [62] measured dissolution enthalpies of Nd_2O_3 in 2M and 4.36M HCl solutions. They reported final ΔH°_{298} for Nd_2O_3 by combining their experimental data and the data on Nd metal dissolution by Stuve [66]. It is observed that ΔH°_{298} from Fitzgibbon's group showed excellent agreement with that of Huber and Holley [60] from combustion method. For further comparison, the experimental result by Fitzgibbon et al., of Nd_2O_3 was combined in this study with the Nd dissolution enthalpy by Merli et al., [48] to obtain ΔH°_{298} for Nd_2O_3. This result is also in good agreement with the result of Huber and Holley.

Yashvili and Gvelesiani [63] reported the dissolution enthalpy of Nd_2O_3 in 6M HCl. Their result was combined with available dissolution enthalpy of Nd by Merli et al., [48] -1831.70±7.80kJ/mol, which was significantly more negative than the other results. Popova and Monaenkova [67] measured the dissolution enthalpy of Nd metal and Nd_2O_3 in 2.19M HCl solution as -686.77.85±1.17kJ/mol and -434.11±0.87kJ/mol, respectively. These give the ΔH°_{298} = -1796.8±1.9KJ/mol [67], which is somewhat agreeable to the less accurate value from Spedding et al., [61]. In this study, a very close value -1808.81kJ/mol of the studies [60, 62] is accepted for ΔH°_{298} for Nd_2O_3.

3.3 Standard Enthalpy of Formation for Middle RE_2O_3

3.3.1 The ΔH°_{298} of C and B – Sm_2O_3

The ΔH°_{298} of C – Sm_2O_3 was measured by Gvelesiani and Yashvili [47], Baker and Pavone [68] using solution calorimetry. The ΔH°_{298} of B – Sm_2O_3 was measured by Huber et al., [69] and Spedding et al., [61] using combustion calorimetry, Gvelesiani and Yashvili [47], Hennig and

Oppermann [70] using solution calorimetry. Baker and Pavone [68] studied the ΔH°_{298} of B form using both techniques. All the experimental data and selected values are listed in Table 14.

In combustion calorimetry studies, Huber et al., [69] obtained ΔH°_{298} of B – Sm_2O_3 as -1815.40±2.01kJ/mol, which was the result after careful correction of impurity compositions. Spedding et al., [61] found ΔH°_{298} of B – Sm_2O_3 as -1777.3KJ/mol, which was significantly more positive than the other literature results [47, 68-70]. The large discrepancy might due to the incompleteness of combustion of Sm in the study of Spedding et al. The ΔH°_{298} of B – Sm_2O_3 obtained by Baker and Pavone [68] is -1824kJ/mol from both combustion and solution calorimetry.

The dissolution enthalpy of B – Sm_2O_3 in 4M HCl solution obtained by Hennig and Oppermann [70] was combined with dissolution enthalpy of Sm metal by Baker and Pavone [68] to obtain ΔH°_{298} =-1824.67±7.99KJ/mol as seen in the study of Cordfunke and Konings [34]. This value was in excellent agreement with Baker and Pavone. Though Cordfunke and Konings ignored the uncertainties night be introduced by combining results measured in HCl solutions with different concentrations. Gvelesiani et al., [47] conducted experiments on both B and C forms and found ΔH°_{298} of C form -1826.32±7.10kJ/mol was more positive in value than B form -1832.17±7.95kJ/mol. This observation was proven not true by Baker and Pavone after their experiments. It is also found in this work that the assessed ΔH°_{298} of the other middle RE_2O_3 (Eu_2O_3 and Gd_2O_3) all have more negative values of C form indicating C form is more stable than B form. Extensive experiments were conducted by Baker and Pavone using both combustion and solution calorimetry. ΔH°_{298} of -1824.18±2.64kJ/mol and -1823.64±1.90kJ/mol for B – Sm_2O_3, and -1827.41±3.05kJ/mol for C form were obtained. Impurities of starting materials were taken into consideration and corrected for the final ΔH°_{298}.

In this study, the ΔH°_{298} of both B and C forms were selected from Baker and Pavone [68] and modified within the uncertainty range to accord with $T_{tr,C\rightarrow B}$ at 1153K (section 2.1) and the trends of $\Delta H^{\circ}_{tr,C\rightarrow B}$ and $\Delta S^{\circ}_{tr,C\rightarrow B}$ (section 6.2.1). The optimized of ΔH°_{298} C and B forms of Sm_2O_3 were -1827.19kJ/mol and -1822.60kJ/mol, respectively.

3.3.2 The ΔH°_{298} of C and B – Eu_2O_3

The ΔH°_{298} of C and B form Eu_2O_3 were investigated by Huber et al.,[71] and Fitzgibbon et al.,[16] using both combustion and solution calorimetry. Yashvili and Gvelesiani [63], Hennig and Oppermann [72] performed experiments on B form, and Stuve [73] studied C form using solution calorimetry technique. All the experimental and selected data were shown in Table 14.

Huber et al., [71] reported ΔH°_{298} of B form -1648.08±3.77kJ/mol from several combustion experiments. In his solution calorimetry study, the $\Delta H^{\circ}_{tr,C\rightarrow B}$ was determined to be 17.99±2.51kJ/mol by measuring the enthalpy difference between dissolution enthalpy of B and C form of Eu_2O_3. Therefore, the ΔH°_{298} of C form -1630.09±4.60kJ/mol was calculated using previous ΔH°_{298} of B – Eu_2O_3 from combustion method and the obtained $\Delta H^{\circ}_{tr,C\rightarrow B}$ Stuve [70] determined ΔH°_{298} = -1619.08±5.02KJ/mol for C – Eu_2O_3 using solution calorimetry. The value was significantly more positive than other values for C – Eu_2O_3 as shown in Table 14. Stuve discussed that his result must be considered provisional as relatively impure Eu metal used and unknown sources of uncertainties during experimental procedures. Yashvili et al., [63] determined ΔH°_{298} = -1725.48±5.10KJ/mol for B – Eu_2O_3 using solution calorimetry. Their result was significantly more negative than the values for B form reported by others [16, 71, 72] as shown in Table 14. The purity of the experimental starting materials in the study of Yashvili et al., was uncertain because the composition was not described in their work. Therefore, Yashvili's study was not considered in this work. Hennig and Oppermann [72] measured the dissolution enthalpy of several Eu compounds including B form of Eu_2O_3. The Eu_2O_3 dissolution enthalpy was combined with the dissolution of Eu by Stuve [70] and Fitzgibbon et al., [14] to obtain -1686.22±5.27kJ/mol and -1730.48±6.11kJ/mol, which were too negative. Consequently, the result of Hennig and Oppermann was not considered in this work.

The most reliable measurements of the ΔH°_{298} of both C and B forms of Eu_2O_3 were obtained by Fitzgibbon et al., [16] after the first paper with Huber et al., [71]. The Eu metal used in the experiment was carefully analyzed for impurities. Numerous experiments on Eu_2O_3 and Eu metal dissolution enthalpies in 2M, 4M and 6M HCl and HNO_3 acid solution were performed to

increase accuracy. ΔH_{298}° = -1651.42±3.35kJ/mol for B – Eu_2O_3 was the average results from both solution and combustion calorimetry. ΔH_{298}° = -1661.10±3.76kJ/mol for C – Eu_2O_3 was obtained using solely solution calorimetry. Fitzgibbon et al., [16] also compared that the dissolution enthalpy of Eu by Stubblefield et al., [74] is about 20 to 40kJ/mol more positive than their data.

In this study, ΔH_{298}° Fitzgibbon et al., [16] were slightly modified to accommodate $T_{tr,C\rightarrow B}$ at 1348K (section 2.1) and the trend of $\Delta H_{tr,C\rightarrow B}^{\circ}$ and $\Delta S_{tr,C\rightarrow B}^{\circ}$ (section 6.2.1). The optimized values of C and B forms of Eu_2O_3 were -1657.95kJ/mol and -1653.45kJ/mol, respectively.

3.3.3 The ΔH_{298}° of C and B – Gd_2O_3

The ΔH_{298}° data for B – Gd_2O_3 were reported by Huber and Holley [75] and Spedding et al., [61] using combustion calorimetry, and Yashvili and Gvelesiani [63] using solution calorimetry. Huber and Holley [75] reported ΔH_{298}° = -1815.7±3.6KJ/mol as shown in Table 14 for Gd_2O_3 by burning Gd metal supplied from Dr. Spedding's lab. Huber and Holley commented that the analytical characterization techniques were limited at that time, thus the chemical state of the impurities remained uncertain. The impurities, including C, N, Ca, O and H, were assumed to form compounds with Gd and potentially reduced purity level by 2.5%. The final ΔH_{298}° was corrected by Huber for those assumed impurities. Spedding et al., obtained ΔH_{298}° = -1782.2kJ/mol using combustion method. Similar to the other results of Lanthanide sesquioxides that reported by Spedding et al., [61], the ΔH_{298}° was much more positive than the other literature values [63, 75]. Spedding et al., commented the reasons might be incompleteness of combustion and limitation of the analytical techniques. Yashvili and Gvelesiani obtained ΔH_{298}° = -1824.22±1.80kJ/mol for B form Gd_2O_3 using solution calorimetry.

Because of similar physical and chemical properties of lanthanide sesquioxides, roughly linear decreasing trend of ΔH_{298}° with decreasing of ionic radii can be obtained. Therefore, ΔH_{298}° of B – Gd_2O_3 should be smaller than B – Sm_2O_3. In this study, the result by Yashvili and Gvelesiani [63] fitted in the trend, therefore, accepted for ΔH_{298}° of B – Sm_2O_3.

The ΔH°_{298} of C – Gd_2O_3 is not available in the literature. The value was estimated by considering $T_{tr,C\rightarrow B}$ at 1561K (section 2.1), the trend of $\Delta H^{\circ}_{tr,C\rightarrow B}$ and $\Delta S^{\circ}_{tr,C\rightarrow B}$ (section 6.2.1). The optimized ΔH°_{298} were -1830.93kJ/mol and -1825.19kJ/mol for C and B form Gd_2O_3, respectively. All the experimental and selected data were shown in Table 14.

3.4 Standard Enthalpy of Formation for Heavy RE_2O_3

The ΔH°_{298} for C – Tb_2O_3 was studied by Stubblefield and Eick [76], Fitzgibbon and Holley [77] using solution calorimetry. It is important to note that terbium oxides consist of Tb_2O_3 and non – stoichiometric oxides, which may increase the difficulties of experiments. All the experimental and selected data were shown in Table 15.

Stubblefield and Eick [76] investigated the solution enthalpies of several stable Tb oxides, including Tb_2O_3, in 6M HNO_3 solution. However, they were unable to obtain the dissolution enthalpy of Tb metal. In order to calculate ΔH°_{298}, they determined the missing enthalpy by linear interpolating enthalpy measurements on various rare earth metals from Spedding and Flynn [58]. The resultant ΔH°_{298} reported by Stubblefield and Eick was -1827.57±8.37kJ/mol. In the more recent assessment paper, Cordfunke and Konings [34] combined their previous assessed enthalpy of metal dissolution with the result of Stubblefield and Eick to yield a more negative ΔH°_{298} -1864.5±8.4kJ/mol.

Fitzgibbon and Holley [77] measured the solution enthalpy of Tb in 1M HCl and the solution enthalpies of a series terbium oxides in 6M HNO_3 solution. According to Fitzgibbon and Holley [77], HNO_3 solution could not be used to dissolve Tb metal because of unwanted reduction of the acid, and HCl solution could not be used on Tb oxides because of undesired oxidation of the acid. It was more problematic that dissolving Tb_2O_3 in HNO_3 had unacceptably slow kinetics for accurate measurements [77]. Therefore, the final result -1865.23±7.53kJ/mol was extrapolated from results of a series of terbium oxides measurements [77], which is in good agreement with the re – evaluated value by Cordfunke and Konings [34]. Therefore, the result of Fitzgibbon and Holley is accepted in this study.

3.4.1 The ΔH_{298}° of C – Dy_2O_3

The ΔH_{298}° of C – Dy_2O_3 was measured by Huber et al., [78] using combustion calorimetry in the first investigation, and both combustion and solution calorimetry techniques in the second study [79]. In the first study, relatively impure Dy metal was used to obtain -1865.39±3.89kJ/mol as shown in Table 15. In the second study, purer samples were employed in combustion method to get -1863.14±4.18kJ/mol. Two dissolution enthalpies of Dy metal and Dy_2O_3 were determined in 4M HCl. The result from solution technique -1863.97±6.69KJ/mol showed an excellent agreement with the second combustion calorimetry result. The average -1863.22±3.56kJ/mol of Huber et al., in their second study [79] was accepted in this work, which was also accepted by Cordfunke and Konings [34].

3.4.2 The ΔH_{298}° of C – Ho_2O_3

Combustion and solution calorimetry were employed by Huber et al., [80] and Morss et al., [44], respectively, to study the ΔH_{298}° of C – Ho_2O_3. Huber et al., obtained the ΔH_{298}° -1880.92±4.81kJ/mol (Table 15) after careful correction of impurity contribution. Morss et al., only measured the enthalpy of Ho_2O_3 in 4M HCl solution and evaluated dissolution enthalpy of Ho from literature. Morss et al., commented the Ho metal dissolution enthalpy from Stuve [81] had substantial uncertainty therefore neglected from their study. Bettonville et al., [82] reported Ho metal dissolution enthalpy in 1M HCl solution. Morss et al., corrected the result from Bettonville et al., to a dissolution enthalpy for 4M HCl. The resultant ΔH_{298}° was -1887.3±13.7kJ/mol. Cordfunke and Konings [34] re – evaluated the dissolution enthalpy of Ho_2O_3 from Morss et al., and the enthalpy of Ho metal from Stuve to yield -1885.7±7.3kJ/mol. In this study, because of uncertainties involved in the study by Stuve, ΔH_{298}° is optimized to be -1884.11±9.26kJ/mol, which is the average of the result of Huber et al., and the result of Moss et al.

3.4.3 The ΔH_{298}° of C – Er_2O_3

The ΔH_{298}° of C – Er_2O_3 was determined by Spedding et al., [61] and Huber et al., [83]

using combustion calorimetry, and Morss et al., [44], Montgometry and Stuve [84] using solution technique. In the study of Huber et al., 0.1% impurities were found after carefully analyzing the starting metal and corrected in ΔH_{298}° -1897.82±1.88kJ/mol. A few years later, Spedding et al., reported the $\Delta H_{298}^{\circ} =$ -1762.84kJ/mol, which was much more positive than other results reported in literature as shown in Table 15, therefore not taken into account in this study. Spedding et al., commented the reason of large discrepancy might due to incompleteness of the combustion reaction, unwanted participation of crucible materials in reaction and limitation of analysis on non – metallic impurities.

Montgometry and Stuve [84] studied the dissolution enthalpy of Er_2O_3 in 1.468M HCl and obtained -370.62±3.68kJ/mol. When their result was combined with the dissolution enthalpy of Er by Spedding and Flynn [58], Bommer and Hohmann [85], two values - 1815.74±3.68kJ/mol and -1847.63±3.68KJ/mol were obtained, respectively. Fuger et al., [86] discussed these two combined results were not sufficiently exothermic, therefore they re-investigated Er dissolution enthalpy in 1.428M HCl solution and found -705.6±1.7kJ/mol. Combining the result of Fuger et al., and Montgometry and Stuve can produce ΔH_{298}° -1898.19±7.08kJ/mol. In 1990s, Morss et al., [44] measured the dissolution enthalpy of Er_2O_3 in 1.40M HCl to be -364.6±3.0kJ/mol. When this result is combined with the result of Fuger et al., [83], ΔH_{298}° -1904.21±6.40kJ/mol as shown in Table 15. The accepted $\Delta H_{298}^{\circ} =$-1900.07kJ/mol of Er_2O_3 is the average of the results from Huber et al., [83], and the combined results involving the study of Fuger et al.

3.4.4 The ΔH_{298}° of C – Tm_2O_3

The ΔH_{298}° of C – Tm_2O_3 was determined by Huber and Holley [87] using combustion calorimetry. Huber reported the metal sample used containing 1.27% and 1.55% impurities and the completeness of the combustion reactions varied from 88.67% to 99.67%. Two results -1894.8±8.3kJ/mol and -1884.3±7.9kJ/mol were obtained from the two samples after impurity corrections and resulted the average -1888.66±5.86kJ/mol as shown in Table 15. This average result is accepted in this study.

3.4.5 The ΔH°_{298} of C – Yb_2O_3 and Lu_2O_3

Limited data were available in the literature for both Yb_2O_3 and Lu_2O_3. The ΔH°_{298} of these two RE_2O_3 were measured by Huber et al., [78, 88] using combustion calorimetry. The starting materials were carefully analyzed as usual as their other studies. The results were -1814.52±2.22kJ/mol and -1878.20±7.53kJ/mol for Yb_2O_3 and Lu_2O_3 respectively. Both of the values are accepted.

3.5 Summary of ΔH°_{298} and Trend

The optimized or accepted ΔH°_{298} of RE_2O_3 are plotted against ionic radii of RE^{3+} in the part (a) of Figure 11, and all experimental data are plotted in part (b). As can be seen in Figure 11(b), there is significant scattering in existing data, but the optimized data in Figure 11 (a) shows clear trend. The typical Lanthanide irregularities are clearly observed for Eu_2O_3 and Yb_2O_3 as shown in part(b). The Eu and Yb elements, which have half-filled and full-filled f-orbitals, are the only divalent crystalline metals in the lanthanide series. The correlation of these irregular thermodynamic properties were well studied by Nugent et al., [89], which introduced the trivalent – divalent transition energy ΔE(M). The ΔH°_{298} of these RE_2O_3 (excluding Eu_2O_3 and Yb_2O_3) almost linearly decrease with decreasing ionic radii, and the trend can be roughly linearly extended to even Gd_2O_3 with C polymorph. The ΔH°_{298} for C – Pm_2O_3 was therefore estimated from the linearity between Gd_2O_3 and Sm_2O_3 because no experimental data were available in literature.

4. Standard Entropy of RE_2O_3

Low temperature C_p data are generally used to calculate standard entropy, S°_{298}. It is interesting to find out that the experimental low temperature (below 298K) C_p of RE_2O_3 typically show thermal anomaly peaks usually around 10K. According to Justice et al.,[90-94], who extensively studied the low temperature C_p of RE_2O_3, mentioned there are three contributions in C_p to be considered for the calculation of S°_{298}: lattice contribution, magnetics contribution (both antiferro – , or ferro – magnetic and para-magnetic contributions), and ground state degeneracy

contribution. The magnetic contributions by antiferro – or ferro – magnetics appeared as "cooperative anomaly" and that of para – magnetics appeared as "Schottky anomaly", according to Justice et al. They also analyzed the crystalline field level of each RE_2O_3 and proposed the method to calculate ground state degeneracy contribution. In the present study, we followed the same approach as Justice et al., proposed to calculate the S°_{298} of each RE_2O_3.

Several rare earth sesquioxides, namely Sc_2O_3 ($3p^6$), Y_2O_3 ($4p^6$), La_2O_3 ($4d^{10}$), Eu_2O_3 ($4f^7$) and Lu_2O_3 ($4f^{14}$), are excluded from the Schottky effect because of absence or lack of unfilled f orbitals, which are the sources of paramagnetic properties.

Justice et al., [90-94] extensively investigated low temperature heat capacity values for (1) A forms of La_2O_3, Pr_2O_3, Ce_2O_3, and Nd_2O_3 and (2) C forms of Gd_2O_3, Yb_2O_3, Dy_2O_3, Ho_2O_3, Er_2O_3, Tm_2O_3 and Lu_2O_3, and (3) B form of Sm_2O_3 from around 5K to 350K. Data for Pm_2O_3 and Tb_2O_3 were not available in literature. In the study of Justice et al., the contribution of magnetic ordering was evaluated from experimental low temperature C_p data by removing lattice contribution. Then, the theoretical magnetic contributions to S°_{298} and lattice contribution to S°_{298} were calculated. In the calculation of lattice contribution, the Debye T^3 approach was of course counted in to calculate the lattice C_p below lowest experimental temperature to 0 K. Then, ground state degeneracy was also added in to calculate total S°_{298}. When the dissociation of lattice contribution and magnetic contribution from experimentally measured C_p data, sometime it was difficult to distinguish each contribution clearly. Therefore, Justices et al., used the standard lattice contribution from La_2O_3 without any magnetism as the lattice C_p of all light RE_2O_3 (A form) to evaluate the magnetic contribution from experimentally observed C_p data. Similarly, they used the lattice C_p of Gd_2O_3 (100 to 298 K) and C_p of Yb_2O_3 (below 100 K) as standard lattice contribution of heavy RE_2O_3 (C form) and obtained the magnetic contribution. Although Lu_2O_3 without any magnetism might be used for lattice C_p of C phase, Justice et al., pointed out the significant lanthanide contractions in Lu_2O_3 which might change the lattice contribution by tens of % from other heavy RE_2O_3. On the other hand, the experimentally measured C_p of Gd_2O_3 and Yb_2O_3 have very small magnetic contribution, so the lattice contribution can be easily approximated from the experimental data. The contribution of ground state degeneracy was calculated as *2Rln(number of degeneracy)* where number of degeneracy was given by Justice et al.

In this work, all available data from the literature were critically reviewed and the standard entropies were evaluated using the same method as Justice et al., suggested. In the assessment process, it was found that the studies of Justice et al., [90-94] were the most consistent and completed, so their low temperature C_p data were used most often in this study to calculate the standard entropy values. Experimental data were not available for all the RE_2O_3. Low temperature heat capacities for C – Sm_2O_3 and B – Gd_2O_3 were not measured, but estimated by Lyutsareva [17] using spectral data. The standard entropy of Pm_2O_3 was calculated in this work using properties of its adjacent RE_2O_3. For Tb_2O_3, magnetic properties measured by Hill [95] were used with the approach by Justice et al., [92] to estimate the S°_{298}. All the reported, evaluated and estimated S°_{298} are listed in Table 17. The available low temperature C_p data are plotted together with high temperature C_p data in Figure 13 to Figure 31. The details of the S°_{298} analysis are given below for each RE_2O_3.

4.1 Standard Entropy of C – Y_2O_3 and C – Sc_2O_3

The low temperature heat capacities for calculating S°_{298} of cubic Y_2O_3 were measured by Goldstein et al., [96] and Gavrichev et al., [97] in the temperature ranges 16 – 300K and 14 – 300K. No trance of thermal anomalies was observed in the experimental ranges from both studies. Using the Debye – like method to extrapolate data below the experimental temperature limits, Goldstein et al., and Gavrichev et al., obtained exactly the same $S^{\circ}_{298} = 98.96$J/mol·K. In this work, 99.13J/mol·K was obtained from the integration of experimental data from the both studies.

Similar to Y_2O_3, thermal anomalies were not observed in the low temperature heat capacity data of cubic Sc_2O_3. Weller and King [98] calculated $S^{\circ}_{298} = 76.99$J/mol·K by adding the integration of C_p from 50 – 298K and Debye – like extrapolation below 50K. Using the same method and the experimental data from Weller and King, 76.60J/mol·K was obtained in this work.

4.2 Standard Entropy of Light RE_2O_3

4.2.1 The S°_{298} of A – La_2O_3

The low temperature heat capacities of A form of La_2O_3 were measured by Justice and Westrum [92] using an adiabatic calorimeter, and Goldstein et al., [96] and King et al., [99] using Nernst vacuum calorimeter. The measurements by Justice and Westrum, Goldstein et al., and King et al., ranged from 5 – 350K, 16 – 300K and 50 – 298K respectively. Since La_2O_3 is one of the sesquioxides without the thermal anomaly, Debye T^3 extrapolation can be used directly to find out data below experimental limits. Using the data from Justice and Westrum, the standard entropy was found 127.24J/mol·K in this study. This value is in excellent agreement with Goldstein's 127.95 ± 0.29 J/mol·K and Justice's 127.32J/mol·K. A little higher value 128.57 ± 0.84 J/mol·K was obtained by King et al.

4.2.2 The S°_{298} of A – Ce_2O_3

The low temperature heat capacities of Ce_2O_3 for calculating of the S°_{298} were investigated by Justice and Westrum [90] in the temperature range between 5 and 350K, Huntelaar et al., [53] at 3 – 420K, Weller and King [98] at 51 – 300K. Ce_2O_3 is one of the non – stoichiometric oxides in the RE_2O_3 series, therefore, pure Ce_2O_3 is very difficult to obtain for experiments. Extra oxygen composition is observed in many experiments.

In the study of Weller and king [98], the starting material Ce_2O_3 contained significant amount of impurities and led to a non – stoichiometric $Ce_2O_{3.33}$. Since their measurements started from 50K, the cooperative transition event below 50K was not included. Therefore, the $S^{\circ}_{298} =$ 150.62±4.18J/mol·K from Weller and King were not taken into consideration in this work.

In the study of Justice and Westrum [90], the starting material Ce_2O_3 was prepared by carbon reduction of pure cerium dioxide and contained 3.4 wt% of impurities. The low temperature heat capacity data showed a sharp prominent feature at 8.5K indicating a cooperative anomaly effect [90]. Because the cooperative anomaly was large, the Schottky effect was hindered and needed to be accounted for in calculation of S°_{298} [90]. The experimentally evaluated entropy from 5 – 298K covering the sharp peak at 8.5K, the Debye – like extrapolation to 0K and the degeneracy

contribution below 5K were summed $S^{\circ}_{298} = 148.11$J/mol·K [90]. A series of thermodynamic properties of Ce_2O_3 were studied by Huntelaar et al., [53]. They produced Ce_2O_3 sample by reduction from CeO_2 and about 1 wt% impurities [53] were contained in the Ce_2O_3 sample. A sharp antiferromagnetic transition was detected at 5.7K, which was lower than 8.5K from Justice and Westrum. A polynomial function was used by Huntelaar et al., to fit the data from 0 – 5K to interpret the heat capacities below experimental limit 3K. As the result, Huntelaar et al., calculated the $S^{\circ}_{298} = 148.91 \pm 0.40$J/mol·K, which was comparable to the result of Justice and Westrum 148.11J/mol·K. In the present study, the result of Huntelaar et al., were re – evaluated to obtain $S^{\circ}_{298} = 148.87$J/mol·K for Ce_2O_3.

4.2.3 The S°_{298} of A – Pr_2O_3

The only source of the low temperature C_p data of Pr_2O_3 is the personal communication between Gruber et al., and Lutsareva [100] in 1997. The low temperature C_p data from 5 to 300K are inconsistent with the high temperature C_p data from Pankratz and Kelley [101]. Gruber et al., adjusted the original low temperature C_p data to estimate the final S°_{298} 152.73J/mol·K of Pr_2O_3. To validate the reliability of the result of Gruber et al., we estimated S°_{298} of Pr_2O_3 as the average of S°_{298} Ce_2O_3 and Nd_2O_3. The average value was 153.83J/mol·K, which is very close to the S°_{298} reported by Gruber et al. The result of Gruber et al. is used in this study for Pr_2O_3.

4.2.4 The S°_{298} of A – Nd_2O_3

The low temperature heat capacities of Nd_2O_3 were measured by Goldstein et al., [96] in the temperature range between 16 and 300K, and Justice and Westrum [92] in the temperature range between 5 and 350K. Goldstein et al., reported S°_{298} 154.47J/mol.K [96] was estimated using from the experimental data and possible magnetic contribution. Justice and Westrum measured the low C_p data and observed the Schottky anomaly peak at about 10K. In addition, the spectroscopic data from the literature was reviewed and compared by Justice and Westrum to their own experimental electronic energy level data. Justice and Westrum reported the final result S°_{298} of 158.45J/mol.K taking into account the additional *2Rln2* for presumed thermal anomaly and lattice

contribution below 5K. In the present study, the experimental results of Justice et al., were re – evaluated to obtain S°_{298} of Nd_2O_3 = 158.78J/mol·K.

4.3 Standard Entropy of Middle RE_2O_3

4.3.1 The S°_{298} of B and C – Sm_2O_3

The only low temperature heat capacities of B – Sm_2O_3 were measured by Justice and Westrum [91] in the temperature range between 5 and 350K. The electronic heat capacities could not be resolved quantitatively because of absence of knowledge on lattice contribution of B form of RE_2O_3 [91]. The experimental data by Justice and Westrum clearly showed the presence of a Schottky anomaly effect, however, the position of the C_p peak was ambiguous to determine especially because lattice contribution could not be separated. Using the same method as other RE_2O_3 which had thermal anomalies, Justice and Westrum calculated the S°_{298} of B – Sm_2O_3 to be 151.04J/mol·K.

The experimental low temperature C_p experimental data for C – Sm_2O_3 were absence in literature. Lyutsareva [17] estimated the S°_{298} of C – Sm_2O_3 using spectral data of Sm^{3+} ion in cubic Y_2O_3 crystals for the electronic contribution and C_p of both C – Eu_2O_3 for the lattice components. The estimated S°_{298} of C – Sm_2O_3 was 155.80±3J/mol·K.

In this work, the experimental data of Justice and Westrum [91] for B – Sm_2O_3 were used for the recalculation based on the same methodology introduced in the previous discussion of other RE_2O_3. A slightly lower value of S°_{298} for B – Sm_2O_3 (150.38J/mol·K) than the result by Justice and Westrum was obtained. For the C – Sm_2O_3, the estimation by Lyutsareva et al., [17] estimation was not used. Instead, the trend of $\Delta S^{\circ}_{tr,C\rightarrow B}$ (section 6.2.1) was used to estimate S°_{298} of C – Sm_2O_3. According to this trend, B form is predicted to have higher S°_{298} than C form. However, the estimation by Lyutsareva et al., told that S°_{298} of B – Sm_2O_3 is lower than that of C – Sm_2O_3. The optimized S°_{298} of C – Sm_2O_3 in the study is 145.94J/mol·K.

4.3.2 The S°_{298} of B and C – Eu_2O_3

The low temperature heat capacity experimental data for both B and C – Eu_2O_3 were measured by Lyutsareva et al., [17] in the temperature range between 8 and 300K. Since the paramagnetic property of Eu_2O_3 is deficient as shown in the insert in Figure 12, both B and C form of Eu_2O_3 show the absence of the Schottky anomaly. In this work, the experimental data Lyutsareva et al., were used to recalculate the S°_{298}. Exactly the same values of 141.45J/mol·K and 142.74J/mol·K as the result of Lyustareva et al., were obtained for C and B – Eu_2O_3 in this work. However, it was both agreed in this study and Zinkevich [2] that the difference between the two S°_{298} should be larger in order to accommodate the thermodynamic consistency for C – B phase transition ($T_{tr}, \Delta H^{\circ}_{tr}, \Delta S^{\circ}_{tr}$). Consequently, minor modifications were made to yield the final results of S°_{298} to be138.95J/mol·K and 144.25J/mol·K for C and B forms respectively.

4.3.3 The S°_{298} B and C – Gd_2O_3

The low temperature C_p data of C – Gd_2O_3 were measured by Justice and Westrum [91] in the temperature range between 7 and 350K. The entire range of thermal anomalies were not observed because of experimental limitations, therefore, by applying the spectral data, the positions of theoretical cooperative and Schottky anomalies were determined to be at 1.3K and 3.8K, respectively [91]. The final S°_{298} calculated by Justice and Westrum was 150.62J/mol·K, which was exactly the same to our recalculation.

The C_p data of B – Gd_2O_3 are unavailable in the literature. Lyutsareva et al., [17] used the similar method as their estimation for C – Sm_2O_3 to obtain the result of C – Gd_2O_3.The estimated S°_{298} was 156.10J/mol·K. In the present study, the result of Justice and Westrum [91] for C – Gd_2O_3 and ΔS°_{tr} of C → B phase change (section 6.2.1) were used. That is, the optimized S°_{298} of B and C – Gd_2O_3 are 150.62J/mol·K and 155.50J/mol·K respectively in this study.

4.4 Standard Entropy of Heavy RE_2O_3

4.4.1 The S°_{298} of C – Dy_2O_3

The low temperature heat capacities of C type Dy_2O_3 were measured by Justice and Westrum [93] in the temperature range 6 to 350K. No other thermal anomaly was discovered experimentally except the double degeneracy at ground state, which contributed *2Rln2* to the final S°_{298} [93]. Using the same method as Justice and Westrum used, 149.48J/mol·K is obtained in this study, which is in excellent agreement with the original S°_{298} 149.79J/mol·K by them.

4.4.2 The S°_{298} of C – Ho_2O_3

Justice and Westrum [93] measured the low temperature heat capacities for C – Ho_2O_3 from 6 to 350K. They further distinguished the thermal anomalies of Schottky and cooperative effects. As Justice and Westrum did, S°_{298} including ground state degeneracy (*2Rln3*) is calculated in this study to be 158.14J/mol·K, which is consistent with the value 158.16 J/mol·K by Justice and Westrum.

4.4.3 The S°_{298} of C – Er_2O_3

The low temperature C_p of C type Er_2O_3 were reported by Justice and Westrum [93] in the temperature range between 5 and 350K. The thermal anomaly peak at 35K was not obviously shown until the lattice contribution was removed from the main heat capacity data. It was proposed by Justice and Westrum that the presence of a probable cooperative anomaly below 10K might cause the hindering of the ground state degeneracy. As the result, the final S°_{298} 153.13J/mol·K of C – Er_2O_3 was calculated by them by adding *2Rln2* as the effect of ground state degeneracy to the entropy calculation. Using the same method, we calculated S°_{298} to be 153.50J/mol·K was obtained in this study.

4.4.4 The S°_{298} of C – Tm_2O_3

The low temperature C_p data for C type of Tm_2O_3 were measured by Justice et al., [94] in the temperature range between 6 and 350K. The lattice contribution was calculated with the same methodology as other cubic RE_2O_3 in the study by Justice and his colleagues, but scaled accordingly because of Lanthanide contraction effect. Justice et al., assumed the ground state degeneracy contribution was singlets , which was excellently supported by magnetic susceptibility data provided by Brown and Hubbard [102] based on the experiments at 1.3 – 4.2K. Consequently, Justice et al., calculated the final S°_{298} to be 139.75J/mol·K. In this work, almost the same result 139.74J/mol·K is recalculated.

4.4.5 The S°_{298} of C – Yb_2O_3

The low temperature C_p data of C – Yb_2O_3 were measured by Justice and Westrum [91] in the temperature range between 5 and 350K. However, even at the lowest temperature point, the peak of the thermal anomaly was still not reached. Justice and Westrum stated that the trace of the thermal anomaly indicated the possible antiferromagnetic ordering at 2.5K [103], which could also be treated as the degeneracy at the ground state. As for the calculation of S°_{298}, Justice and Westrum also took into account for the degeneracy at the ground state *2Rln2*. The recalculated S°_{298} from this study is 133.77J/mol·K, which is very close to the original value by Justice and Westrum at 133.05J/mol·K.

4.4.6 The S°_{298} of C – Lu_2O_3

The low temperature C_p of C – Lu_2O_3 was measured by Justice et al., [94] in the temperature range between 6 and 350K. Compare to other RE_2O_3, the effect of thermal anomaly is absent due to filled f – orbital of Lu_2O_3. Therefore, the calculation of the S°_{298} is much simpler than other RE_2O_3. By summing the integration of the available low temperature C_p data and extrapolation from 6K to 0K using the Debye method, 109.96J/mol·K is obtained for S°_{298} of C – Lu_2O_3 by Justice et al., and 109.91J/mol·K in this study.

4.5 Estimation of Missing S°_{298} for Pm_2O_3 and Tb_2O_3

The low temperature C_p of Pm_2O_3 and Tb_2O_3 were not available in the literature. In the study of Zinkevich [2], the estimated S°_{298} of Pm_2O_3 and Tb_2O_3 were 155.60J/mol·K and 156.91J/mol· K, respectively.

All the available experimental S°_{298} and calculated/optimized S°_{298} in this study are plotted in Figure 12. The paramagnetic moment (insert of Figure 14) and assessed standard entropies in Figure 12 show similar trend with atomic number. From the change of S°_{298} of cubic RE_2O_3, S°_{298} of C – Pm_2O_3 is estimated to be 152.95J/mol·K (average of the values of C – Sm_2O_3 and C – Eu_2O_3).

In the case of C – Tb_2O_3, simple linear average of the value of adjacent RE_2O_3 is less reasonable because of the mismatch between high paramagnetic moment (Figure 12) and low S°_{298} of neighbouring Dy_2O_3. Fortunately, Hill [95] measured the low temperature magnetic ("electronic" according to the study by Justice et al., [90-94]) heat capacities below 22K and estimated the magnetic entropy from 0 to 22K. Using the available data from Hill, the contribution of magnetic S_{mag} to S°_{298} was calculated in this study. Then, S_{mag} at 298K was added to the lattice contribution of C – RE_2O_3 calculated using the method by Justice et al., to obtain the final S°_{298} to be 157.57J/mol·K.

5. Heat Capacity of RE_2O_3

All the available heat capacity data RE_2O_3 are plotted in Figure 13 to Figure 31. Even though, RE_2O_3 have multiple polymorph modifications, the available heat capacity data only covered the most stable phases for the light (A phase) and heavy (C phase) RE_2O_3. For the middle RE_2O_3, C_p data for both C and B phases were available. All the high temperature C_p data were calculated from original heat content data. In the figures, low temperature C_p data which were mainly obtained from adiabatic calorimetry are also plotted to examine the consistency of C_p data.

Pankratz et al., [101, 104-108], as one of the main contributors for C_p measurement, measured the heat content values of the entire RE_2O_3 except La_2O_3 and Pm_2O_3. The second important research group was Tsagreishvilli et al., [109-113] who measured heat content data of RE_2O_3 series (RE = Sc, Eu, Dy, Ho, Tm and Yb). Shpil'rain et al., [32] performed heat content measurements covering phase transition of C→H→L of Y_2O_3. Experimental data were not available for radioactive Pm_2O_3. The heat capacity function for Pm_2O_3 was estimated by taking the average of the C_p function coefficients of Nd_2O_3 and Sm_2O_3.

For each RE_2O_3, when more than one set of experimental data are available, the most reliable set or combined data sets from several authors were carefully assessed and used to generate the best heat capacity functions using computer-assisted regression program. The typical C_p function coefficients were used in this work is:

$$C_p = a + bT + cT^{-2} + dT^2$$

In the optimization of C_p function for T>298K, the C_p data starting from 200K or less were used to get the smooth continuous functions from low temperature C_p. The optimized coefficients of all C_p functions of all the RE_2O_3 are listed in Table 18. In Figure 13 to Figure 31, the results of Zinkevich [2] are also plotted in dashed lines for comparison. The details of C_p evaluation for each RE_2O_3 are below.

5.1.1 Heat capacity of C – Y_2O_3

Extensive data [18, 32, 108, 114-117] were found for C – Y_2O_3 as shown in Figure 13. Low temperature data are from Goldstein et al., [96].

Curtis [117] reported a series of properties of Y_2O_3, including heat content from 473K to 1473K. Pankratz et al., [108] and Landa et al., [114] measured heat content using drop calorimetry from 298 to 1799K and from 1300 to 2100K respectively. The heat content values from Yashvili et al., [116], who used 99.94% purity Y_2O_3 ranged from 389K to 1615K. Seminko et al., [115] investigated $H_T - H_{298}$ from 1194K to 2468K. The heat content values from Shpil'rain et al., [32]

ranged from 1883K to 2919K, which covered three phases, C, H and L. Kolitsch [18] investigated the heat capacity using stepwise heating and continuous heating in the temperature range between 650 and 1650K. As shown in Figure 13, experimental data from Curtis were already scattering below 800K, while the result by Pankratz et al., and Yashvili et al., overlapped with great consistency. Above 1200K, data of Pankratz et al., started to show scattering and reached maximum variation at around 1400K. Although Seminko et al., and Shpil'rain et al., studied heat content above 2000K, their data scattering was too severe to obtain a reasonable C_p function. In this work, the data from Landa et al., Kolitsch, Yashvili et al., and Pankratz et al. below 1200K were used to construct the heat capacity function. As can be seen in Figure 13, the C_p curve from Zinkevich [2] deviates gradually from the present C_p function with increasing temperature.

5.1.2 Heat Capacity of C – Sc_2O_3

The experimental heat content data were measured by Pankratz and Kelley [104] and Tsagareishvili et al., [110] at 298 – 1800K and 298 – 1600K, respectively. Shpil'rain et al., [21] was the only researcher who reported enthalpy measurements up to 2930K including liquid phase. Leonidov et al., [40] has studied various properties related to Sc_2O_3 including heat capacities in his thesis. As presented in Figure 14, the optimized C_p data from Leonidov showed great agreement with the results of Pankratz and Kelley, and Tsagareishvili et al., and also exhibited smooth connection with low temperature C_p data from Weller and King [98]. Data from Shpil'rain et al., were overly scattered as usual. In this work, the optimized data by Lenonidov et al., were employed to calculate the C_p function. The C_p optimized by Zinkevich [2] was somewhat lower than the result from this work. Zinkevich might have used the scattered data from Pankratz and Kelley above 1400K (Figure 14).

5.2 Heat Capacity of Light RE_2O_3

5.2.1 The Heat Capacity of A – La_2O_3

Heat content data of La_2O_3 were reported by Blomeke and Ziegler [118] and King et al., [99] at 383 – 1172K and 30 – 2000K, respectively. As seen in Figure 15, the data by King et al.,

showed great consistency with the low temperature C_p data from Justice and Westrum [92], Goldstein et al., [96], and also the result of Blomeke and Ziegler for high temperature C_p. Therefore, the results of King et al., Blomeke and Ziegler were used together to produce the C_p function in this work. The results from Zinkevich [2] agreed excellently with this work.

5.2.2 The Heat Capacity of A – Ce_2O_3

The heat capacity experimental data above room temperature were obtained by Pankratz and Kelley [105], Kuznetsov and Rezukhina [119] at 398 – 1500K and 578 – 1116K, respectively. Low temperature C_p data were measured by Weller and King [98], Justice and Westrum [90] and Huntelaar et al., [53]. A few extrapolation data points for high temperature C_p were also reported by Huntelaar et al. The results of Kuznetsov and Rezukhina were systematically lower than the extrapolation from low temperature C_p data. Even though, Pankratz and Kelley reported considerable number of experimental data, the quality was too poor to fix a C_p function. The poor accuracy of the results of Pankratz and Kelley might result from the starting non – stoichiometric material ($Ce_2O_{3.3}$) instead of the stoichiometric compound Ce_2O_3. The $\alpha - \beta$ transition reported by Pankratz and Kelley were neither discussed clearly in their own study nor supported by any other literature. α was measured as Hexagonal structure, while β was not characterized by Pankratz and Kelley. Therefore, the results by Pankratz and Kelley, Kuznetsov and Rezukhina were excluded from the optimization of C_p function. In this work, the data extrapolated by Huntelaar et al., up to about 800K were used to optimize the C_p function of A – Ce_2O_3. The C_p data calculated from Zinkevich [2] are slightly higher than the present line (Figure 16).

5.2.3 The Heat Capacity of A – Pr_2O_3

Heat content data for Pr_2O_3 were reported by Pankratz [101] in the range between 400 and 1600K, and the low temperature C_p data were limited to the personal communication between Gruber and Lutsareva [100]. As discussed previously (section 4.2.3) on standard entropy, the experimental data from Lutsareva were quantitatively adjusted by Gruber to align the high temperature C_p from Pankratz. In this work, whole range of the data by Pankratz were used to calculate the C_p function.

5.2.4 The Heat Capacity of A – Nd_2O_3

High temperature heat content data for Nd_2O_3 were measured by Blomeke and Ziegler [118] at 383 – 1172K and Pankratz et al., [108] at 400 – 1800K. Data reported by both authors showed consistency with the low temperature C_p data measured by Goldstein et al., [96] and Justice and Westrum [92]. However, some scattering were observed in the data by Pankratz above 1300K as shown in Figure 18. Therefore, all available data below 1300K by Blomeke and Ziegler, and Pnakratz et al., were used to produce the C_p function of A – Nd_2O_3. As presented in the figure, the C_p line produced by Zinkevich [2] was reasonable until 1300K shows the deviation from the present optimized C_p function.

5.3 Heat Capacity of Middle RE_2O_3

5.3.1 The Heat Capacity of C and B – Sm_2O_3

Sm_2O_3 is stable in either C or B form at room temperature, therefore, heat content data for the two polymorphs were measured. Pankratz and Kelley [106] reported data for C and B structures 405 – 1150K and 403 – 1798K, respectively. Gvelesiani et al., [120] reported data for C – Sm_2O_3 at 394 – 1147K and B – Sm_2O_3 at 396 – 1617K. Both studies on C – Sm_2O_3 were discontinued around 1150K because C→B phase transition occurs at 1153K (section 2.1). The C_p function of C – Sm_2O_3 was optimized using data from both Pankratz and Kelley, and Gvelesiani et al. As shown in Figure 19, the C_p line produced by Zinkevich [2] started to deviate from this work after 1150K.

In the study of Pankratz and Kelley [106] on B – Sm_2O_3, a thermal anomaly was observed near 1195K as shown in Figure 20. Since the cause of this anomaly was neither discussed by Pankratz nor reported in the study Gvelesiani et al., [120], the anomaly was excluded in the evaluation of C_p. The C_p function was optimized using the whole ranges of data from both studies. It should be noted that both data sets are consistent with the data from Justice and Westrum [91]. The optimized C_p in this work shows negligible difference comparing to C_p optimized by Zinkevich [2].

5.3.2 The Heat Capacity of C and B – Eu_2O_3

Experimental heat content data on C – Eu_2O_3 were reported by Pankratz and Kelley [106], Tsagareishvili and Gvelesiani [109], Gilchrist and Preston [121] in the temperature ranges at 400 – 1350K, 400 – 1200K and 298 – 973K respectively as shown in Figure 21. These C_p data are consistent with low temperature C_p data from Lyutsareva [17]. Due to the phase transition of C→B at 1348K, heat content data of C – Eu_2O_3 were not available above this temperature. The C_p function was optimized by employing all the data [106, 109, 121]. The C_p established by Zinkevich [2] was slightly higher than the C_p from this work.

The heat content data on B – Eu_2O_3 were obtained by researchers Pankratz and Kelley [106], Gvelesiani et al., [120] and Gilchrist and Preston [121] at 400 – 1800K, 383 – 1589K, and 298 – 973K, respectively. The results of Gvelesiani et al., are consistent with other results until 1200K. Then, a significant scattering is shown. It should be also noted that all C_p results are consistent with low temperature C_p from Lyutsareva [17], as can be seen in Figure 22. In this work, all C_p data except the part of data by Gvelesiani et al., were used to obtain the optimized C_p function of B – Eu_2O_3.

5.3.3 The Heat Capacity of C and B – Gd_2O_3

The heat contents of C – Gd_2O_3 were reported only by Pankratz and Kelley [106] in the temperature range at 400 – 1550K. The C_p derived from the heat content data are plotted in Figure 23 and they are consistent with the low temperature C_p data by Justice and Westrum [91]. The C_p of B – Gd_2O_3 were investigated by Pankratz and Kelley [106] and Shpil'rain et al., [122] in the temperature ranges at 400 – 1802K and 1600 – 2400K, respectively. The C_p function of C – Gd_2O_3 is optimized based on the data by Pankratz and Kelley.

For B – Gd_2O_3, the result of Sphil'rain et al., [122] were not employed in the present C_p optimization because of poor accuracy as shown in Figure 24. Therefore, the C_p function of B – Eu_2O_3 was calculated only using the results of Pankratz and Kelley [106]. For both C and B – Gd_2O_3, the present C_p functions are in an excellent agreement with the functions by Zinkevich [2].

5.4 Heat Capacity of Heavy RE_2O_3

5.4.1 The Heat Capacity of C –Tb_2O_3

Heat contents of C – Tb_2O_3 were investigated by Pankratz [101] at 400 – 1600K. Low temperature C_p data have not been measured. Therefore, the C_p function was determined only based on the results of Pankratz. The resultant C_p in this study is similar to that of Zinkevich [2] as shown in Figure 25.

5.4.2 The Heat Capacity of C – Dy_2O_3

High temperature heat content data for C – Dy_2O_3 were measured by Pankratz and Kelley [105] in the temperature range at 400 – 1800K. Tsagareishvili and Gvelesiani [113] also measured the heat contents in the temperature range between 400 and 1600K. The C_p derived from both studies are plotted in Figure 26. As can be seen both C_p are consistent with low temperature C_p by Justice and Westrum [91]. The scattering of the results by Pankratz and Kelley becomes significant above 1000K, which is originated from anomaly in heat content. This anomaly was not found by Tsagareishvili and Gvelesiani. Therefore, the C_p function was optimized using experimental C_p data below 1000K from both Pankratz and C_p data from Tsagareishvili and Gvelesiani. The C_p function in this study and Zinkevich [2] were in excellent agreement as seen in Figure 26.

5.4.3 The Heat Capacity of C – Ho_2O_3

Heat content data for Ho_2O_3 were measured by Pankratz and King [107], Tsagareishvili and Gvelesiani [112] in the temperature range from 400 to 1800K. The C_p values derived from both studies are consistent with the low temperature C_p data [93]. Therefore, available data above room temperature were all taken into account for the optimization of C_p function of C – Ho_2O_3, and the result is shown with all available experimental data in Figure 27.

5.4.4 The Heat Capacity of C – Er_2O_3

Heat contents of C – Er_2O_3 were measured by Pankratz and King [107] from 400K to 1800K. The C_p derived [107] is in consistent with low temperature C_p reported by Justice and Westrum [93]. The C_p data from Pankratz and King were used to obtain the C_p function. The experimental data and the C_p curve from this study are plotted in Figure 28.

5.4.5 The Heat Capacity of C – Tm_2O_3

High temperature heat content data of C – Tm_2O_3 were reported by Pankratz and King [107] from 400K to 1800K, Tsagareshvili and Gvelesiani [109] at 400 – 1600K. Similar to the results by Pankratz [105] for Dy_2O_3, a thermal anomaly was observed for Tm_2O_3 near 1680K. The similar explanation was given by Pankratz but we found not convincing. Therefore, data above 1600K were excluded from calculation for C_p function. It is observed in Figure 29 that C_p function by Zinkevich [2] showed excellent agreement with this study.

5.4.6 The Heat Capacity of C – Yb_2O_3

Heat content values for C – Yb_2O_3 were measured by Pankratz and King [107] in the temperature between 400 and 1800K, Tsagareishvili and Gvelesiani [109] at 400 – 1600K. Similar to Dy_2O_3 and Tm_2O_3, thermal anomaly was observed by Pankratz and King at 1365K with heat absorption of 628J/mol. As usual, the thermal anomaly was excluded from calculation of C_p function. The resultant C_p curve from this study and experimental data are plotted in Figure 30.

5.4.7 The Heat Capacity of C – Lu_2O_3

Heat capacities of the C – Lu_2O_3 above room temperature were derived from the heat content data by Pankratz and Kelley [105] in the temperature range between 400 and 1800K. As presented in Figure 31, the derived C_p data are consistent with the low temperature C_p reported by Justice et al., [94]. The C_p function from this study also strongly supported by Zinkevich [2] and can reproduce the experimental data by Pankratz and Kelley.

6. The Enthalpy and Entropy Changes of Phase Transitions

Rare earth sesquioxides have different polymorph stabilities under various temperature and pressure conditions. The T_{tr} of stable and metastable phase transformations at 1atm was introduced above (section 2.1 to 2.6). In this section, P_{tr} will be introduced as the other factor to induce phase transitions. Then, the enthalpy and entropy of phase transitions, ΔH_{tr}° and ΔS_{tr}° will be derived from available thermodynamic information.

The ΔH_{298}°, S_{298}° and C_p derived above can only construct Gibbs energy functions of the most stable phases which are stable at room temperature. The knowledge of ΔH_{tr}° and ΔS_{tr}° allow to extend to a completed thermodynamic database with 6 Gibbs energy functions for C, B, A, H, X and L phases of each RE_2O_3. In this study, when the C_p of given polymorph RE_2O_3 is unavailable, its C_p was assumed to be the same to that of the nearest stable polymorph of each RE_2O_3

Equation 2

$$\Delta G_{tr}^{\circ} = \Delta H_{tr}^{\circ} - T\Delta S_{tr}^{\circ}$$

Equation 3

$$\Delta H_{tr}^{\circ} = \left(\Delta H_{298,j}^{\circ} - \Delta H_{298,i}^{\circ}\right) + \int_{298}^{T} C_{p,tr}\, dT$$

Equation 4

$$\Delta S_{tr}^{\circ} = \left(\Delta S_{298,j}^{\circ} - \Delta S_{298,i}^{\circ}\right) + \int_{298}^{T} C_{p,tr}/T\, dT$$

where "i" and "j" are two adjacent polymorphs of RE_2O_3. At the phase transition temperature, T_{tr}, $\Delta G_{tr}^{\circ} = 0$.

Equation 5

$$\Delta H_{tr}^{\circ} = \Delta S_{tr}^{\circ} \times T_{tr}$$

If the T_{tr} is known, the ΔS_{tr}° can be calculated from ΔH_{tr}° or vice versa.

with the assumption of $\Delta C_{p,tr} = 0$,

Equation 6

$$\Delta H_{tr}^{\circ} = (\Delta H_{298,j}^{\circ} - \Delta H_{298,i}^{\circ})$$

Equation 7

$$\Delta S^{\circ}_{tr} = (\Delta S^{\circ}_{298,j} - \Delta S^{\circ}_{298,i})$$

For example, if the ΔH°_{298}, S°_{298} and C_p of stable C phase at room temperature are known, the Gibbs energy of B phase can be calculated from T_{tr}, and ΔH°_{tr} and ΔS°_{tr} with assumed C_p or experimental determined C_p of B phase. The Gibbs energy functions of other phases stable at high temperature or metastable (A, H, X, L) can be built up step by step using the same approach. In each step, as the accuracy of ΔH°_{tr} and ΔS°_{tr} between transition phases determines the accuracy of Gibbs energy of polymorphs of RE_2O_3, special attentions were given to find the most reliable ΔH°_{tr} and ΔS°_{tr} using systematic analysis of all RE_2O_3 simultaneously.

The ΔH°_{tr} and ΔS°_{tr} were usually not directly measured, so various approaches were applied depending on available data types. In general, in the present study the following approaches for C→B transition, Clausius – Clapeyron relationship were used. For B→A transition, DFT calculated data and limited heat content data were available. For A→H, H→X and X→L, the limiting slope rule and binary phase diagram was applied to determineΔH°_{tr}. The details of the methodologies for each phase transition are explained below.

6.1 Methodologies for Determining ΔH°_{tr} and ΔS°_{tr}

6.1.1 The C→B Transition

Many ΔH°_{298}, S°_{298} and C_p are available for both B and or C forms of Sm_2O_3, Gd_2O_3 and Eu_2O_3, as discussed above (section 3.3 and 4.3). Then, by using the relationship In Equation 5, the unknown values can be calculated.

The Clausieus – Clapeyron relationship allows to proceed by using pressure induced phase transition data to calculate ΔH°_{tr} and ΔS°_{tr} for other RE_2O_3 in light and heavy groups. Before applying this relationship, two assumptions must be set: (1) same C_p functions of every phase of RE_2O_3, and (2) molar volume is independent of temperature or pressure. As mentioned above,

when no C_p data available for a given phase, it is assumed that the C_p of a given polymorph is the same as C_p of nearest stable polymorph at room temperature. In fact, when C_p of C and B polymorphs of Sm_2O_3, Eu_2O_3, and Gd_2O_3, the difference in C_p depending on the crystal structure was not significant. So this assumption can be reasonable. Regarding the molar volume assumption, the thermal expansibility and compressibility data are very scarce, so this assumption can be still acceptable.

The Clausieus – Clapeyron relationship between the most stable phase and the subsequent higher phase can be expressed as:

Equation 8

$$\frac{dP}{dT} = \frac{\Delta S}{\Delta V} = \frac{\Delta S^{\circ}_{298,tr}}{\Delta V_{298,tr}}$$

Once $\Delta S^{\circ}_{298,tr}$ is calculated from the experimental phase transition T – P relations, the ΔH°_{tr} can be calculated from the known T_{tr} at 1atm.

The transition pressure data for applying Clausieus – Clapeyron relationship were not only measured using *in situ* experiments, but also calculated from DFT (Density Functional Theory). The available experimental and calculated data are summarized in Table 19.

6.1.2 The B→A Transition

The $\Delta H^{\circ}_{tr,B\rightarrow A}$ of the entire RE_2O_3, excluding Eu_2O_3 and Yb_2O_3, were obtained by Wu et al., [123] using DFT calculation. In their study, the energies of formation of both B and A were reported and the energy difference was assumed as the transition energy ΔH°_{tr}.

The continuous heat content data including the event of B→A transition for Gd_2O_3 were measured by Barkhatov et al., [20]. So ΔH°_{tr} of Gd_2O_3 can be obtained from their experiment and ΔS°_{tr} can be calculated from ΔH°_{tr} and T_{tr}. In addition, a few pressure induced phase transition data, including experimentally measured data and calculated data using *ab initio* method were reported

[124-129]. In this case, the Clausieus – Clapeyron relationship was applied to obtain $\Delta H^{\circ}_{tr,B\rightarrow A}$ and $\Delta S^{\circ}_{tr,B\rightarrow A}$.

6.1.3 The A→H, H→X and X→L Transitions

The thermodynamic enthalpy and entropy data for A→H, H→X and melting are very limited. Barkhatov et al., [20] measured heat content data of Gd_2O_3 and reported an unexpectedly large ΔH°_{tr} for A→H transition (34.73±3.35KJ/mol), which is not accepted in this study. Therefore, the so – called limiting slope rule, which connects ΔH°_{tr} (or ΔS°_{tr}) to liquidus of binary phase diagram is used to derive ΔH°_{tr} and ΔS°_{tr} in this study. In the binary system,

Equation 9

$$\frac{dT}{dX_i} = \frac{2RT_{tr}}{\Delta S^{\circ}_{tr}}$$

where $\frac{dT}{dX_i}$ is the slope of liquidus, and T_{tr} and ΔS°_{tr} are the transition temperature and entropy, respectively. In order to apply such rule, the solid which form liquidus is ideally a stoichiometric phase. Among available binary RE_2O_3 oxide systems, a series of $RE_2O_3 – Al_2O_3$ systems show a stoichiometric RE_2O_3 phase. Therefore, $RE_2O_3 – Al_2O_3$ systems were used for this analysis. Fortunately, assessment of the $RE_2O_3 – Al_2O_3$ phase diagram by Wu and Pelton [28] is available. In fact, when Wu and Pelton performed their optimization of the binary systems, they used the same limiting slope rule to evaluate the ΔH°_{tr} and ΔS°_{tr} of A→H, H→X and X→L transitions.

For example, the optimized phase diagram of the $Nd_2O_3 – Al_2O_3$ systems [28] is presented in Figure 32 along with experimental data [26]. As can be seen in "circle 1", the liquidus slope near melting temperature can give the ΔS°_{tr} of X – Nd_2O_3. The same analysis was performed for all binary $RE_2O_3 – Al_2O_3$ systems. The slope of liquidus of Nd_2O_3 at the A – H and H – X transitions (circled area 2 and 3 in Figure 32) shows negligible changes. This observation is a strong indication for the small entropy differences between A and H, and H and X. The similar observations were found for all the $RE_2O_3 – Al_2O_3$ binary systems [28]. This finding allowed to

apply the same value ΔS_{tr} =2.5J/mol.K on both A→H and H→X transitions of the entire RE_2O_3 family.

The entropies of fusion of entire RE_2O_3 family (except Sc_2O_3), regardless of solid polymorph for melting, their diverse last solid phases, were extracted from Wu and Pelton [28] , Roth [130] for the $RE_2O_3 - Al_2O_3$ phase diagrams using the limiting slope rule. The ΔS°_{fus} of Sc_2O_3 with magnitudes 100.42KJ/mol and 127KJ/mol were reported by shpil'rain et al., [21] and Leonidov et al., [40] respectively.

For Lu_2O_3, ΔS°_{fus} extracted from Wu and Pelton's [28] $Lu_2O_3 - Al_2O_3$ phase diagram also represent $\Delta S^{\circ}_{tr,C\to L}$. The complexity was significantly increased because more energy terms were involved, namely: (1) transition energies of C→B and B→A, (2) $\Delta S^{\circ}_{tr,A\to H}$, $\Delta S^{\circ}_{tr,H\to X}$, $T_{tr,C\to L}$ and (3) $\Delta H^{\circ}_{tr,H\to X}$ to calculated properties of A→H and X→L. During calculation, it was found either of the two unknowns $T_{tr,X\to L}$ or $T_{tr,A\to H}$ must be determined in order to obtain $\Delta H^{\circ}_{tr,X\to L}$ and $\Delta H^{\circ}_{tr,A\to H}$. In this study, $T_{tr,X\to L}$ was fixed first because of relatively fair consistency of adjacent sesquioxides in comparison with data of $T_{tr,A\to H}$ as shown in Figure 4 and Figure 6. The similar situation also occurred for Sc_2O_3 that $\Delta H^{\circ}_{tr,A\to H}$ and $\Delta H^{\circ}_{tr,H\to X}$ were calculated by taking average of the corresponding values of the rest of the RE_2O_3. Examples for detailed determination of discrete energy terms were illustrated in detail in section 6.2.3.

6.1.4 The Shock Induced C→A Phase Transition

Shock induced phase change C→A was observed for Sc_2O_3 and Sm_2O_3 [129, 131, 132]. In addition, the same type C→A transition was also reported for Gd_2O_3 and Y_2O_3 [131]. This transition is not stable transition, or reversible [131]. So these transition data were not taken into account in the present study.

6.2 The Optimized Results of ΔH_{tr} and ΔS_{tr}

6.2.1 The ΔH°_{tr} and ΔS°_{tr} of C→B Phase Transition

The ΔH_{tr}° and ΔS_{tr}° of C→B phase transition obtained in this study are plotted using in Figure 33 and Figure 34, and listed in Table 20. In general, ΔH_{tr}° and ΔS_{tr}° are decreasing and increasing linearly with ionic radii, respectively.

The experimental ΔH_{298}° [16, 47, 68, 71] and S_{298}° data [17, 91] for the three middle rare earth sesquioxides Sm_2O_3, Eu_2O_3 and Gd_2O_3 are available. Large uncertainties were found in the ΔH_{298}° for Eu_2O_3 [16, 71]. The ΔH_{tr}° value at 298K for Eu_2O_3 calculated from Lyutsareva's experimental entropies [17] did not locate along the general linear trend as shown in Figure 33 . The ΔH_{298}° values for Sm_2O_3 and Gd_2O_3 calculated using the estimated entropies by Lyutsareva et al., and experimental entropies by Justice and Westrum [91] aligned perfectly with the general linear trend as shown in Figure 33. The ΔH_{tr}° and ΔS_{tr}° for the three middle RE_2O_3 were selected accordingly with the best set of standard ΔH_{298}° and S_{298}° (section 3.3).

The data of pressure induced C→B phase transition obtained from various authors [19, 128, 133-136] using both experimental techniques and DFT method were estimated in this study to apply the Clausieus – Clapeyron relationship. Among all the pressure data, the results of Hoekstra [19] were the most widely accepted in literature because of the broad range of his work from Sm_2O_3 to Er_2O_3 at three different temperatures. As shown in Figure 33 and Figure 34, values calculated from Hoekstra were also supported by the values obtained from the experimental ΔH_{298}° and S_{298}° [16, 17, 47, 68, 71, 91], especially for Sm_2O_3 and Gd_2O_3. Therefore, the result of Hoekstra were generally accepted in this study.

According to experimental T_{tr} data (section 2.1), stable C→B transformation does not occur at 1 atm in the lanthanide oxide series before Pm_2O_3 (La_2O_3 – Nd_2O_3) and after Ho_2O_3 (Y_2O_3 – Lu_2O_3). The unavailability of the study by Hoekstra [19] was observed starting from Tm_2O_3 as seen in Figure 33 and Figure 34. For heavy RE_2O_3 after Tm_2O_3 and two rare earth like oxides Y_2O_3 and Sc_2O_3, a linear extrapolation based on the results calculated from the phase transition P – T relation by Hoekstra was used to obtain hypothetical ΔH_{tr}° and ΔS_{tr}° . For light RE_2O_3 before Pm_2O_3, the same linear relationship was used to estimate ΔH_{tr}° and ΔS_{tr}°. But found the B – Nd_2O_3 was more stable than A – Nd_2O_3 at room temperature. Therefore, the ΔH_{tr}° of Nd_2O_3 was slightly modified to 1.38KJ/mol, which was slightly lower than the original value calculated from the linear

trend established from the results of Hoekstra. Using the adjusted ΔH_{tr}° for Nd_2O_3 and carefully selected ΔH_{tr}° for Sm_2O_3 – Gd_2O_3, a separate linear trend was established to describe enthalpy of C→B phase change in the range La_2O_3 – Gd_2O_3. In this way, the stable A phase for light RE_2O_3 can be still calculated at room temperature. It should be noted that the estimated ΔH_{tr}° is negative for La_2O_3, Ce_2O_3 and Pr_2O_3. The discontinuity in the linear trend for ΔH_{tr}° was also found at Gd_2O_3 in the assessment of Zinkevich [2]. For optimized ΔS_{tr}° of RE_2O_3 the values varied from 5J/mol·K to 4 J/mol·K when RE_2O_3 is varied from La_2O_3 to Lu_2O_3.

Although the present optimized ΔH_{tr}° and ΔS_{tr}°.for C→B transition results are similar to those of Zinkevich [2], one of the fundamental difference is in the T_{tr}. Some of the C→B transition temperatures used by Zinkevich were very different from the experimental temperatures [7, 13-15, 18] especially for the middle RE_2O_3 as shown in Figure 10.Therefore, the present optimization is more accurate than the work by Zinkevich. In addition, the ΔH_{tr}°, ΔS_{tr}° and T_{tr} for La_2O_3 to Nd_2O_3 were not optimized by Zinkevich.

6.2.2 The ΔH_{tr}° and ΔS_{tr}° of B→A Phase Transition

The ΔH_{tr}° and ΔS_{tr}° of B→A phase transition data were plotted in Figure 35 and Figure 36, and listed in *Table 21*. Although not all RE_2O_3 have stable B→A transition, the ΔH_{tr}° data for the entire RE_2O_3 family, except Eu_2O_3 and Yb_2O_3, were calculated by Wu et al., [123] using DFT. The available ΔH_{tr}° and ΔS_{tr}° data show decreasing trends with increasing of ionic radii.

Prior to the study by Wu et al., [123], thermodynamic data of B→A transition were only available for Sm_2O_3, Eu_2O_3 and Gd_2O_3 from P – T transition experiments [124-129]. Similar to the previous C→B transition, Clausieus – Clapeyron relationship was employed to obtain ΔS_{tr}°, which were applied together with assessed $T_{tr,B\rightarrow A}$ (see Figure 3). The only calorimetric ΔH_{tr}° was obtained by Barkhatov et al., [20] for heat content data of Gd_2O_3. As shown in Figure 35, the ΔH_{tr}° from DFT calculations by Wu et al., [123] is reliable because the ΔH_{tr}° from their work show good agreement with not only the calorimetric ΔH_{tr}° [20] but also the ΔH_{tr}° derived from P – T transition data [124-129]. The ΔH_{tr}° for the two exceptions Eu_2O_3 and Yb_2O_3 can be estimated from the trend

of the available results from Wu et al. The estimated ΔH_{tr}° for Eu_2O_3 overlaps with the experimental data from Chen et al., [125] and Guo et al., [128] as shown in Figure 35. The DFT data of Wu et al. and the estimated data of Eu_2O_3 and Yb_2O_3 are accepted in this study for ΔH_{tr}° of B→A transition.

Regarding the entropy of transition, the data presented in Figure 36 can be divided into three parts. The first part is from Pm_2O_3 to Dy_2O_3, where stable B→A transition occurs and the assessed T_{tr} is available (see Figure 3). ΔS_{tr}° for these RE_2O_3 were calculated from ΔH_{tr}° and T_{tr}. The second part includes Ho_2O_3 – Lu_2O_3, Y_2O_3 and Sc_2O_3. ΔS_{tr}° of these RE_2O_3 were calculated from ΔH_{tr}° estimated T_{tr} of metastable B→A transition. The third part is light RE_2O_3. Wu et al. calculated negative ΔH_{tr}° values and T_{tr} is not properly estimated. If the general trend of ΔS_{tr}° for the first and second parts are followed, negative ΔS_{tr}° can be predicted for light RE_2O_3. However, negative ΔS_{tr}° seems to be less probable, because the entropy is highly dependent on the structure of RE_2O_3. So A phase higher entropy than B phase, regardless of RE_2O_3. If ΔS_{tr}° is two positive, A phase can be more stable than B phase at room temperature. Therefore, ΔS_{tr}° of light RE_2O_3 were all assigned to be 0.05J/mol·K in this study.

Large disagreement on ΔS_{tr}° was observed between results optimized in this study and Zinkevich [2]. The difference becomes large between Pm_2O_3 to La_2O_3. For Pm_2O_3, the reason of large difference between Zinkevich and the present study is due to T_{tr}. Zinevich used T_{tr} = 936K for Pm_2O_3, while the present study accepts the T_{tr} = 2013K from experimental study [12]. Therefore, the optimized ΔS_{tr}° of Pm_2O_3 in this study should be more reliable than that of Zinkevich. Most probably, the ΔS_{tr}° of B→A transition of La_2O_3 to Nd_2O_3 by Zinkevich would be over-estimated.

6.2.3 The ΔH_{tr}° and ΔS_{tr}° of A→H, H→X and X→L Transitions

As discussed in section 6.1.3, ΔS_{tr}° of A→H and H→X were set to be 2.5J/mol·K in this study. Then, from ΔS_{tr}° and T_{tr}, ΔH_{tr}° can be calculated as shown in Table 22. The fusion entropies $\Delta S_{tr,X\to L}^{\circ}$ for La_2O_3 – Dy_2O_3, $\Delta S_{tr,H\to L}^{\circ}$ for Ho_2O_3 – Yb_2O_3, $\Delta S_{tr,C\to L}^{\circ}$ for Lu_2O_3 extracted from Wu

and Pelton [123], and $\Delta S^{\circ}_{tr,H\rightarrow L}$ for Y_2O_3 extracted from Roth [130] and $\Delta S^{\circ}_{tr,C\rightarrow L}$ for Sc_2O_3 extracted from Shpil'rain et al., [21] were listed in Table 22. If all these ΔH°_{tr} and ΔS°_{tr} of A→H, H→X, and X→L are combined with ΔH°_{tr} and ΔS°_{tr} of C→B and B→A, and ΔH°_{298} and ΔS°_{298} of the most stable phase at room temperature, ΔH°_{298} and ΔS°_{298} of all phases can be determined as listed in *Table 23*. Although the standard transition sequence of RE_2O_3 is C→B→A→H→X→L. Four types of combined transitions were observed: B→H, C→H, H→L and C→L. The ΔH°_{tr} and ΔS°_{tr} of these combined transitions can be calculated suing the Hess's law using data from Table 23.

The calculated $\Delta H^{\circ}_{tr,A\rightarrow H}$, $\Delta H^{\circ}_{tr,B\rightarrow H}$ and $\Delta H^{\circ}_{tr,C\rightarrow H}$ are plotted in Figure 37 and compare with the results of Zinkevich [2] and limited experimental data from Barkhatov et al., [20] and Shpil'rain et al., [32]. The estimated $\Delta H^{\circ}_{tr,C\rightarrow H}$ for Y_2O_3 in this study shows excellent agreement with the experimental data reported by Shpil'rain et al., as seen in Figure 37. The $\Delta H^{\circ}_{tr,A\rightarrow H}$ reported by Zinkevich are significantly higher than the results from this study. The estimation by Zinkevich on $\Delta H^{\circ}_{tr,,A\rightarrow H}$ was entirely based on the study of Barkhatov et al., on Gd_2O_3, which is proved not reliable from the discussion of liquidus slope in 6.1.3.

Up till this stage, all the available information for constructing the thermodynamic database of the entire RE_2O_3 were completed. All the assessed and estimated standard enthalpies and entropies were shown in Table 23. The C_p functions were previously discussed in section. In total, 102 Gibbs energy functions for 17 RE_2O_3 with 6 different phases were produced. The thermodynamic database was then applied to produce binary $RE'_2O_3 - RE''_2O_3$ phase diagrams for validation purposes.

7. Main Differences between the Study of Zinkevich and This Work

As shown in each section, most of the results accepted in this study were compared with the results from Zinkevich [2]. Some of the main differences were observed in T_{tr} of C→B and

B→A, and ΔH_{tr}° and ΔS_{tr}° of B→A, A→H and meltings, which caused large differences of ΔH_{tr}° and ΔS_{tr}° in B→H C→H, and H→X transitions.

7.1 Transition Temperature

For the temperature of C→B transition as shown in *Table 1*, the results of this study, which were obtained from critical review of available experimental data (section 2.1), were much higher than the results from Zinkevich [2], which were extracted from optimized Y_2O_3 – RE_2O_3 (RE = Sm, Eu and Gd) phase diagrams. In his phase diagrams, the limited binary phase diagram data of C + B phase are not sufficient to support low T_{tr} of C→B. The magnitude of $T_{tr,\ C\rightarrow B}$ of Pm_2O_3 from the study of Zinkevich, which is almost half of the experimental value, is obtained entirely from linear extrapolation without any experimental proof.

For the temperature of B→A transition as shown in *Table 1*, the result of Zinkevich [2] for Pm_2O_3 936K is less than half in magnitude compare to experimental result 2013K accepted in this study. The low temperature from Zinkevich might due to the assumed parabolic trend of ΔS_{tr}° used for prediction of Pm_2O_3. The ΔS_{tr}° predicted by Zinkevich was probably used subsequently to calculate $T_{tr,\ B\rightarrow A}$.

Table 1 Main differences of transition temperatures between the study of Zinkevich [2] and this work

Sesquioxides	**T, K**	**T, K**
	Zinkevich	This work
	C→B	
Pm_2O_3	457	973
Sm_2O_3	676	1153
Eu_2O_3	894.5	1348
Gd_2O_3	1425	1561
	B→A	
Pm_2O_3	936	2013

7.2 The Enthalpy and Entropy of Transitions

The ΔH_{tr}° of $B \rightarrow A$ transition from Zinkevich [2] do not have unacceptably large differences with the values selected in this study from the DFT calculated results of Wu et al., [123] as seen in Table 2. It should be noted that B→A transition is metastable that the negative value of ΔH_{tr}° or the small empirical ΔS_{tr}°=0.05J/mol.K used in this study does not give influential effect on future thermodynamic calculations. The positive values of ΔS_{tr}° in the study of Zinkevich are the results of prediction using a parabolic trend as mentioned in previous section 7.1.

One of the main disagreement between this work and the study of Zinkevich [2] is the ΔH_{tr}° and ΔS_{tr}° of A→H transition as seen in Table 2. It is found that the ΔH_{tr}° value from Barkhatov used by Zinkevich gives exceptionally large ΔS_{tr}°, which causes A phase is overly stable. The assumed ΔS_{tr}°=2.5J/mol.K of this study is used because of our observation from well – established Al_2O_3 – RE_2O_3 phase diagrams mainly from the study of Wu and Pelton [28]. Subsequently, using the critically assessed T_{tr}, ΔH_{tr}° of A→H is calculated. Because of the questionable data used by Zinkevich for A→H transition, the results of the combined transitions B→H and C→H are less reasonable. For examples in Table 2, the same ΔS_{tr}°=13.99J/mol.K is used for both A→H and B→H transitions ; ΔS_{tr}° of A→H and B→H transitions is larger than C→H transition, which is supposed to include more polymorphic configurations C→B→A→H.

The experimental ΔH_{tr}° and ΔS_{tr}° of meltings (X→L, H→L, C→L) are unavailable except for Sc_2O_3 and Y_2O_3, therefore, all the values must be properly estimated. The methodologies used by Zinkevich [2] and this study are very different that results show large disagreements as seen in Table 2. In the study of Zinkevich, an empirical equation involving factors of volume change, Grüneisen parameter and heat capacity was used. In this study, the limiting slope rule was applied on optimized Al_2O_3 – RE_2O_3 phase diagrams, which have strongly supported experimental data near pure RE_2O_3 sides. Subsequently, the properties of $H \rightarrow X$ were calculated with known properties of meltings and properties of other discrete transitions. The disagreements in meltings also cause the differences in H→X transition between both studies.

Table 2 Main differences of the enthalpy and entropy of transitions between the study of Zinkevich [2] and this work

Sesquioxides	**ΔH_{tr}°, kJ/mol**	**ΔS_{tr}°, J/mol.K**

	Zinkevich	This work	Zinkevich	This work
		B→A		
$La_2O_3 – Nd_2O_3$ Pm_2O_3	-4.14 – 0.4 1.5	-4.85 – 0.55 0.83	2.22 – 1.68 1.60	0.05 0.41
		A→H		
$La_2O_3 – Gd_2O_3$	32.35 – 34.7	5.78 – 6.72	13.99	2.50
		B→H		
$Tb_2O_3 – Ho_2O_3$	34.13 – 34.73	11.95 – 14.51	13.99	4.90 – 5.78
		C→H		
Y_2O_3, $Er_2O_3 – Yb_2O_3$	25.10 – 25.61	26.39 – 32.23	9.65	10.15 – 12.15
		H→X		
$La_2O_3 – Dy_2O_3$	10.84 – 12.12	5.95 – 6.64	4.57	2.50
		X→L		
$La_2O_3 – Dy_2O_3$	71.70 – 109.28	51.75 – 70.08	26.63 – 41.66	20.05 – 26.21
		H→L		
Y_2O_3, $Ho_2O_3 – Yb_2O_3$	83.10 – 87.04	43.63 – 49.73	30.22 – 32.35	16.14 – 18.44
		C→L		
Lu_2O_3	80.57	67.89	29.16	24.70

8. Thermodynamic Modeling of Binary R'$_2O_3$ – R"$_2O_3$

In this study, the Gibbs energy of all stable and metastable C, B, A, H, X and L phases of 17 RE_2O_3 including Sc_2O_3 and Y_2O_3 were optimized. Based on these Gibbs energies, the binary R'$_2O_3$ – R"$_2O_3$ systems were optimized in this study. There is no thermodynamic properties data in the binary systems. The only available data are phase diagrams. So all the available phase diagrams were reproduced using the regular solution model. As these RE_2O_3 shows the systematic changes in physical – chemical properties, we believe that there would be a trend in the regular solution parameters in the binary RE_2O_3 systems. In the present study, liquid phase was assumed as an ideal solution. The regular solution model applied to solid solutions can be expressed as:

Equation 10

$$g_{soln} = X_{RE'_2O_3}\overset{\circ}{g}_{RE'_2O_3} + X_{RE"_2O_3}\overset{\circ}{g}_{RE"_2O_3} + 2RT\left(X_{RE'_2O_3} lnX_{RE'_2O_3} + X_{RE"_2O_3} lnX_{RE"_2O_3}\right) + \omega X_{RE'_2O_3} X_{RE"_2O_3}$$

where $g^{\circ}_{RE'_2O_3}$, and $g^{\circ}_{RE''_2O_3}$ are the Gibbs energy functions for pure RE_2O_3 component in either stable or metastable forms, $X_{RE'_2O_3}$ and $X_{RE''_2O_3}$ are mole fractions of RE_2O_3 component, ω is a regular solution parameter. In the entropy of mixing term, 2 moles of energy of mixing per one mole of solution was considered because of $(RE^{3+}, RE^{3+})_2O_3$ solution has two mole of sites for mixing per mole of formula. It should be noted that Zinkevich [2] did the similar optimization of the binary RE_2O_3 systems. But he used the "1" mole of entropy of mixing per mole of formula, which is less accurate.

The calculated binary phase diagrams were presented from Figure 38 to Figure 48. Adylov et al., [137] investigated the phase diagrams of Y_2O_3 – Nd_2O_3. Shevthenko et al., [138] measured the phase diagrams of Y_2O_3 – Sm_2O_3, and Gd_2O_3. The phase diagram of Y_2O_3 – Eu_2O_3 was measured by Andrievskaya and Lopato [139] in their study of ternary systems ZrO_2 – Y_2O_3 – Eu_2O_3. Y_2O_3 – Dy_2O_3 binary phase diagram was measured by Nigmanov and Shevthenko [140]. In their studies [137-140], phases above 2000K were measured using DTA technique. Samples with phases lower than 2000K were obtained by annealing and the compositions were characterized using X – ray analysis. A series of binary phase diagrams consist of La_2O_3 with other Re_2O_3 (RE = Nd, Sm, Gd, Dy, Ho, Er) were investigated by Coutures and Foex [10] using thermal analysis.

Some disagreements were observed between calculated phase diagrams and experimental data in the Y_2O_3 – Sm_2O_3, Y_2O_3 – Eu_2O_3 and Y_2O_3 – Nd_2O_3 systems. In the binary Y_2O_3 – Nd_2O_3 phase diagram as shown in Figure 38, the boundary of "C + B" two phase region overlapped with the two experimental data [137] marked with cross. The boundary of "B + A" two phase region did not match with experimental data points reported by Adylov et al., [137]. In the Y_2O_3 – Sm_2O_3 and Y_2O_3 – Eu_2O_3 binary systems as shown in Figure 39 and Figure 40, some mismatches were observed between calculated two phase boundaries and experimental data [138, 139]. It should be noted that regular solution model is an extremely simple model. More accurate Y_2O_3 related binary phase diagrams can be produced using a more sophisticated solution model.

On the contrary of the Y_2O_3 related binary phase diagrams, excellent matches between the calculated La_2O_3 related phase diagrams and experimental data [10] were observed from Figure

43 to Figure 48. Most of the experimental data from Coutures and Foex [10] described the phase boundaries of H and X phases, only a few data were available for A phase as shown in Figure 45 to Figure 47. Therefore, the reliability of the calculated phase boundaries for C and B phases was probably ambiguous. It is observed that the stability of A phase decreases in the binary system of the La_2O_3 – Nd_2O_3 to La_2O_3 – Er_2O_3, and B phase appears with strong stability in the La_2O_3 – Sm_2O_3 system. B phase is eventually replaced by C phase in the La_2O_3 – Er_2O_3 system.

The optimized regular solution parameters are listed in Table 3. All parameters are positive, which tells the repulsive interactions between RE' and RE". In general, with the closer the ionic radii between the two RE_2O_3 components, the smaller the parameters are needed for C, B and A phases. The parameters of H and X phases show opposite trend. For example, Dy_2O_3 is closer to Y_2O_3 compare to Nd_2O_3, the parameters used in C, B and A phases appears to be smaller in the Y_2O_3 – Dy_2O_3 interaction than the Y_2O_3 – Nd_2O_3 interaction. For H and X phases, the parameters of Y_2O_3 – Dy_2O_3 system are larger than those of Y_2O_3 – Nd_2O_3 system. This trend found may not be used to roughly predict the phase diagram of the binary R'$_2O_3$ – R"$_2O_3$ systems.

In comparison with the phase diagrams and solution parameters reported by Zinkevich [2], it is found that the accuracies of the phase diagrams are comparable, however the parameters used in this work are much smaller. The large differences are observed especially in A and H phases. The reason for this is unreliably large experimental ΔH_{tr} of A→H transition was accepted by Zinkevich (see Figure 37). Therefore, large parameters were necessary to bring down the stability of H phase in the binary RE_2O_3 systems.

9. Conclusion

All the available thermodynamic data and phase transition data of RE_2O_3 have been critically and systematically evaluated in this study to obtain the best set of 102 Gibbs energy functions of 17 RE_2O_3 including Sc_2O_3 and Y_2O_3. For all stable and metastable C, B, A. H, X and L phases, ΔH°_{298}, S°_{298}, C_p, and phase transition temperature are prepared.

- The temperature of each discrete and combined transitions were reviewed and the best set of values were selected based on rigorous assessment of all the available data in the

literature. The transition temperatures of metastable phase transformations were also predicted according to the thermodynamic enthalpy and entropy of transition data.

- For the standard enthalpies of formation, the experimental techniques and reaction schemes were critically reviewed and compared. The best set of data for ΔH_{298}° was obtained based on experimental accuracy and systematic changes along with atomic number of RE. From the systematic trend, ΔH_{298}° of Pm_2O_3 which has not been available in the literature was reasonably predicted.
- The standard entropies of RE_2O_3 were examined by recalculation using the available experimental low temperature heat capacity data. During the calculation process, the concepts of lattice and magnetic contributions were considered. The unavailable S_{298}° of Tb_2O_3 and Pm_2O_3 were estimated properly either using the properties of adjacent RE oxides or the predicted lattice and magnetic C_p.
- The C_p data above room temperature were carefully assessed. C_p functions were produced by fitting the selected experimental data into the general C_p function form and plotted up to 3000 K. For the middle RE_2O_3, two C_p functions were produced because of their dual stabilities of C and B phases at room temperature. The C_p functions of B phase of the middle RE_2O_3 were adopted for higher temperature phases A, H, X and L because unavailability of the data. However, for the rest of RE_2O_3, C_p function was available for the phase stable at room temperature (C in heavy RE_2O_3 and A for light RE_2O_3). This function was adopted for all other stable and metastable phases (C, B, A, H, X, L).
- For C→B transition, the ΔH_{tr}° and ΔS_{tr}° were obtained from various data sources, including: assessed standard energies of the middle RE_2O_3, pressure – temperature phase transition data, and *ab initio* calculations. All the results obtained using various methodologies were discussed that a linear trend was established between ΔH_{tr} and ionic radii (and also ΔS_{tr} vs. ionic radii) to estimate the ΔH_{tr}° and ΔS_{tr}° for the C→B transition of the entire RE_2O_3.
- For B→A transition, the ΔH_{tr} data from *ab initio* calculations were mostly employed in this study because of its great reliability and consistency. The ΔS_{tr}° values were mostly determined by considering the assessed T_{tr}. However, the ΔS_{tr}° for the light RE_2O_3 were slightly modified to ensure stability of A phase at room temperature.
- For A→H and H→X transitions, a very small ΔS_{tr}° was estimated in this work because of the observations of small RE_2O_3 liquidus slope changes in the RE_2O_3 – Al_2O_3 phase

diagrams where such transition occurs in literature. For X-LΔS°_{fus} were calculated from $RE_2O_3 - Al_2O_3$ phase diagrams by applying the limiting slope rule. The ΔH_{tr} values were mostly determined by considering the assessed T_{tr}, while some ΔH_{tr} were determined by considering temperature and energies of combined transitions B→H, C→H, H→L and C→L.

The optimized Gibbs energy functions were tested for the thermodynamic modeling of the binary $RE'_2O_3 - RE''_2O_3$ systems. In the modeling, a simple regular solution model was applied for all solid solutions and liquid was assumed as ideal solution. It was found that much smaller regular solution parameters were required to reproduce the available phase diagram data compared to the previous thermodynamic assessment.

The Gibbs energy database of RE_2O_3 constructed in this work can be readily used for the building of new thermodynamic database for binary, ternary and multicomponent systems containing RE_2O_3.

10. Appendix

Table 3 The optimized regular solution parameters for selected $R'_2O_3 – R''_2O_3$ systems

R'	R"	C	B	A	H	X	L
Y	Nd	836	1881	2090	2508	2090	0
Y	Sm	418	0	0	2759	2090	0
Y	Eu	836	627	0	5016	4096	0
Y	Gd	418	0	0	9196	7942	0
Y	Dy	0	209	0	6437	4932	0
La	Nd	0	0	2842	8485	6688	0
La	Sm	0	2090	3177	1254	836	0
La	Gd	3762	3762	5852	230	418	0
La	Dy	8360	9823	10241	0	0	0
La	Ho	12540	8778	7733	0	0	0
La	Er	12540	15884	9948	0	0	0

Table 4 Summary of C→B phase transition temperatures: ASS: assessment; DT: decrease temperature; DTA: differential thermal analysis; EST: estimation; IT: increase temperature; QM: quenching method; TA: thermal analysis; XRD: X – ray diffraction; UNK: unknown method.

Sesquioxides	Ionic radii, Å	T_{trans}, K	Techniques	References	
Y_2O_3	0.892	2756[a]	EST	This work	
Sc_2O_3	0.73	5099[a]	EST	This work	
La_2O_3	1.061	-786[a]	EST	This work	
Ce_2O_3	1.034	-369[a]	EST	This work	
Pr_2O_3	1.013	-21[a]	EST	This work	
Nd_2O_3	0.995	285[a]	EST	This work	
Pm_2O_3	0.982	973	QM, XRD	Chikalla, 1972	[12]
		457	EST, ASS	Zinkevich, 2007	[2]
		973	ASS	This work	
Sm_2O_3	0.964	1173 – 1273	QM, XRD	Roth, 1960	[13]
		1153	QM, XRD	Warshaw, 1961	[7]
		676	EST, ASS	Zinkevich, 2007	[2]
		1153	ASS	This work	
Eu_2O_3	0.950	1323	QM, XRD	Curtis, 1959	[15]
		1348	QM, XRD	Roth, 1960	[13]
		1373	QM, XRD	Warshaw, 1961	[7]
		894.5	EST, ASS	Zinkevich, 2007	[2]
		1348	ASS	This work	
Gd_2O_3	0.938	1523	QM, XRD	Roth, 1960	[13]
		1508	QM, XRD	Warshaw, 1961	[7]
		1561	UNK	Kolitsch, 1995	[18]

		1425	EST, ASS	Zinkevich, 2007	[2]
		1561	ASS	This work	
Tb_2O_3	0.923	2113	QM, XRD	Warshaw, 1961	[7]
		1829	XRD, IT	Foex, 1966	[3]
		1679	XRD, DT	Foex, 1966	[3]
		1823	EST, ASS	Zinkevich, 2007	[2]
		1823	ASS	This work	
Dy_2O_3	0.908	2223	TA	Foex, 1966	[3]
		2223	DTA	Tresvyatkii, 1971	[9]
		2140	TA	Coutures, 1974	[10]
		2253	DTA	Shevthenko, 1985	[11]
		2263	EST, ASS	Zinkevich, 2007	[2]
		2238	ASS	This work	
Ho_2O_3	0.894	2456	TA	Foex, 1966	[3]
		2463	DTA	Tresvyatkii, 1971	[9]
		2459	TA	Coutures, 1974	[10]
		2463	DTA	Shevthenko, 1985	[11]
		2458	EST, ASS	Zinkevich, 2007	[2]
		2460	ASS	This work	
Er_2O_3	0.881	2593	DTA	Tresvyatkii, 1971	[9]
		2593	EST, ASS	Zinkevich, 2007	[2]
		2600	ASS	This work	
Tm_2O_3	0.869	2913[a]	EST	This work	
Yb_2O_3	0.858	3195[a]	EST	This work	
Lu_2O_3	0.848	3315[a]	EST	This work	

[a]: estimated value from this work

Table 5 Summary of B→A phase transition temperatures: ASS: assessment; DTA: differential thermal analysis; ECM: electric conductivity measurements; EST: estimation; TA: thermal analysis

Sesquioxides	**Ionic radii, Å**	**T_{trans}, K**	**Techniques**	**References**	
Y_2O_3	0.892	2645	EST	This work	
Sc_2O_3	0.73	3265	EST	This work	
La_2O_3	1.061	<0[b]	EST	This work	
Ce_2O_3	1.034	<0[b]	EST	This work	
Pr_2O_3	1.013	<0[b]	EST	This work	
Nd_2O_3	0.995	<0[b]	EST	This work	
Pm_2O_3	0.982	2013	DTA	Chikalla, 1972	[12]
		1873	Ignition	Weigel, 1965	[8]
		936	EST, ASS	Zinkevich, 2007	[2]
		2013	ASS	This work	
Sm_2O_3	0.964	2173	TA	Foex, 1966	
		2193	DTA	Tresvyatkii, 1971	[9]
		2098	TA	Coutures, 1974	[10]
		2143	DTA	Shevthenko, 1985	[11]
		2173	EST, ASS	Zinkevich, 2007	[2]

		2170	ASS	This work	
Eu_2O_3	0.950	2323	TA	Foex, 1966	[3]
		2323	EST, ASS	Zinkevich, 2007	[2]
		2323	ASS	This work	
Gd_2O_3	0.938	2403	TA	Foex, 1966	[3]
		2443[a]	DTA	Tresvyatkii, 1971	[9]
		2383	TA	Coutures, 1976	[10]
		2436±10	ECM	Barkhatov, 1981	[20]
		2443[a]	DTA	Shevthenko, 1985	[11]
		2443	EST, ASS	Zinkevich, 2007	[2]
		2383	ASS	This work	
Tb_2O_3	0.923	2448[a]	DTA	Tresvyatkii, 1971	[9]
		2433[a]	DTA	Shevthenko, 1985	[11]
		2441	ASS	This work	
Dy_2O_3	0.908	2463[a]	DTA	Tresvyatkii, 1971	[9]
		2463[a]	DTA	Shevthenko, 1985	[11]
		2483	ASS	This work	
Ho_2O_3	0.894	2570[b]	EST	This work	
Er_2O_3	0.881	2622[b]	EST	This work	
Tm_2O_3	0.869	2668[b]	EST	This work	
Yb_2O_3	0.858	2712[b]	EST	This work	
Lu_2O_3	0.848	2752[b]	EST	This work	

[a]: mixed transition; [b]: estimated value from this work

Table 6 Summary of A→H phase transition temperatures: ASS: assessment; ECM: electric conductivity measurement; DTA: differential thermal analysis; EST: estimation; TA: thermal analysis

Sesquioxides	**Ionic radii, Å**	**T_{trans}, K**	**Techniques**	**References**	
Y_2O_3	0.892	2905	EST	This work	
Sc_2O_3	0.73	2332	EST	This work	
La_2O_3	1.061	2313	TA	Foex, 1966	[3]
		2313	DTA	Tresvyatkii, 1971	[9]
		2312	TA	Coutures, 1974	[10]
		2303	DTA	Shevthenko, 1985	[11]
		2313	ASS	Zinkevich, 2007	[2]
		2313	ASS	This work	
Ce_2O_3	1.034	2383	DTA	Tresvyatkii, 1971	[9]
		2393	DTA	Shevthenko, 1985	[11]
		2338	ASS	Zinkevich, 2007	[2]
		2388	ASS	This work	
Pr_2O_3	1.013	2318	DTA	Tresvyatkii, 1971	[9]
		2303	DTA	Shevthenko, 1985	[11]
		2353	ASS	Zinkevich, 2007	[2]

		2313	ASS	This work	
Nd_2O_3	0.995	2335	TA	Foex, 1966	[3]
		2373	DTA	Tresvyatkii, 1971	[9]
		2379	TA	Coutures, 1974	[10]
		2333	DTA	Shevthenko, 1985	[11]
		2373	ASS	Zinkevich, 2007	[2]
		2376	ASS	This work	
Pm_2O_3	0.982	2408	DTA	Chikalla, 1972	[12]
		2390	ASS	Zinkevich, 2007	[2]
		2408	ASS	This work	
Sm_2O_3	0.964	2388	TA	Foex, 1966	[1]
		2403	DTA	Tresvyatkii, 1971	[9]
		2369	TA	Coutures, 1974	[10]
		2343	DTA	Shevthenko, 1985	[11]
		2403	ASS	Zinkevich, 2007	[2]
		2369	ASS	This work	
Eu_2O_3	0.95	2413	TA	Foex, 1966	[3]
		2413	ASS	Zinkevich, 2007	[2]
		2413	ASS	This work	
Gd_2O_3	0.938	2425	TA	Foex, 1966	[3]
		2458[a]	DTA	Tresvyatkii, 1971	[9]
		2405	TA	Coutures, 1974	[10]
		2481	ECM	Barkhatov, 1981	[20]
		2473[a]	DTA	Shevthenko, 1985	[11]
		2481	ASS	Zinkevich, 2007	[2]
		2447	ASS	This work	
Tb_2O_3	0.923	2448[a]	DTA	Tresvyatkii, 1971	[9]
		2435[b]	EST	This work	
		2473[a]	DTA	Shevthenko, 1985	[11]
Dy_2O_3	0.908	2463[a]	DTA	Shevthenko, 1985	[11]
		2466[b]	EST	This work	
Ho_2O_3	0.894	2468[a]	DTA	Tresvyatkii, 1971	[9]
		2411[b]	EST	This work	
Er_2O_3	0.881	2540[b]	EST	This work	
Tm_2O_3	0.869	2083[b]	EST	This work	
Yb_2O_3	0.858	1788[b]	EST	This work	
Lu_2O_3	0.848	2292[b]	EST	This work	

[a]: mixed transition; [b]: estimated value from this work

Table 7 Summary of H→X phase transition temperatures: ASS: assessment; DTA: differential thermal analysis; EST: estimation; TA: thermal analysis

Sesquioxides	Ionic radii, Å	T_{trans}, K	Techniques	References	
Y_2O_3	0.892	2704[b]	EST	This work	
Sc_2O_3	0.73	2750[b]	EST	This work	
La_2O_3	1.061	2389	TA	Foex, 1966	[3]
		2413	DTA	Tresvyatkii, 1971	[9]
		2371	TA	Coutures, 1976	[10]
		2373	DTA	Shevthenko, 1985	[11]
		2373	ASS	Zinkevich, 2007	[2]
		2378	ASS	This work	
Ce_2O_3	1.034	2443	DTA	Tresvyatkii, 1971	[9]
		2443	DTA	Shevthenko, 1985	[11]
		2413	ASS	Zinkevich, 2007	[2]
		2443	ASS	This work	
Pr_2O_3	1.013	2426	TA	Foex, 1966	[3]
		2393	DTA	Tresvyatkii, 1971	[9]
		2403	DTA	Shevthenko, 1985	[11]
		2443	ASS	Zinkevich, 2007	[2]
		2407	ASS	This work	
Nd_2O_3	0.995	2448	TA	Foex, 1966	[3]
		2473	DTA	Tresvyatkii, 1971	[9]
		2483	TA	Coutures, 1976	[10]
		2453	DTA	Shevthenko, 1985	[11]
		2473	ASS	Zinkevich, 2007	[2]
		2478	ASS	This work	
Pm_2O_3	0.982	2498	DTA	Chikalla, 1972	[12]
		2498	ASS	Zinkevich, 2007	[2]
		2498	ASS	This work	
Sm_2O_3	0.964	2537	TA	Foex, 1966	[3]
		2553	DTA	Tresvyatkii, 1971	[9]
		2520	TA	Coutures, 1976	[10]
		2498	DTA	Shevthenko, 1985	[11]
		2523	ASS	Zinkevich, 2007	[2]
		2526	ASS	This work	
Eu_2O_3	0.95	2543	TA	Foex, 1966	[3]
		2543	ASS	Zinkevich, 2007	[2]
		2543	ASS	This work	
Gd_2O_3	0.938	2622	TA	Foex, 1966	[3]
		2613	DTA	Tresvyatkii, 1971	[9]

		2641	TA	Coutures, 1976	[10]
		2643	DTA	Shevthenko, 1985	[11]
		2633	ASS	Zinkevich, 2007	[2]
		2642	ASS	This work	
Tb_2O_3	0.923	2613 – 2643[a]	DTA	Tresvyatkii, 1971	[9]
		2643	DTA	Shevthenko, 1985	[11]
		2643	ASS	Zinkevich, 2007	[2]
		2643	ASS	This work	
Dy_2O_3	0.908	2633[a]	DTA	Tresvyatkii, 1971	[9]
		2650	TA	Coutures, 1976	[10]
		2658	DTA	Shevthenko, 1985	[11]
		2653	ASS	Zinkevich, 2007	[2]
		2654	ASS	This work	
Ho_2O_3	0.894	2700[b]	EST	This work	
Er_2O_3	0.881	2706[b]	EST	This work	
Tm_2O_3	0.869	2729[b]	EST	This work	
Yb_2O_3	0.858	2751[b]	EST	This work	
Lu_2O_3	0.848	2770[b]	EST	This work	

[a]: mixed transition; [b]: estimated value from this work

Table 8 Summary of X→L phase transition temperatures: ASS: assessment; DTA: differential thermal analysis; EST: estimation; TA: thermal analysis; TC:

Sesquioxides	**Ionic radii, Å**	**T_{trans}, K**	**Techniques**	**References**	
Y_2O_3	0.892	2702[b]	EST	This work	
Sc_2O_3	0.73	2247[b]	EST	This work	
La_2O_3	1.061	2578	TA	Foex. 1966	[3]
		2583	DTA	Tresvyatkii, 1971	[9]
		2583	TA	Mizuno, 1974	[23]
		2579	TA	Coutures, 1976	[10]
		2583	DTA	Shevthenko, 1985	[11]
		2578	ASS	Zinkevich, 2007	[2]
		2581	ASS	This work	
Ce_2O_3	1.034	2513	DTA	Tresvyatkii, 1971	[9]
		2513	DTA	Shevthenko, 1985	[11]
		2503	ASS	Zinkevich, 2007	[2]
		2513	ASS	This work	
Pr_2O_3	1.013	2569	TA	Foex, 1966	[3]
		2533	DTA	Tresvyatkii, 1971	[9]
		2563	TA	Mizuno, 1977	[27]
		2553	DTA	Shevthenko, 1985	[11]
		2573	ASS	Zinkevich, 2007	[2]
		2555	ASS	This work	

Nd_2O_3	0.995	2545±20	Melting	Lambertson, 1952	[22]
		2572	TA	Foex, 1966	[3]
		2593	DTA	Tresvyatkii, 1971	[9]
		2605	TA	Coutures, 1976	[10]
		2576	TA	Mizuno,1977	[26]
		2573	DTA	Shevthenko, 1985	[11]
		2593	ASS	Zinkevich, 2007	[2]
		2574	ASS	This work	
Pm_2O_3	0.982	2593	DTA	Chikalla, 1972	[12]
		2593	ASS	Zinkevich, 2007	[2]
		2593	ASS	This work	
Sm_2O_3	0.964	2603	TA	Foex, 1966	[3]
		2613	DTA	Tresvyatkii, 1971	[9]
		2591	TA	Coutures, 1976	[10]
		2597	TA	Mizuno, 1977	[24]
		2583	DTA	Shevthenko, 1985	[11]
		2608	ASS	Zinkevich, 2007	[2]
		2597	ASS	This work	
Eu_2O_3	0.95	2598	TA	Foex, 1966	[3]
		2633	TA	Mizuno, 1977	[25]
		2623	ASS	Zinkevich, 2007	[2]
		2616	ASS	This work	
Gd_2O_3	0.938	2665	TA	Foex, 1966	[3]
		2718	DTA	Tresvyatkii, 1971	[9]
		2670	TA	Coutures, 1974	[10]
		2683	TA	Mizuno, 1977	[25]
		2683	DTA	Shevthenko, 1985	[11]
		2693	ASS	Zinkevich, 2007	[2]
		2683	ASS	This work	
Tb_2O_3	0.923	2673	TA	Foex, 1966	[3]
		2673[a]	DTA	Tresvyatkii, 1971	[9]
		2673	DTA	Shevthenko, 1985	[11]
		2683	ASS	Zinkevich, 2007	[2]
		2673	ASS	This work	
Dy_2O_3	0.908	2675	TA	Foex, 1966	[3]
		2633[a]	DTA	Tresvyatkii, 1971	[9]
		2673	TA	Coutures, 1974	[10]
		2643	TA	Mizuno, 1977	[29]
		2673	DTA	Shevthenko, 1985	[11]
		2681	ASS	Zinkevich, 2007	[2]
		2674	ASS	This work	
Ho_2O_3	0.894	2684[b]	EST	This work	
Er_2O_3	0.881	2685[b]	EST	This work	
Tm_2O_3	0.869	2691[b]	EST	This work	
Yb_2O_3	0.858	2709[b]	EST	This work	
Lu_2O_3	0.848	2727[b]	EST	This work	

[a]: mixed transition; [b]: estimated value from this work

Table 9 Summary of C→H phase transition temperatures: ASS: assessment; DC: drop calorimetry; DTA: differential thermal analysis; ECM: electric conductivity measurements; EST: estimation; TA: thermal analysis

Sesquioxides	Ionic radii, Å	T_{trans}, K	Techniques	References	
Y_2O_3	0.892	2623	DTA	Tresvyatkii, 1971	[9]
		2600±30	DC&ECM	Shpil'rain, 1979	[21]
		2663	DTA	Shevthenko, 1985	[11]
		2660±5	EST	Grobner, 1995	[30]
		2581±15	DTA	Navrotsky, 2005	[31]
		2600	ASS	Zinkevich, 2007	[2]
		2600	ASS	This work	
Er_2O_3	0.881	2593	DTA	Shevthenko, 1985	[11]
		2566	TA	Foex, 1966	[3]
		2592	TA&DTA	Maister, 1984	[33]
		2518	TA	Coutures, 1974	[10]
		2593	ASS	Zinkevich, 2007	[2]
		2593	ASS	This work	
Tm_2O_3	0.869	2623	DTA	Shevthenko, 1985	[11]
		2583	TA	Foex, 1966	[3]
		2630	TA	Coutures, 1976	[10]
		2623	ASS	Zinkevich, 2007	[2]
		2623	ASS	This work	
Yb_2O_3	0.858	2653[a]	DTA	Tresvyatkii, 1971	[9]
		2692	TA	Foex, 1966	[3]
		2653	DTA	Shevthenko, 1985	[11]
		2653	ASS	Zinkevich, 2007	[2]
		2653	ASS	This work	

[a]: mixed transition.

Table 10 Summary of B→H phase transition temperatures: ASS: assessment; DTA: differential thermal analysis; TA: thermal analysis

Sesquioxides	Ionic radii, Å	T_{trans}, K	Techniques	References	
Gd_2O_3	0.938	2468[a]	DTA	Tresvyatkii, 1971	[9]
		2443[a]	DTA	Shevthenko, 1985	[11]
Tb_2O_3	0.923	2446[a]	DTA	Tresvyatkii, 1971	[9]
		2438	TA	Foex, 1966	[3]
		2443 [a]	DTA	Shevthenko, 1985	[11]
		2440	ASS	Zinkevich, 2007	[2]
		2438	ASS	This work	
Dy_2O_3	0.908	2463[a]	DTA	Tresvyatkii, 1971	[9]
		2476	TA	Foex, 1966	[3]
		2477	TA	Coutures, 1976	[10]

		2473[a]	DTA	Shevthenko, 1985	[11]
		2463	ASS	Zinkevich, 2007	[2]
		2468	ASS	This work	
Ho_2O_3	0.894	2511	TA	Foex, 1966	[3]
		2468[a]	DTA	Tresvyatkii, 1971	[9]
		2509	TA	Coutures, 1976	[10]
		2473	DTA	Shevthenko, 1985	[11]
		2483	ASS	Zinkevich, 2007	[2]
		2510	ASS	This work	
Er_2O_3	0.881	2593[a]	DTA	Tresvyatkii, 1971	[9]

[a]: mixed transition.

Table 11 Summary of H→L phase transition temperatures: ASS: assessment; DC: drop calorimetry; DTA: differential thermal analysis; ECM: electric conductivity measurements; TA: thermal analysis

Sesquioxides	**Ionic radii, Å**	**T_{trans}, K**	**Techniques**	**References**	
Y_2O_3	0.892	2683	DTA	Tresvyatkii, 1971	[9]
		2703±15	DC&ECM	Shpil'rain, 1979	[21]
		2713	DTA	Shevthenko, 1985	[11]
		2705±5	EST	Grobner, 1995	[30]
		2655±15	DTA	Navrotsky, 2005	[31]
		2712	ASS	Zinkevich, 2007	[2]
		2703	ASS	This work	
Ho_2O_3	0.894	2677	TA	Foex, 1966	[3]
		2643	DTA	Tresvyatkii, 1971	[9]
		2710	TA	Coutures, 1976	[10]
		2713	DTA	Shevthenko, 1985	[11]
		2688	ASS	Zinkevich, 2007	[2]
		2686	ASS	This work	
Er_2O_3	0.881	2686	TA	Foex, 1966	[3]
		2663	DTA	Tresvyatkii, 1971	[9]
		2685	TA	Coutures, 1976	[10]
		2693	DTA	Shevthenko, 1985	[11]
		2691	ASS	Zinkevich, 2007	[2]
		2688	ASS	This work	
Tm_2O_3	0.869	2708	TA	Foex, 1966	[3]
		2683	DTA	Shevthenko, 1985	[11]
		2698	ASS	Zinkevich, 2007	[2]
		2696	ASS	This work	
Yb_2O_3	0.858	2706	TA	Foex. 1966	[3]
		2673	DTA	Tresvyatkii, 1971	[9]
		2723	DTA	Shevthenko, 1985	[11]
		2708	ASS	Zinkevich, 2007	[2]
		2715	ASS	This work	

Table 12 Summary of ΔH°_{298} of Y_2O_3 and Sc_2O_3, ASS: assessed; EST: estimation; CC: combustion calorimetry; SC: solution calorimetry

Sesquioxides	ΔH°_{298}, KJ/mol	Uncertainties, KJ/mol	Technique	Reference	
Sc_2O_3	-1871.42	0.98	CC	Mah, 1962	[37]
	-1908.86	2.30	CC	Huber, 1962	[38]
	-1904.47	2.09	CC	Huber, 1963	[39]
	-1917.53	2.93	SC		
	-1908.6	2.0	ASS	Leonidov, 1997	[40]
	-1904.47			This work	
Y_2O_3	-1905.60	2.26	CC	Huber, 1957	[41]
	-1919.4	2.8	CC	Lavut, 1990	[42]
	-1930		EST	Wang, 1988	[43]
	-1932.8[a]	5.2	SC	Morss, 1993	[44]
	-1932.8			This work	

[a] The ΔH°_{298} was calculated using the reported enthalpy of Y_2O_3 solution and Wang's [43] Y metal dissolution enthalpy

Table 13 Summary of ΔH°_{298} of the light rare earth sesquioxides La_2O_3 – Nd_2O_3, and estimated ΔH°_{298} of Pm_2O_3 ASS: assessed; CC: combustion calorimetry; EST: estimation; SC: solution calorimetry; TTD: transposed temperature drop calorimetry

Sesquioxides	ΔH°_{298}, KJ/mol	Uncertainties, KJ/mol	Technique	Reference	
La_2O_3	-1793.10	0.80	CC	Huber, 1953	[45]
	-1794.50	2.68	SC	Fitzgibbon, 1965	[46]
	-1792.50[a]	2.89	SC		
	-1797.86	5.44	SC	Gvelesiani, 1967	[47]
	-1791.09 [a]	5.56	SC		
	-1791.6	2.0	ASS	Cordfunke, 2001	[34]
	-1791.78			This study	
Ce_2O_3	-1819.80	4.14	CC	Kuznetsov, 1960	[49]
	-1786.61	2.93	CC	Mah, 1961	[50]
	-1796.23	2.84	CC	Baker, 1968	[51]
	-1813.10	0.80	SC	Huntelaar, 2000	[53]
	-1805.80	5.80	TTD	Putnum, 2000	[54]
	-1813.0	2.0	ASS	Cordfunke, 2001	[34]
	-1809.85			This study	
Pr_2O_3	-1823.40	6.69	SC	Stubblefield, 1956	[56]
	-1809.66	3.01	SC	Fitzgibbon, 1973	[57]
	-1809.9	3.0	ASS	Cordfunke, 2001	[34]
	-1809.66			This study	
Nd_2O_3	-1808.10	1.00	CC	Huber, 1952	[60]
	-1798.07		CC	Spedding, 1959	[61]
	-1807.90[b]	0.92	SC	Fitzgibbon, 1968	[62]

	-1805.38 [a]	3.00			
	-1782.80	1.26	SC	Yashvili, 1971	[63]
	-1831.70 [a]	7.00	SC	Morss, 1989	[64]
	-1796.80	1.90	SC	Monaenkova, 1996	[65]
	-1806.9	3.0	ASS	Cordfunke, 2001	[34]
	-1808.81			This study	
Pm_2O_3	-1811	21	EST	Cordfunke, 2001	[34]
	-1824.22			This study	

[a] The ΔH_{298}° was calculated using the reported enthalpy of Nd_2O_3 solution and Merli's [48] Nd metal dissolution enthalpy.
[b] The ΔH_{298}° was calculated using the reported enthalpy of Nd_2O_3 solution and Stuve's [66] Nd metal dissolution enthalpy.

Table 14 Summary of ΔH_{298}° of the middle rare earth sesquioxides Sm_2O_3 – Gd_2O_3, ASS: assessed; CC: combustion calorimetry; SC: solution calorimetry

Sesquioxides	**ΔH_{298}°, KJ/mol**	**Uncertainties, KJ/mol**	**Technique**	**Reference**	
Sm_2O_3 (B)	-1815.40	2.01	CC	Huber, 1955	[69]
	-1777.3		CC	Spedding, 1959	[61]
	-1832.17	7.95	SC	Gvelesiani, 1967	[47]
	-1824.18	2.64	CC	Baker, 1972	[68]
	-1823.64	1.90	SC		
	-1824.67[a]	7.99	SC	Hennig, 1997	[70]
	-1823.0	4.0	ASS	Cordfunke, 2001	[34]
	-1822.60			This study	
Sm_2O_3 (C)	-1826.32	7.10	SC	Gvelesiani, 1967	[47]
	-1827.41	3.05	SC	Baker, 1972	[68]
	-1826.8	4.8	ASS	Cordfunke, 2001	[34]
	-1827.19			This study	
Eu_2O_3 (B)	-1648.08	3.77	CC	Huber, 1964	[71]
	-1725.48	5.10	SC	Yashvili, 1971	[63]
	-1651.42	3.35	SC&CC	Fitzgibbon, 1972	[16]
	-1624.58[b]	9.37	SC		
	-1686.22[c]	5.27	SC	Hennig, 1998	[72]
	-1730.48[d]	6.11	SC		
	-1650.4	4.0	ASS	Cordfunke, 2001	[34]
	-1653.45			This study	
Eu_2O_3(C)	-1630.09	4.60	SC	Huber, 1964	[71]
	-1619.08	5.02	SC	Stuve, 1965	[73]
	-1661.10	3.76	SC	Fitzgibbon, 1972	[16]
	-1622.91[b]	8.08	SC		
	-1662.5	6.0	ASS	Cordfunke, 2001	[34]
	-1657.95			This study	

Gd_2O_3 (B)	-1815.60	3.60	CC	Huber, 1955	[75]
	-1782.2		CC	Spedding, 1959	[61]
	-1824.22	1.80	SC	Yashvili, 1971	[63]
	-1819.7	3.6	ASS	Cordfunke, 2001	[34]
	-1825.19			This study	
Gd_2O_3 (C)	-1830.93			This study	

[a]**:** The ΔH_{298}° was calculated using the reported enthalpy of Sm_2O_3 solution and Baker's [68] Sm metal dissolution enthalpy.
[b]: The ΔH_{298}° was calculated using the reported enthalpy of Eu_2O_3 solution and Stubblefield's [74] Eu metal dissolution enthalpy.
[c]: The ΔH_{298}° was calculated using the reported enthalpy of Eu_2O_3 solutin and Stuve's [73] Eu metal dissolution enthalpy.
[d]: The ΔH_{298}° was calculated using the reported enthalpy of Eu_2O_3 solutin and Fitzgibbon's [16] Eu metal dissolution enthalpy.

Table 15 Summary of ΔH_{298}° of the heavy rare earth sesquioxides Tb_2O_3 – Lu_2O_3, ASS: assessed; CC: combustion calorimetry; SC: solution calorimetry

Sesquioxides	ΔH_{298}°, KJ/mol	Uncertainties, KJ/mol	Techniques	References	
Tb_2O_3	-1827.57	8.37	SC	Stubblefield, 1956	[76]
	-1865.23	7.53	SC	Fitzgibbon, 1968	[77]
	-1864.5[a]	8.4	ASS	Cordfunke, 2001	[34]
	-1865.2	6.0			
	-1865.23			This work	
Dy_2O_3	-1865.39	3.89	CC	Huber, 1956	[78]
	-1863.14	4.18	CC	Huber, 1971	[79]
	-1863.97	6.69	SC		
	-1863.4	5.0	ASS	Cordfunke, 2001	[34]
	-1863.22			This work	
Ho_2O_3	-1880.92	4.81	CC	Huber, 1957	[80]
	-1887.3	13.7	SC	Morss, 1993	[44]
	-1883.3	8.2	ASS	Cordfunke, 2001	[34]
	-1884.11	9.26		This work	
Er_2O_3	-1897.82	1.88	CC	Huber, 1956	[83]
	-1762.84		CC	Spedding, 1959	[61]
	-1815.74[b]	3.68	SC	Montegomery, 1961	[84]
	-1847.63[c]	3.68			
	-1898.19[d]	7.08			
	-1904.21[d]	6.04	SC	Morss, 1993	[44]
	-1900.1	6.5	ASS	Cordfunke, 2001	[34]
	-1900.07			This work	
Tm_2O_3	-1894.8	8.3	CC	Huber, 1960	[87]
	-1884.3	7.9			
	-1888.66	5.86			
	-1889.3	5.7	ASS	Cordfunke, 2001	[34]
	-1888.66			This work	
Yb_2O_3	-1814.52	2.22	CC	Huber, 1956	[78]
	-1814.5	6.0	ASS	Cordfunke, 2001	[34]
	-1814.52			This work	
Lu_2O_3	-1878.20	7.53	CC	Huber, 1960	[88]
	-1877.0	7.7	ASS	Cordfunke, 2001	[34]
	-1878.20			This work	

[a]: The ΔH_{298}° was calculated using the assessed enthalpy of Tb solution and Stubblefield's [76] Tb_2O_3 dissolution enthalpy.
[b]: The ΔH_{298}° was calculated using the reported enthalpy of Er_2O_3 and Spedding's [58] Er solution enthalpy.
[c]: The ΔH_{298}° was calculated using the reported enthalpy of Er_2O_3 and Bommer's [85] Er solution enthalpy.
[d]: The ΔH_{298}° was calculated using the reported enthalpy of Er_2O_3 and Fuger's [86] Er solution enthalpy.

Table 16 List of references of the experimental ΔH°_{298} for La_2O_3 – Lu_2O_3

A-hexagonal phase at room temperature				
Symbols	**La_2O_3 (1.061)**	**Ce_2O_3 (1.034)**	**Pr_2O_3 (1.013)**	**Nd_2O_3 (0.995)**
Circle	Huber 1953, CC	Kuznetsov 1960, CC	Stubblefield 1956, SC	Huber 1952, CC
Square	Montgomery 1959, SC	Mah 1961, CC	Fitzgibbon 1973, SC	Spedding 1952, CC
Triangle	Fitzgibbon 1965, SC	Baker 1968, CC		Fitzgibbon 1968 & Stuve 1965, SC
Inverted- Triangle	Gvelesiani 1967, SC	Huntelaar 2000, SC		Fitzgibbon 1968 & Merli 1998, SC
Diamond	Gvelesiani 1967 & Merli 1998, SC	Putnam 2000, SC		Yashvili 1971, SC
Centered-cross	This work	This work		Morss 1989 & Merli 1998, SC
Upper cross				Popova 1989, SC
Star				This work

Both B-monoclinic and C-cubic phases at room temperature			
Symbols	**Sm_2O_3 (0.964)**	**Eu_2O_3 (0.95)**	**Gd_2O_3 (0.938)**
Circle	(B) Huber 1955, CC	(B) Huber 1964, SC	(B) Huber, 1955, CC
Square	(B) Spedding 1959, CC	(B) Yashvili 1971, SC	(B)Spedding, 1959, CC
Triangle	(B) Gvelesiani 1967, SC	(B) Fitzgibbon 1972, SC	(B) Yashvili, 1971, SC
Inverted triangle	(B) Baker 1972, CC	(B) Fitzgibbon 1972 & Stubblefield 1965, SC	(B) This work
Diamond	(B) Baker 1972, SC	(B) Hennig 1998 & Stuve 1965, SC	(C) This work
Centered cross	(B) Henning 1997 & Baker 1972, SC	(B) Hennig 1998 & Fitzgibbon 1972, SC	
Upper cross	(B) This work	(B) This study	
Top filled circle	(C) Gvelesiani 1967, SC	(C) Huber 1964, SC	
Left filled triangle	(C) Baker 1972, SC	(C) Stuve 1965, SC	
Top filled square	(C) This work	(C) Fitzgibbon 1972, SC	
Bottom filled diamond		(C) Fitzgibbon 1972 & Stubbefield 1965, SC	
Small filled diamond		(C) This work	

C-cubic phase at room temperature				
Symbols	**Tb_2O_3 (0.923)**	**Dy_2O_3 (0.908)**	**Ho_2O_3 (0.894)**	**Er_2O_3 (0.881)**
Circle	Stubblefield 1956, SC	Huber 1956, CC	Huber 1957, SC	Huber 1956, CC
Square	Fitzgibbon 1968, SC	Huber 1971, CC	Morss 1993, CC	Spedding 1959, CC
Triangle	Cordfunke 2001, ASS	Huber 1971, SC	Cordfunke 2001, ASS	Montgomery 1961 & Spedding 1959, SC
Inverted triangle	This work	This work	This work	Montgomery 1961 & Bommer 1941, SC
Diamond				Montgomery 1961 & Fuger 1980, SC
Centered cross				This work

C-cubic phase at room temperature			
Symbols	**Tm_2O_3 (0.869)**	**Yb_2O_3 (0.858)**	**Lu_2O_3 (0.848)**
Circle	Huber, 1960, CC	Huber, 1956, CC	Huber, 1960, CC
Square	Huber, 1960, CC		

Table 17 Summary of standard entropy values of entire RE_2O_3

Sesquioxides	Structure	S°_{298}, J/mol·K	Uncertainties, J/mol·K	References	
Sc_2O_3	C	76.99		Weller, 1963	[98]
		76.60		This work	
Y_2O_3	C	98.96		Goldstein, 1959	[96]
		98.96		Gavrichev, 1993	[97]
		99.13		This work	
La_2O_3	A	127.95	0.29	Goldstein, 1959	[96]
		128.57	0.84	King, 1961	[99]
		127.32		Justice, 1963	[92]
		127.24		This work	
Ce_2O_3	A	148.11		Justice, 1968	[90]
		150.62	4.18	Weller, 1963	[98]
		148.80	0.4	Huntelaar, 2001	[53]
		148.87		This work	
Pr_2O_3	A	152.73		Gruber, 2002	[100]
		153.83		This work	
Nd_2O_3	A	154.47		Goldstein, 1959	[96]
		158.54		Justice, 1963	[96]
		158.78		This work	
Pm_2O_3	C	152.95		This work	
Sm_2O_3	B	151.04		Justice, 1963	[91]
		150.38		This work	
	C	155.80	3	Lyutsareva, 1994	[17]
		145.95		This work	
Eu_2O_3	B	142.74		Lyutsareva, 1994	[17]
		144.25		This work	
	C	141.45		Lyutsareva, 1994	[17]
		138.95		This work	
Gd_2O_3	B	156.10	3	Lyutsareva, 1994	[17]
		155.50		This work	
	C	150.62		Justice, 1963	[91]
		150.62		This work	
Tb_2O_3		157.57		This work	
Dy_2O_3	C	149.79		Justice, 1963	[93]
		149.48		This work	
Ho_2O_3	C	158.16		Justice, 1963	[93]
		158.14		This work	
Er_2O_3	C	153.13		Justice, 1963	[93]
		153.50		This work	
Tm_2O_3	C	139.75	0.4	Justice 1969	[94]
		140.06		This work	
Yb_2O_3	C	133.05		Justice, 1963	[91]
		133.77		This work	
Lu_2O_3	C	109.96		Justice, 1969	[94]
		109.91		This work	

Table 18 Optimized coefficients heat capacity function of entire RE_2O_3

RE_2O_3	**a**	**b, T**	**c, T^{-2}**	**d, T^2**	**Phase Applied**
Sc_2O_3 (C)	114.91125	0.014466	-2229209	2.4676E-07	C, B, A, H, X, L
Y_2O_3 (C)	114.55891	0.0200833	-1480281.19	-1.7319E-06	C, B, A, H, X, L
La_2O_3 (A)	120.29480	0.013597	-1407346.41	1.2217E-07	C, B, A, H, X, L
Ce_2O_3 (A)	124.47103	0.014008	-1229146.52	1.8138E-06	C, B, A, H, X, L
Pr_2O_3 (A)	119.00680	0.027437	-453272.57	-1.7672E-08	C, B, A, H, X, L
Nd_2O_3 (A)	114.45302	0.033685	-1151754.12	-3.0074E-06	C, B, A, H, X, L
Pm_2O_3(C)	121.96825	0.026824	-1505548.64	-3.01E-06	C, B, A, H, X, L
Sm_2O_3 (C)	129.48348	0.019963	-1859343.17		C
Sm_2O_3 (B)	128.22586	0.019444	-1700690.29		B, A, H, X, L
Eu_2O_3 (C)	133.64516	0.018570	-1207017.95	-1.6595E-06	C
Eu_2O_3 (B)	127.56237	0.024691	-1141112.51	-2.5575E-06	B, A, H, X, L
Gd_2O_3 (C)	120.49465	0.011643	-1646124.13		C
Gd_2O_3 (B)	114.8587	0.0138	-1000494.21	2.4885E-07	B, A, H, X, L
Tb_2O_3 (B)	120.8339	0.021744	-610864		C, B, A, H, X, L
Dy_2O_3 (C)	121.5356	0.016945	-832086.1	-1.1438E-06	C, B, A, H, X, L
Ho_2O_3 (C)	118.781	0.015921	-691226.40	-2.5075E-06	C, B, A, H, X, L
Er_2O_3 (C)	118.94703	0.014742	-1274185.88	-2.9546E-06	C, B, A, H, X, L
Tm_2O_3 (C)	124.69408	0.009921	-875245.94	-2.0546E-06	C, B, A, H, X, L
Yb_2O_3 (C)	128.06732	0.006391	-1277222.67	-5.0061E-07	C, B, A, H, X, L
Lu_2O_3 (C)	116.7154	0.014939	-1705012.07	-1.9454E-06	C, B, A, H, X, L

Table 19 Summary of pressure – temperature data for phase transitions. AA: anvil apparatus; XRD: X – ray diffraction; SI: shock induced; RM: Raman spectrometry; DFT: density functional theory; ADXD: angled dispersive X – ray diffraction; MS: Mössbauer spectroscopy.

Sesquioxides	Phase transitions	P, GPa	Techniques	T, K	References	
Sc_2O_3	C→B	13	AA, XRD	1273	Reid, 1969	[141]
	C→A	40.90±1.3	SI	~298	Atou, 1994	[132]
Y_2O_3	C→B	12.8	AA, XRD	298	Ma, 2002	[142]
		12	AA, RM	298	Husson, 1999	[143]
		13	AA, XRD	298	Halevy, 2010	[144]
	C→B (A)	11.81	SI	~298	Atou, 1990	[131]
	B→A	19	AA, RM	298	Husson, 1999	[143]
		24.5	AA, XRD	298	Halevy, 2010	[144]
	C→A	11.25	SI	~298	Atou, 1990	[131]
La_2O_3			N/A			
Ce_2O_3			N/A			
Pr_2O_3			N/A			
Nd_2O_3			N/A			
Pm_2O_3			N/A			
Sm_2O_3	C→B	3.89	DFT	0	Guo, 2008	[128]
		9.9	AA, XRD	300	Guo, 2008	[128]
	B→A	3.35	AA, XRD	298	Atou, 1989	[124]
		2.5	RM, XRD	298	Atou 1992	[126]
		3	DFT	298	Wu, 2007	[123]
		4.7	AA, XRD	298	Guo, 2008	[128]
		3.98	DFT	0	Guo, 2008	[128]
		2.5	AA, RM, XRD	298	Sheng, 2013	[129]
		2.6	AA, RM	298	Hongo, 2007	[127]
	C→A	4.2	AA, RM, XRD	298	Sheng, 2013	[129]
Eu_2O_3	C→B	2	AA, RM, XRD	298	Dilawar, 2013	[136]
		0.55	AA, XRD	823	Hoekstra, 1965	[19]
		0.05	AA, XRD	1273	Hoekstra, 1965	[19]
	B→A	4.7	AA, XRD	298	Chen, 1994	[125]
Gd_2O_3	C→B	4.87	DFT	0	Guo, 2008	[128]
	C→B (A)	4.00	SI	~298	Atou, 1990	[131]
	C→B	0.77	AA, XRD	823	Hoekstra, 1965	[19]
		0.27	AA, XRD	1273	Hoekstra, 1965	[19]
	B→A	7.96	DFT	0	Guo, 2008	[128]
Tb_2O_3	C→B	1.09	AA, XRD	823	Hoekstra, 1965	[19]
		0.59	AA, XRD	1273	Hoekstra, 1965	[19]
		0.09	AA, XRD	1723	Hoekstra, 1965	[19]
Dy_2O_3	C→B	1.49	AA, XRD	823	Hoekstra, 1965	[19]
		0.99	AA, XRD	1273	Hoekstra, 1965	[19]
		0.49	AA, XRD	1723	Hoekstra, 1965	[19]

		1.53	AA, XRD	823	Seck, 1969	[145]
		1.08	AA, XRD	1273	Seck, 1969	[145]
		0.65	AA, XRD	1723	Seck, 1969	[145]
Ho_2O_3	C→B	8.9	AA. ADXD	298	Sheng, 2011	[135]
		2.00	AA, XRD	823	Hoekstra, 1965	[19]
		1.50	AA, XRD	1273	Hoekstra, 1965	[19]
		1.00	AA, XRD	1723	Hoekstra, 1965	[19]
Er_2O_3	C→B	7.05	DFT	0	Guo, 2008	[128]
		9.9	AA, XRD	300	Guo, 2007	[134]
		2.49	AA, XRD	823	Hoekstra, 1965	[19]
		1.99	AA, XRD	1273	Hoekstra, 1965	[19]
		1.49	AA, XRD	1723	Hoekstra, 1965	[19]
	B→A	19.4	DFT	0	Guo, 2008	[128]
Tm_2O_3	C→B	3.00	AA, XRD	823	Hoekstra, 1965	[19]
		2.50	AA, XRD	1273	Hoekstra, 1965	[19]
		2.00	AA, XRD	1723	Hoekstra, 1965	[19]
Yb_2O_3	C→B	13	AA, MS, XRD	298	Meyer, 1995	[133]
		3.47	AA, XRD	823	Hoekstra, 1965	[19]
		2.97	AA, XRD	1273	Hoekstra, 1965	[19]
		2.47	AA, XRD	1723	Hoekstra, 1965	[19]
	C→A	15.05	SI	~298	Atou, 1990	[131]
Lu_2O_3	C→B	4.07	AA, XRD	823	Hoekstra, 1965	[19]
		3.57	AA, XRD	1273	Hoekstra, 1965	[19]
		3.07	AA, XRD	1723	Hoekstra, 1965	[19]
		~17	ADXD	298	Lin, 2010	[146]

Table 20 Summary of the enthalpy and entropy changes of C→B phase transition.

Sesquioxides	Ionic radii, Å	ΔH_{tr}, KJ/mol	ΔS_{tr}, J/mol.K	References	
Sc_2O_3	0.73	47.22	37.09	Reid, 1969	[141]
		14.02[a]	2.75[a]	This study	
		31.38	3.058	Zinkevich, 2007	[2]
Y_2O_3	0.892	53.44	21.61	Ma, 2002	[142]
		11.11[a]	4.03[a]	This study	
		54.28	21.95	Halevy, 2010	[144]
		50.10	20.26	Husson, 1999	[143]
		11.09	3.97	Zinkevich, 2007	[2]
La_2O_3	1.061	-4.21[a]	5.36[a]	This study	
Ce_2O_3	1.034	-1.90[a]	5.15[a]	This study	
Pr_2O_3	1.013	-0.10[a]	4.98[a]	This study	
Nd_2O_3	0.995	1.38[a]	4.84[a]	This study	
Pm_2O_3	0.982	4.61[a]	4.74[a]	This study	
		2.15	4.71	Zinkevich, 2007	[2]
Sm_2O_3	0.964	5.27	4.57	Hoekstra, 1965	[19]
		5.8	5.03	Gvelesiani, 1967	[47]
		3.77	4.35	Baker, 1972	[68]
		10	3.37	Guo, 2008	[128]
		4.59	4.33	This work	
		3.31	4.90	Zinkevich, 2007	[2]
		5.49	4.76	Lyutsareva 1994 & Justice, 1963	[17, 91]
Eu_2O_3	0.95	17.20	12.76	Huber, 1964	[71]
		9.7	7.2	Fitzgibbon, 1972	[16]
		6.10	4.08	Hoekstra, 1965	[19]
		10.48	7.70	Dilawar, 2013	[136]
		4.40	4.91	Zinkevich, 2007	[2]
		4.49	5.30	This work	
		1.74	1.29	Lyutsareva 1994	[17]
Gd_2O_3	0.938	5.3	3.4	Kolitsch, 1995	[18]
		7.23	4.63	Hoekstra, 1965	[19]
		5.33	3.37	Zinkevich, 2007	[2]
		6.68	5.48	This work	
		8.55	5.48	Lyutsareva 1994 & Justice, 1963	[17, 91]
Tb_2O_3	0.923	7.62	4.06	Hoekstra, 1965	[19]
		7.68	4.211	Zinkevich, 2007	[2]
Dy_2O_3	0.908	9.07	4.05	Hoekstra, 1965	[19]

		9.255	4.09	Zinkevich, 2007	[2]
Ho_2O_3	0.894	37.52	15.23	Sheng, 2011	[135]
		10.13	4.11	Hoekstra, 1965	[19]
		9.79	3.98	Zinkevich, 2007	[2]
Er_2O_3	0.881	24	9.25	Guo, 2007	[134]
		10.03	3.87	Hoekstra, 1965	[19]
		13.07	3.8	Zinkevich, 2007	[2]
Tm_2O_3	0.869	11.04[a]	3.79[a]	This study	
		12.46	3.89	Zinkevich, 2007	[2]
Yb_2O_3	0.858	50.17	16.05	Meyer, 1995	[133]
		12.11[a]	3.79[a]	This study	
		15.35	3.73	Zinkevich, 2007	[2]
Lu_2O_3	0.848	12.33[a]	3.72[a]	This study	
		16.60	3.66	Zinkevich, 2007	[2]

[a]: estimated hypothetical values using the established trend

Table 21 Summary of the enthalpy and entropy changes of B→A phase transition.

Sesquioxides	**Ionic radii, Å**	**ΔH_{tr}, KJ/mol**	**ΔS_{tr}, J/mol.K**	**References**	
Sc_2O_3	0.73	30.18	9.24[a]	Wu, 2007	[123]
Y_2O_3	0.892	9.57	3.62[a]	Wu, 2007	[123]
La_2O_3	1.061	-4.14	2.22	Zinkevich, 2007	[2]
	1.061	-4.85	0.05[a]	Wu, 2007	[123]
Ce_2O_3	1.034	-2.28	1.96	Zinkevich, 2007	[2]
	1.034	-3.37	0.05[a]	Wu, 2007	[123]
Pr_2O_3	1.013	-0.84	1.8	Zinkevich, 2007	[2]
	1.013	-1.94	0.05[a]	Wu, 2007	[123]
Nd_2O_3	0.995	0.4	1.68	Zinkevich, 2007	[2]
	0.995	-0.55	0.05[a]	Wu, 2007	[123]
Pm_2O_3	0.982	0.83	0.41	Wu, 2007	[123]
	0.982	1.5	1.6	Zinkevich, 2007	[2]
Sm_2O_3	0.964	2.48	1.14	Wu, 2007	[123]
	0.964	3.32	1.53	Zinkevich, 2007	[2]
	0.964	3.36	1.55	Atou, 1989	[124]
	0.964	2.37	1.1	Atou, 1992	[126]
	0.964	4.46	2.06	Guo, 2008	[128]
	0.964	3.25	1.5	Guo, 2008	[128]
	0.964	2.38	1.1	Sheng, 2013	[129]
	0.964	2.47	1.14	Hongo, 2007	[127]
Eu_2O_3	0.95	3.5	1.5	Zinkevich, 2007	[2]

	0.95	3.82	1.65	Chen, 1994	[125]
		3.40	1.47	This work	
Gd_2O_3	0.938	5.27	2.21	Wu, 2007	[123]
	0.938	6.3	2.58	Zinkevich, 2007	[2]
	0.938	7.96	3.26	Guo, 2008	[128]
	0.938	6.28	2.57	Barkhatov, 1981	[20]
Tb_2O_3	0.923	5.87	2.40	Wu, 2007	[123]
Dy_2O_3	0.908	8.54	3.44	Wu, 2007	[123]
Ho_2O_3	0.894	8.48	3.30[a]	Wu, 2007	[123]
Er_2O_3	0.881	12.06	4.60[a]	Wu, 2007	[123]
Tm_2O_3	0.869	14.22	5.33[a]	Wu, 2007	[123]
Yb_2O_3	0.858	14.13[a]	5.77[a]	This work	
Lu_2O_3	0.848	17.44[a]	6.33[a]	Wu, 2007	[123]

Table 22 Summary of enthalpies of discrete transitions A→H, H→X and X→L; the entropies of fusion: except values for Y_2O_3 and Sc_2O_3, all the rest were extracted from the study of Wu et al., [123]

RE_2O_3	Ionic Radii, Å	$\Delta H_{tr,A\to H}$, kJ/mol	$\Delta H_{tr,H\to X}$, kJ/mol	$\Delta H_{tr,X\to L}$, kJ/mol	$\Delta S_{tr,X\to L}$, kJ/mol	$\Delta S_{tr,H\to L}$, J/mol	$\Delta S_{tr,C\to L}$, J/mol
Sc_2O_3	0.73	5.83	6.88	43.52	19.37		100.42[b]
Y_2O_3	0.892	5.71	6.76	36.87	13.64	16.14[a]	
La_2O_3	1.061	5.78	5.95	51.75	20.05		
Ce_2O_3	1.034	5.97	6.11	57.42	22.85		
Pr_2O_3	1.013	5.78	6.02	64.89	25.40		
Nd_2O_3	0.995	5.94	6.20	58.46	22.71		
Pm_2O_3	0.982	6.02	6.25	58.27	22.47		
Sm_2O_3	0.964	5.92	6.32	55.48	21.36		
Eu_2O_3	0.95	6.03	6.36	55.50	21.21		
Gd_2O_3	0.938	6.12	6.61	67.21	25.05		
Tb_2O_3	0.923	6.09	6.61	61.52	23.02		
Dy_2O_3	0.908	6.17	6.64	70.08	26.21		
Ho_2O_3	0.894	6.03	6.75	38.92	14.50	17.00	
Er_2O_3	0.881	6.35	6.77	40.07	14.92	17.42	
Tm_2O_3	0.869	5.21	6.82	42.90	15.94	18.44	
Yb_2O_3	0.858	4.47	6.88	38.75	14.31	16.81	
Lu_2O_3	0.848	5.73	6.92	25.46	9.34		67.89

[a]: the entropy of fusion was obtained from Roth's [130] study.
[b]: the entropy of fusion was obtained from Shpil'rain's [21] study.

Table 23 Summary of optimized standard enthalpies of formation and standard entropies of 6 phases (C, B, A, H, X and L) for entire RE_2O_3

Sesquioxides	$\Delta H^{\circ}_{298,C}$	$S^{\circ}_{298,C}$	$\Delta H^{\circ}_{298,B}$	$S^{\circ}_{298,B}$	$\Delta H^{\circ}_{298,A}$	$S^{\circ}_{298,A}$	$\Delta H^{\circ}_{298,H}$	$S^{\circ}_{298,H}$	$\Delta H^{\circ}_{298,X}$	$S^{\circ}_{298,X}$	$\Delta H^{\circ}_{298,L}$	$S^{\circ}_{298,L}$
Sc_2O_3	-1904.47	76.60	-1890.45	79.35	-1860.27	88.59	-1854.44	91.09	-1847.57	93.59	-1804.05	112.96
Y_2O_3	-1932.80	99.13	-1921.69	103.16	-1912.12	106.78	-1906.41	109.28	-1899.65	111.78	-1862.78	125.42
La_2O_3	-1782.71	127.24	-1786.93	127.19	-1791.78	127.24	-1786.00	129.74	-1780.05	132.24	-1728.30	152.29
Ce_2O_3	-1804.58	148.76	-1806.48	148.82	-1809.85	148.87	-1803.88	151.37	-1797.77	153.87	-1740.36	176.72
Pr_2O_3	-1807.62	153.83	-1807.72	153.78	-1809.66	153.83	-1803.88	156.33	-1797.86	158.83	-1732.97	184.23
Nd_2O_3	-1809.64	158.78	-1808.26	158.73	-1808.81	158.78	-1802.87	161.28	-1796.68	163.78	-1738.21	186.49
Pm_2O_3	-1824.22	152.37	-1819.61	157.11	-1818.78	157.52	-1812.76	160.02	-1806.51	162.52	-1748.24	184.99
Sm_2O_3	-1827.19	145.95	-1822.60	150.38	-1820.12	151.52	-1814.20	154.02	-1807.88	156.52	-1752.40	177.89
Eu_2O_3	-1657.95	138.95	-1653.45	144.25	-1650.05	145.72	-1644.02	148.22	-1637.66	150.72	-1582.16	171.94
Gd_2O_3	-1830.93	150.62	-1825.19	155.50	-1819.92	157.71	-1813.80	160.21	-1807.20	162.71	-1739.99	187.76
Tb_2O_3	-1865.23	157.57	-1857.61	161.63	-1851.74	164.03	-1845.66	166.53	-1839.05	169.03	-1777.53	192.05
Dy_2O_3	-1863.22	149.48	-1854.15	153.53	-1845.61	156.97	-1839.44	159.47	-1832.81	161.97	-1762.73	188.18
Ho_2O_3	-1884.11	158.14	-1873.98	162.25	-1865.50	165.53	-1859.47	168.03	-1852.72	170.53	-1813.80	185.03
Er_2O_3	-1904.21	153.50	-1894.15	157.37	-1882.09	161.97	-1875.77	164.47	-1869.00	166.97	-1828.93	181.89
Tm_2O_3	-1888.66	140.05	-1877.62	143.85	-1863.40	149.18	-1858.19	151.68	-1851.36	154.18	-1808.46	170.12
Yb_2O_3	-1814.52	133.77	-1802.41	137.65	-1786.76	143.42	-1782.29	145.92	-1775.41	148.42	-1736.66	162.72
Lu_2O_3	-1878.20	109.61	-1865.87	113.63	-1848.42	119.97	-1842.69	122.47	-1835.77	124.97	-1810.31	134.31

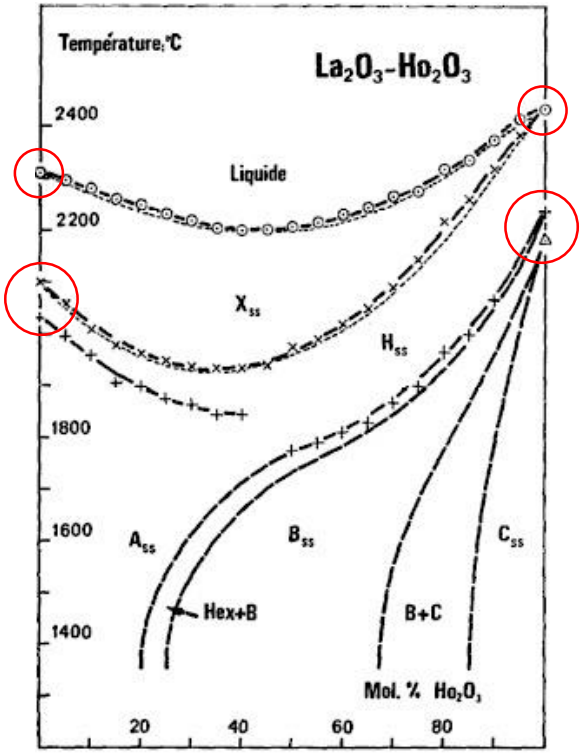

Figure 1 An example of binary RE_2O_3 phase diagram by Coutures and Foex [10]: binary La_2O_3 – Ho_2O_3 system; red circles indicate the extrapolated T_{tr}.

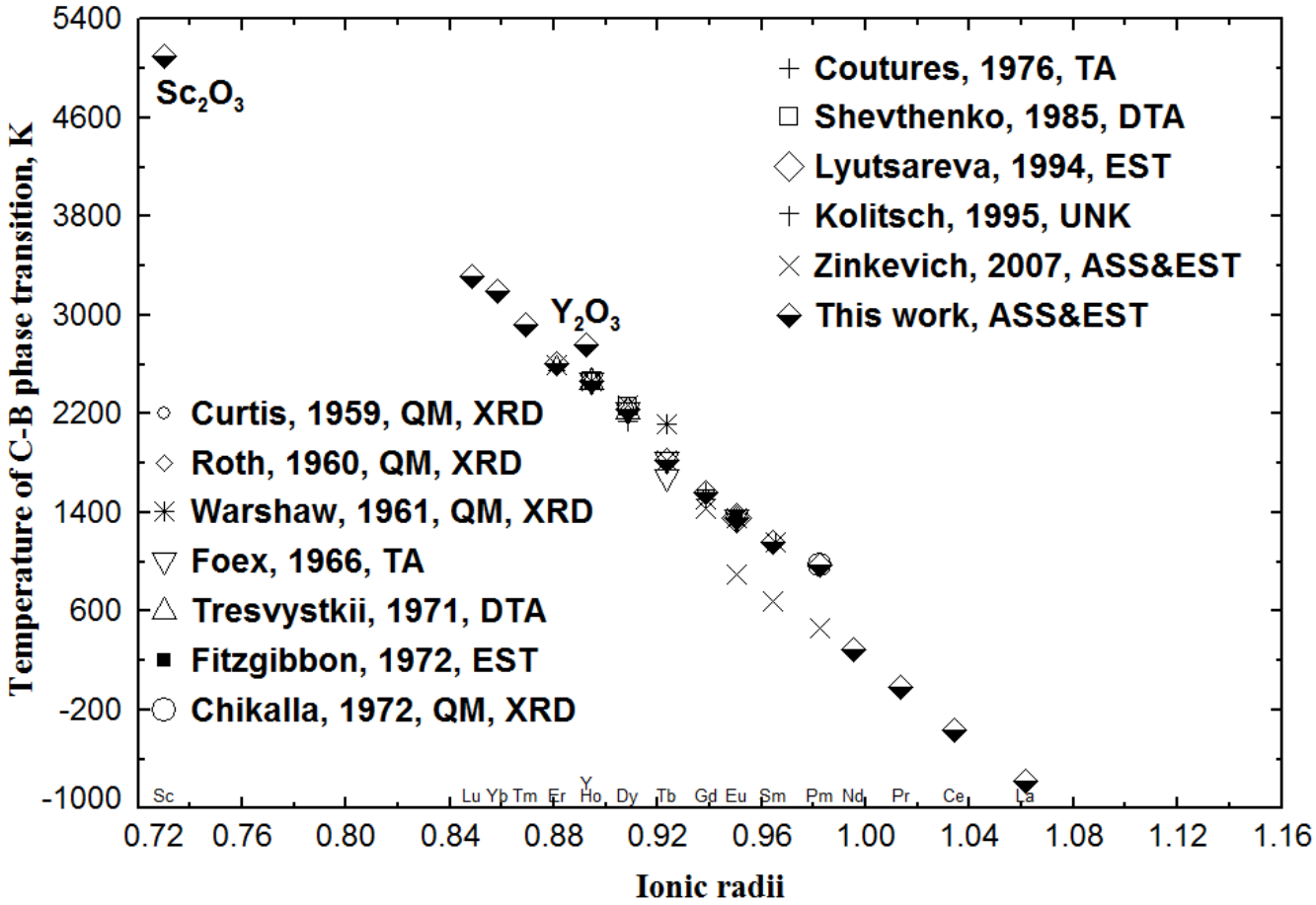

Figure 2 Summary of C→B phase transition temperatures depending on RE ionic radii; ASS: assessment; EST: estimation; DTA: differential thermal analysis; QM: quenching method; XRD: X – ray diffraction; TA: thermal analysis; UNK: method unknown; ionic radii in unit Å.

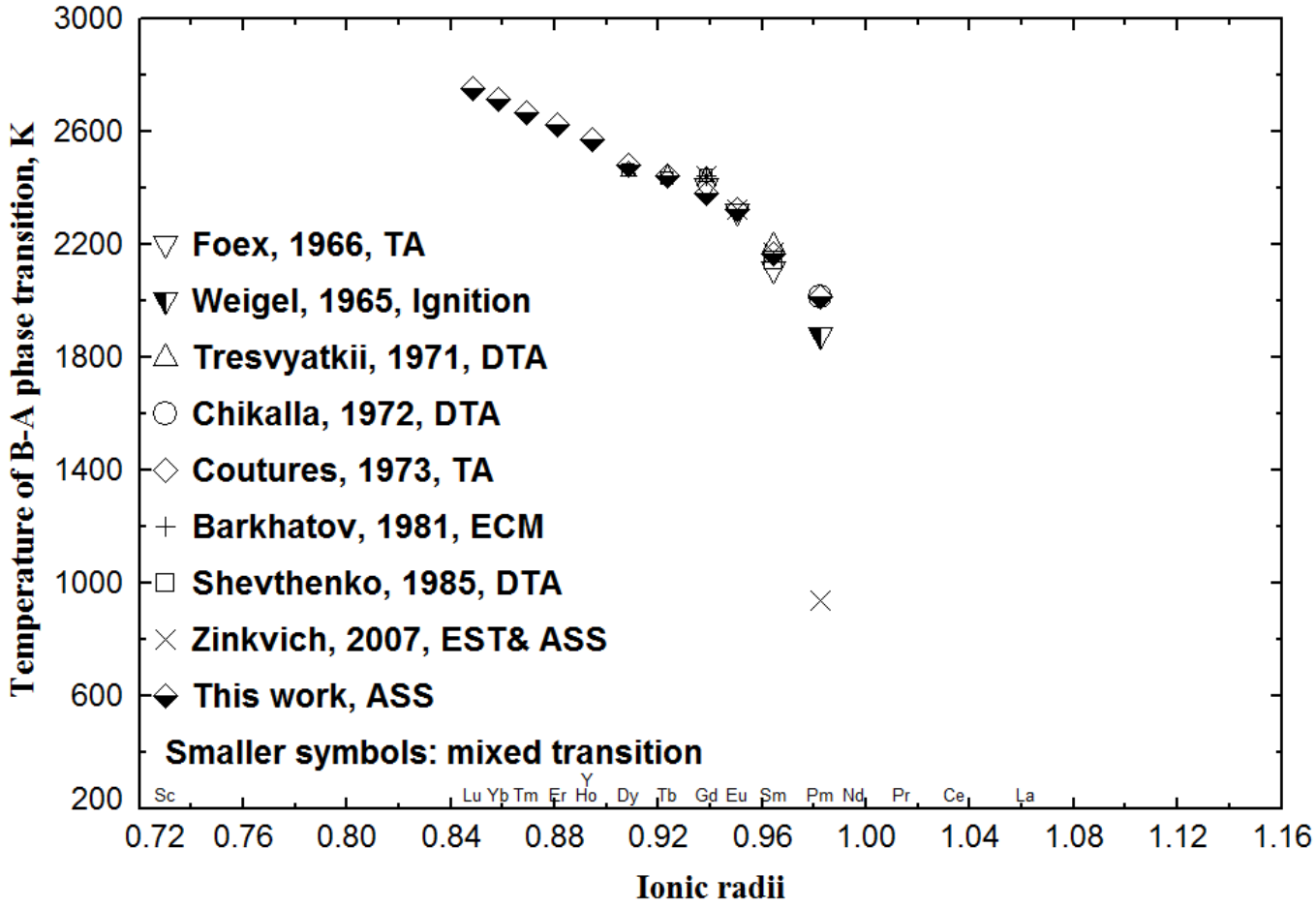

Figure 3 Summary of B→A phase transition temperatures depending on RE ionic radii; ASS: assessment; EST: estimation; ECM: electric conductivity measurement; DTA: differential thermal analysis; QM: quenching method; XRD: X – ray diffraction; TA: thermal analysis; ionic radii in unit Å.

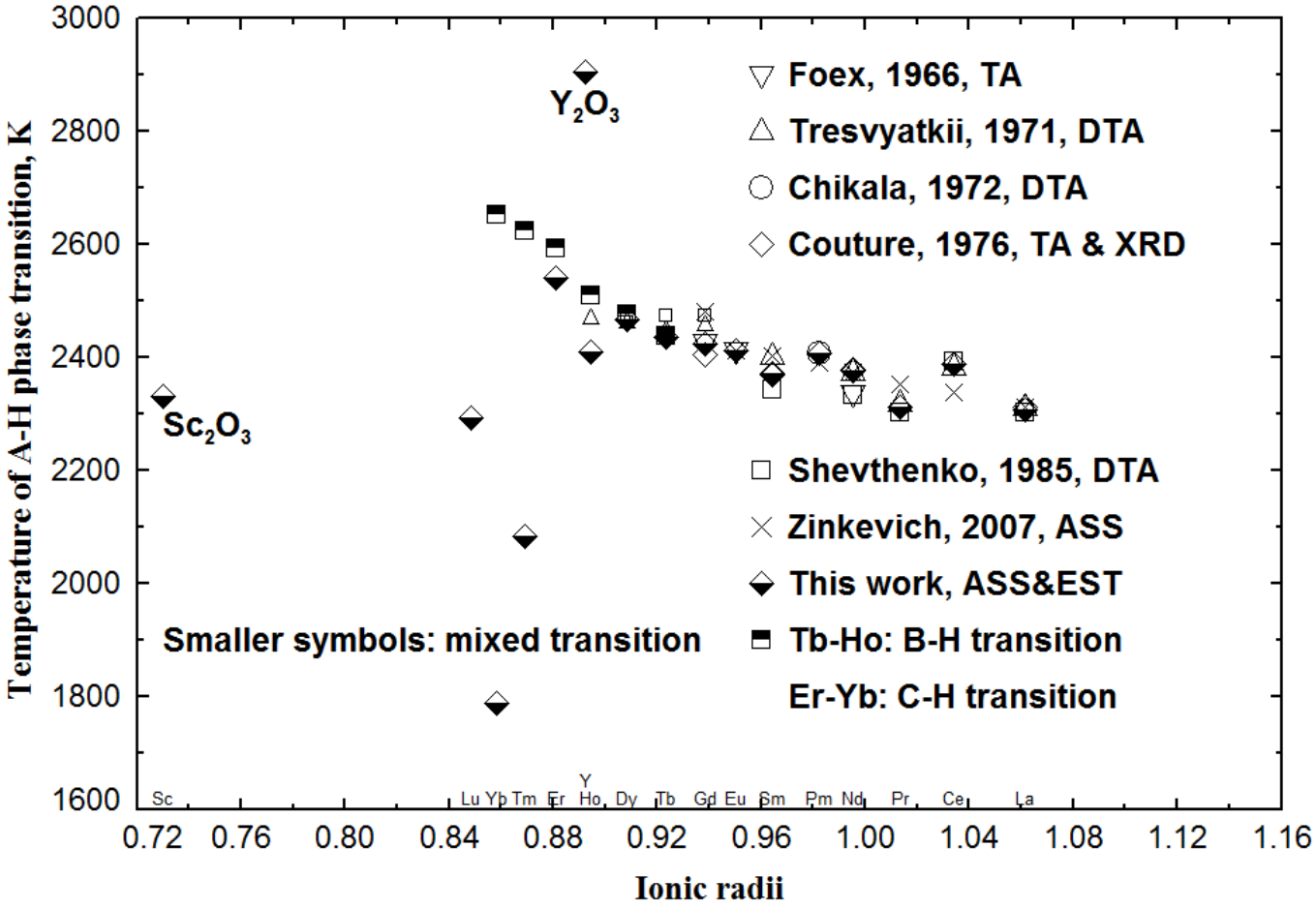

Figure 4 Summary of A→H phase transition temperatures depending on RE ionic radii; ASS: assessment; EST: estimation; DTA: differential thermal analysis; XRD: X – ray diffraction; TA: thermal analysis; ionic radii in unit Å.

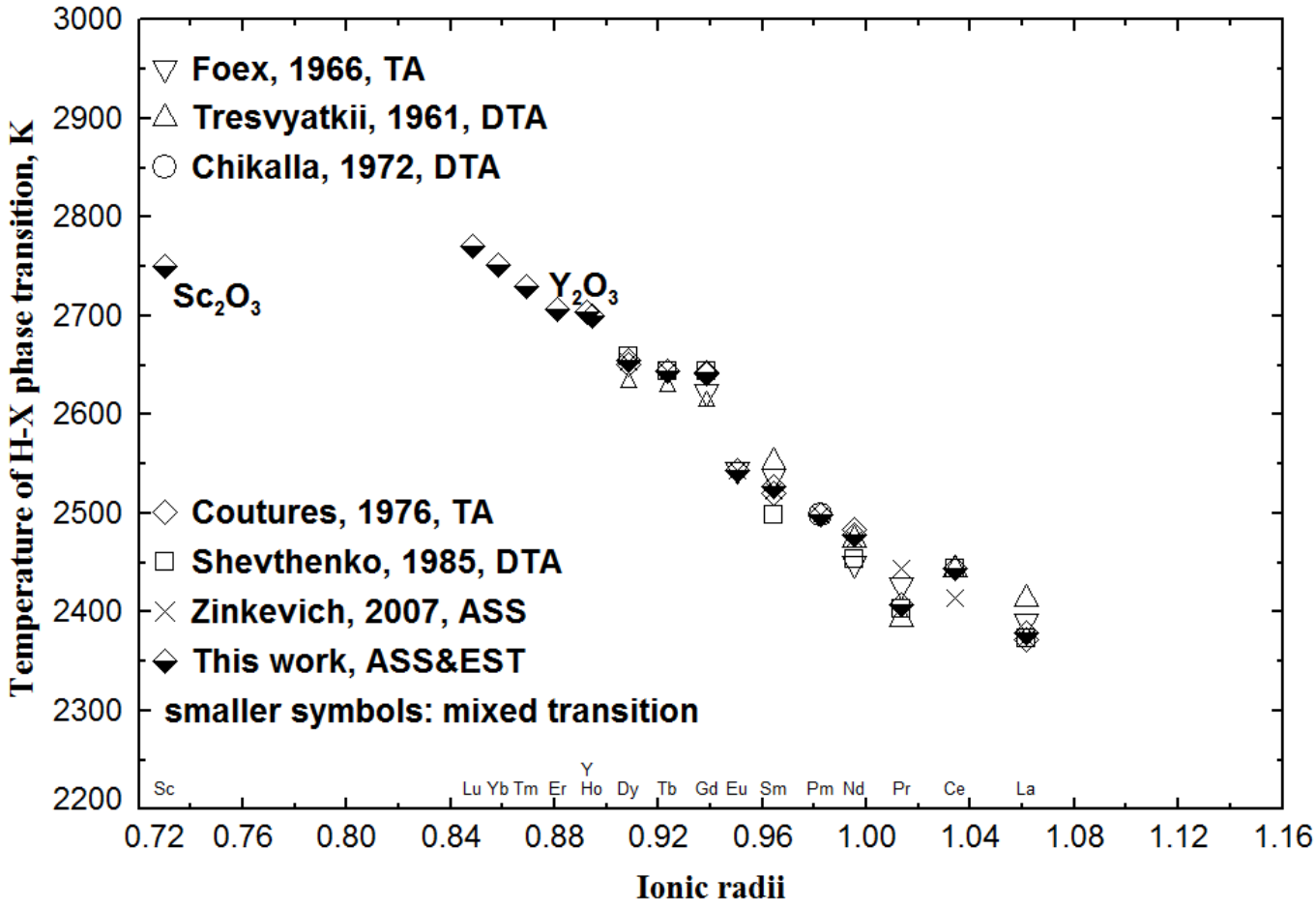

Figure 5 Summary of H→X phase transition temperatures depending on RE ionic radii; ASS: assessment; EST: estimation; DTA: differential thermal analysis; XRD: X – ray diffraction; TA: thermal analysis; ionic radii in unit Å.

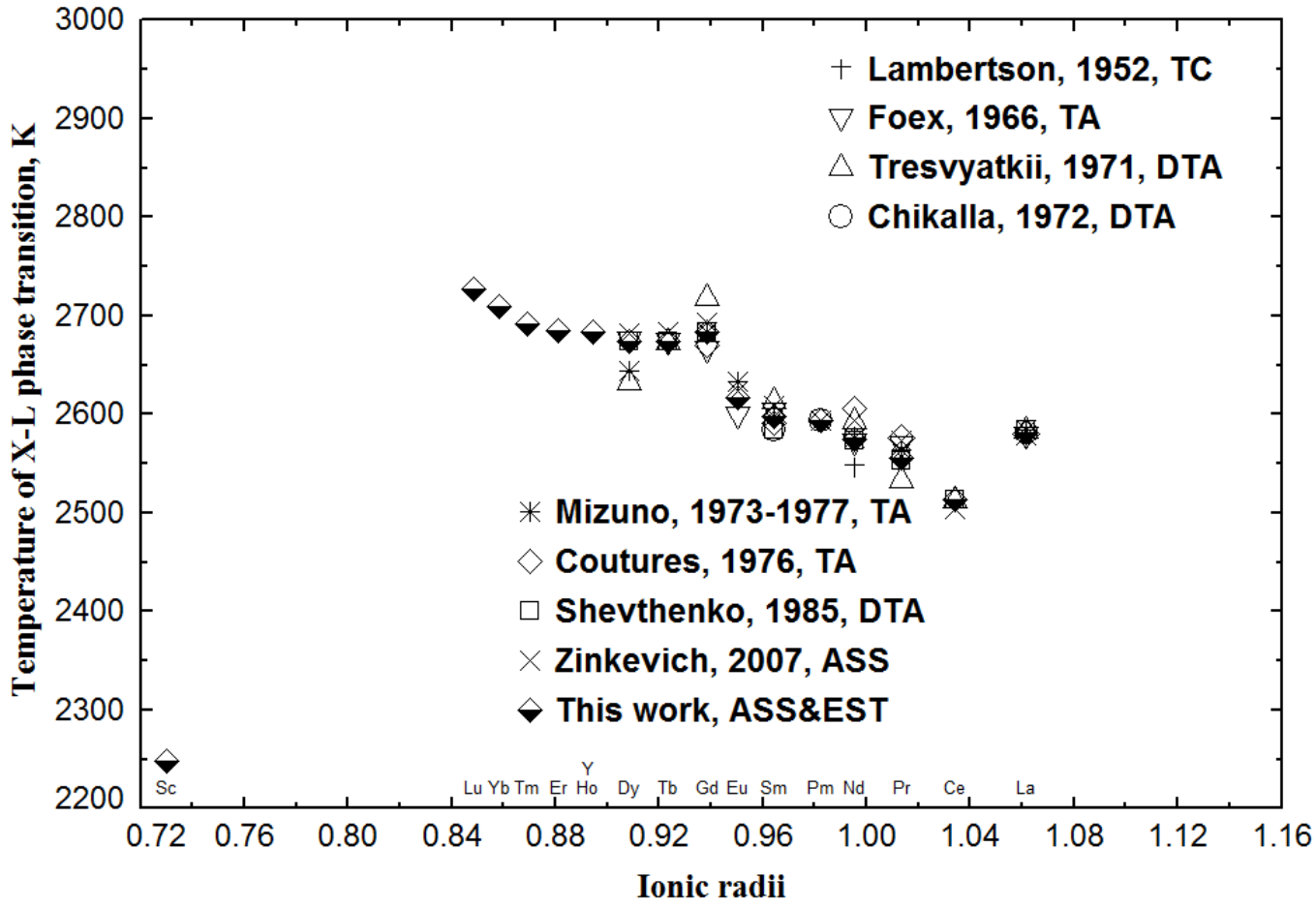

Figure 6 Summary of X→L phase transition temperatures depending on RE ionic radii; ASS: assessment; EST: estimation; DTA: differential thermal analysis; XRD: X – ray diffraction; TA: thermal analysis; ionic radii in unit Å.

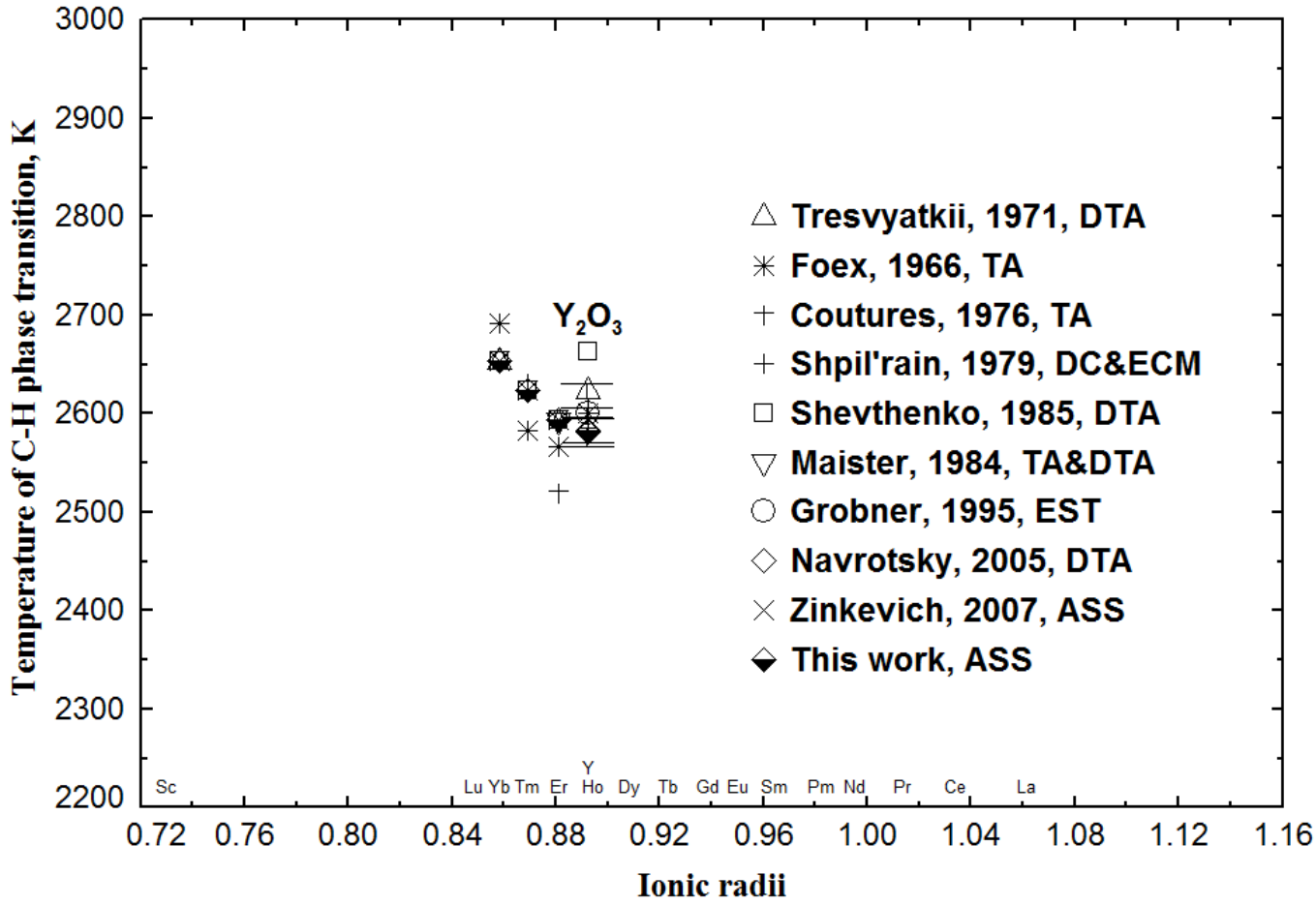

Figure 7 Summary of C→H phase transition temperatures depending on RE ionic radii; ASS: assessment; ECM: electric conductivity measurement; EST: estimation; DTA: differential thermal analysis; XRD: X – ray diffraction; TA: thermal analysis; ionic radii in unit Å.

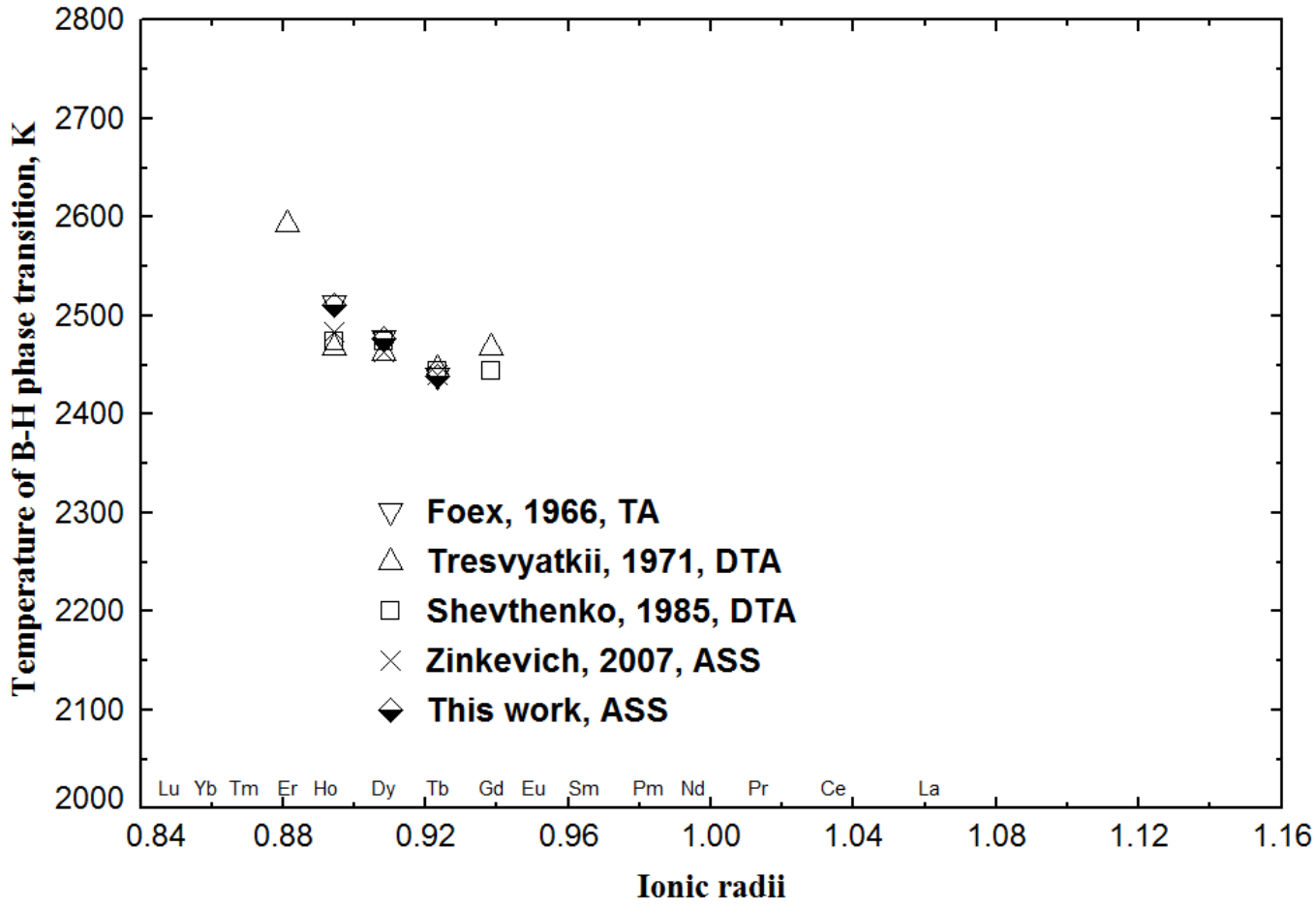

Figure 8 Summary of B→H phase transition temperatures depending on RE ionic radii; ASS: assessment; DTA: differential thermal analysis; XRD: X – ray diffraction; TA: thermal analysis; ionic radii in unit Å.

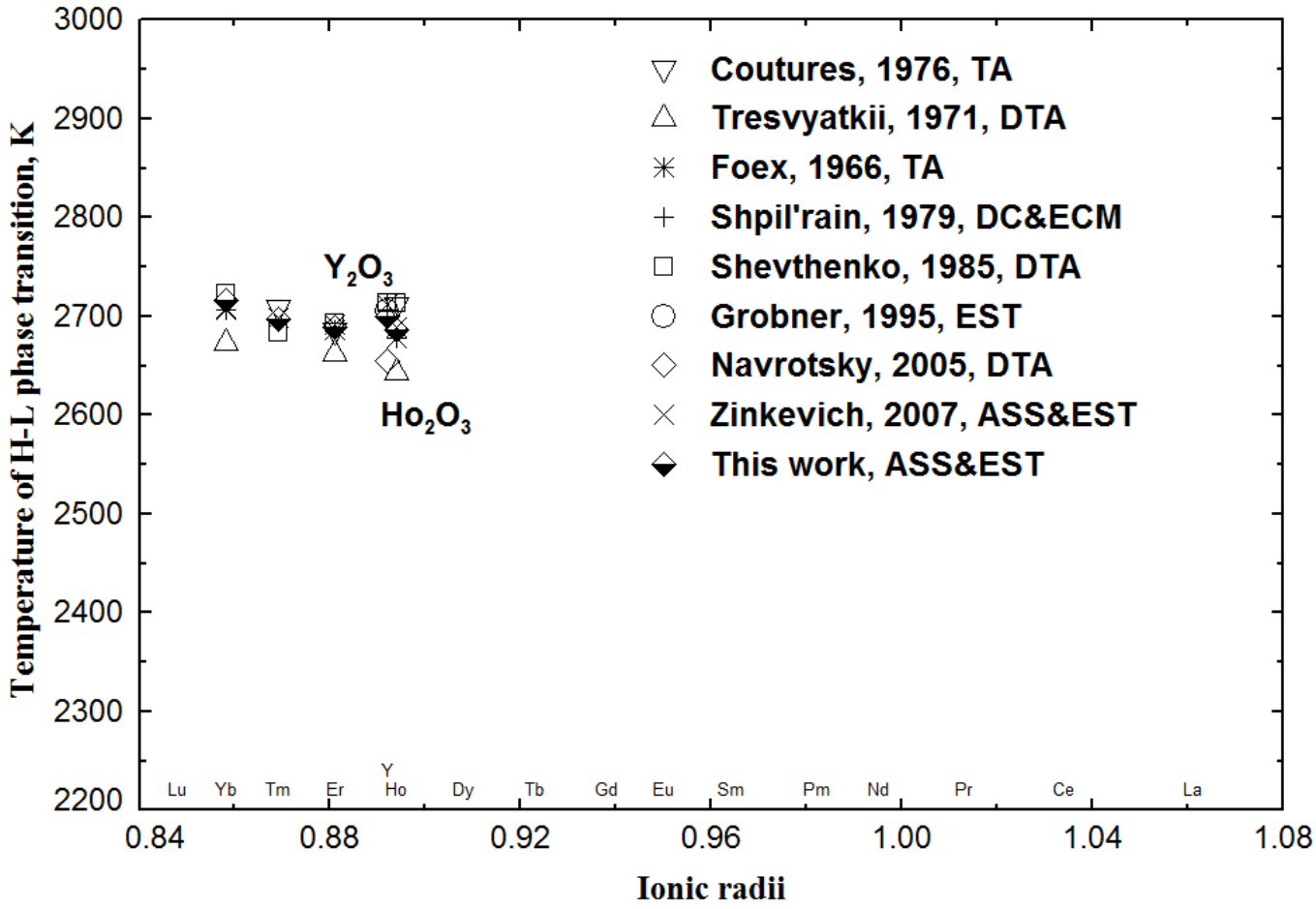

Figure 9 Summary of H→L phase transition temperatures depending on RE ionic radii; ASS: assessment; ECM: electric conductivity measurement; EST: estimation; DC: drop calorimetry; DTA: differential thermal analysis; XRD: X – ray diffraction; TA: thermal analysis; ionic radii in unit Å.

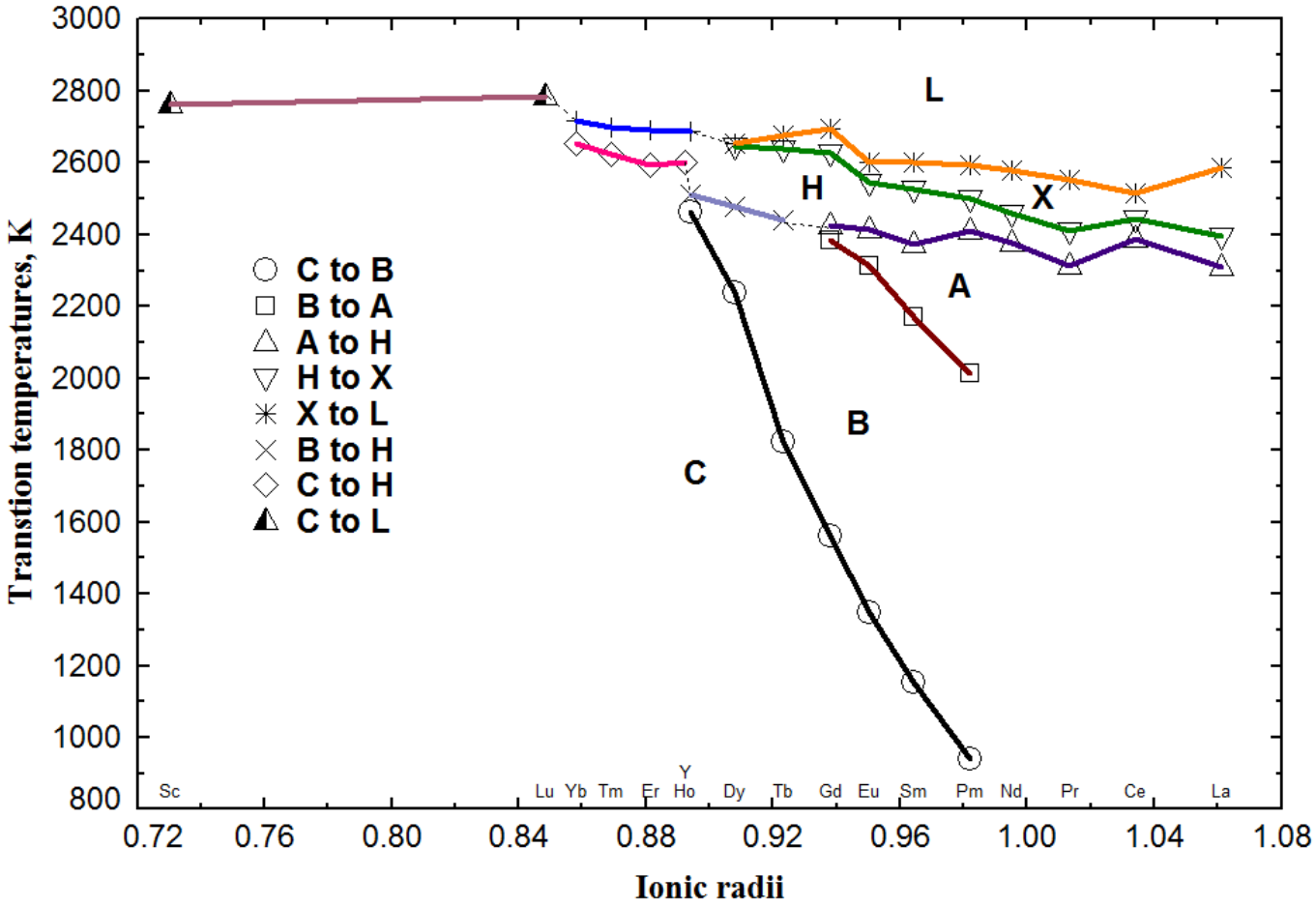

Figure 10 The optimized phase transition diagram of entire RE_2O_3 in this study; C: cubic; B: monoclinic; A: hexagonal; H: high temperature hexagonal; X: high temperature cubic; L: liquid; ionic radii in unit Å.

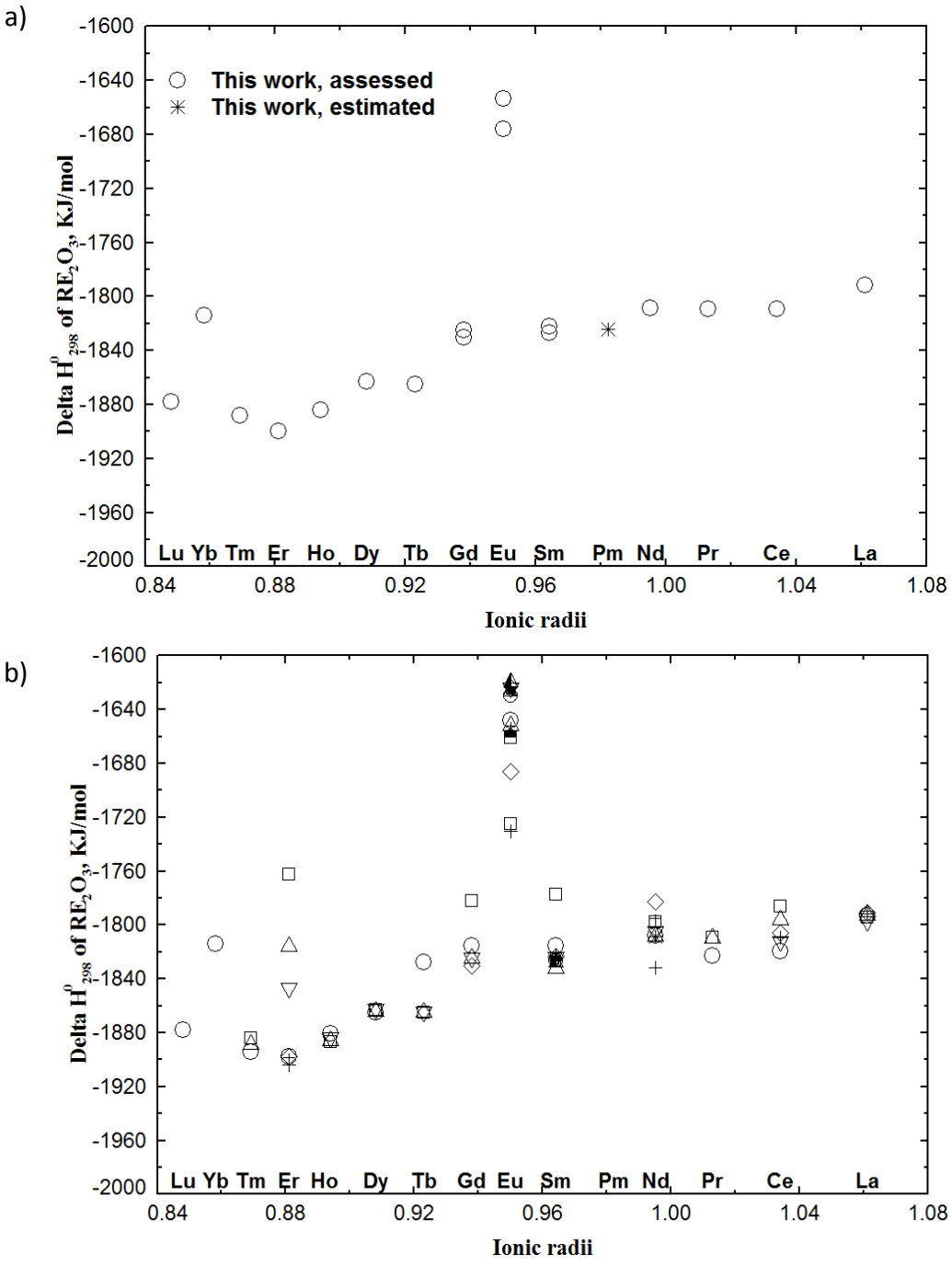

Figure 11 Standard enthalpy of formation of RE_2O_3. (a) Optimized ΔH°_{298} in this study and (b) experimental ΔH°_{298} in the literature; ionic radii in unit Å. References of (b) are listed in Table 16.

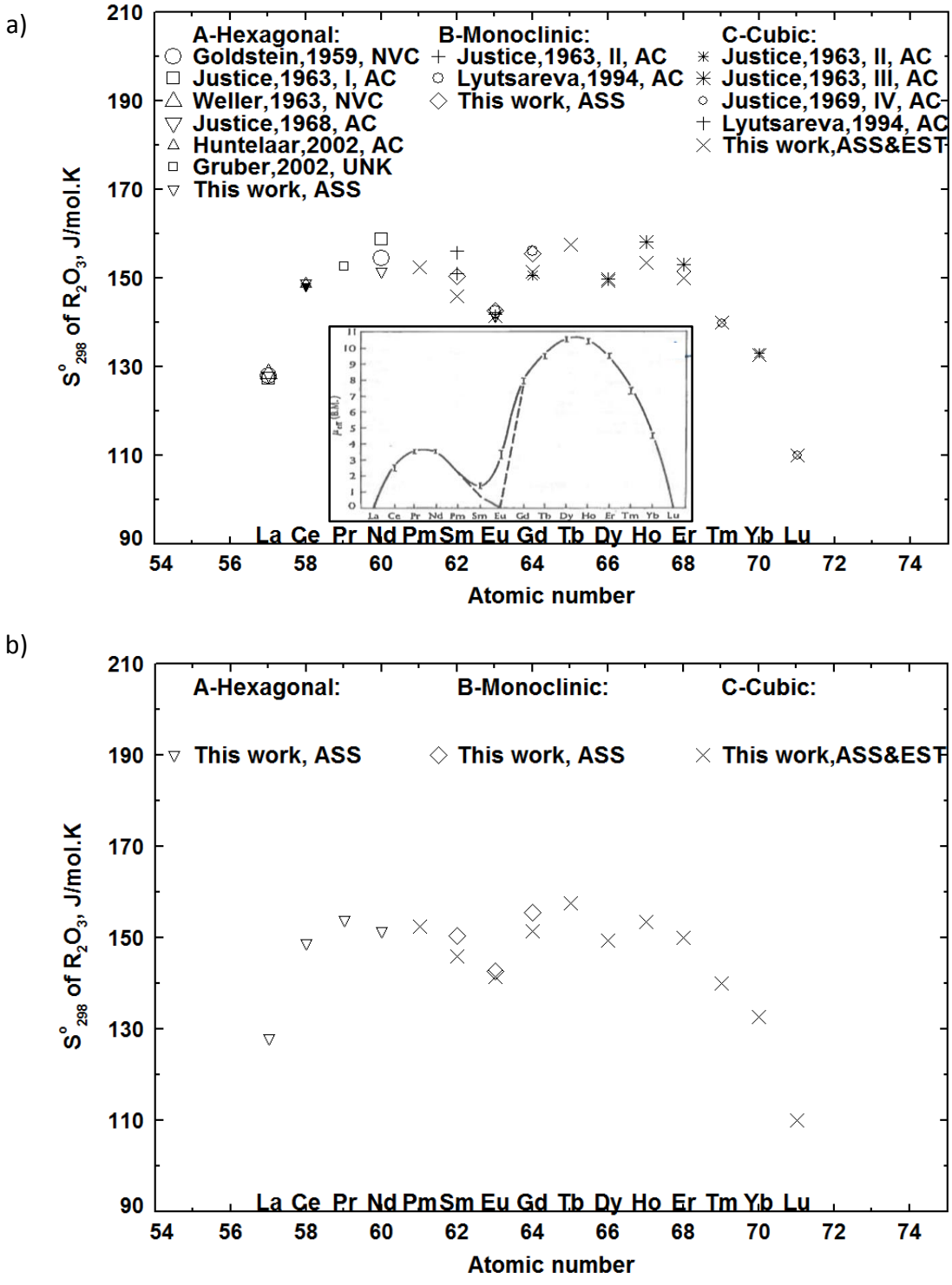

Figure 12 The standard entropies of Lanthanide sesquioxides;(a) experimental results; (b) optimized results; AC: adiabatic calorimetry; ASS: assessed; EST: estimation; NVC Nernst vacuum calorimetry; the small figure in the middle indicated the effective paramagnetic moment of RE^{3+} [145], dotted line: at 0K; solid line: at room temperature.

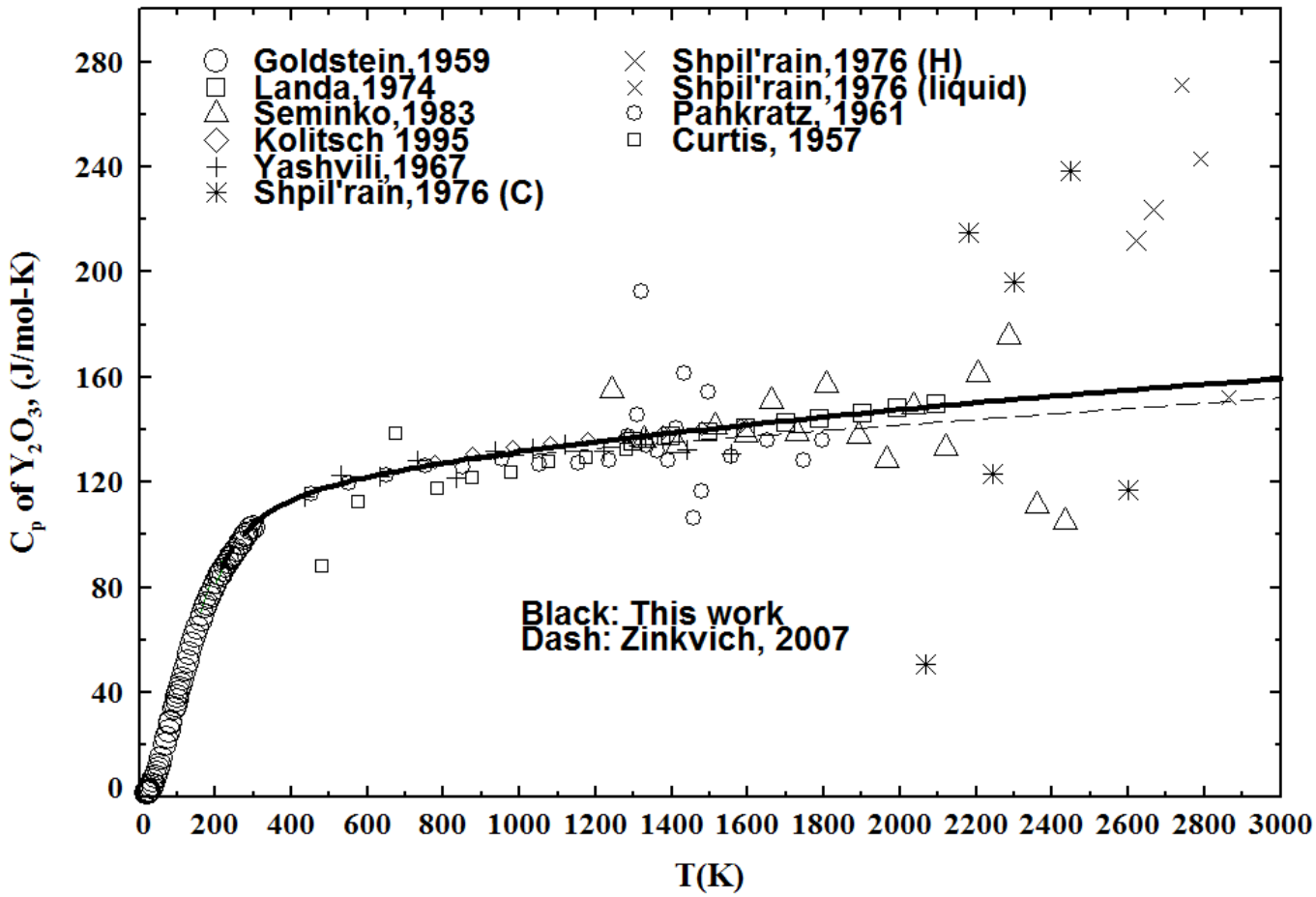

Figure 13 Optimized heat capacity of C – Y_2O_3 along with experimental data

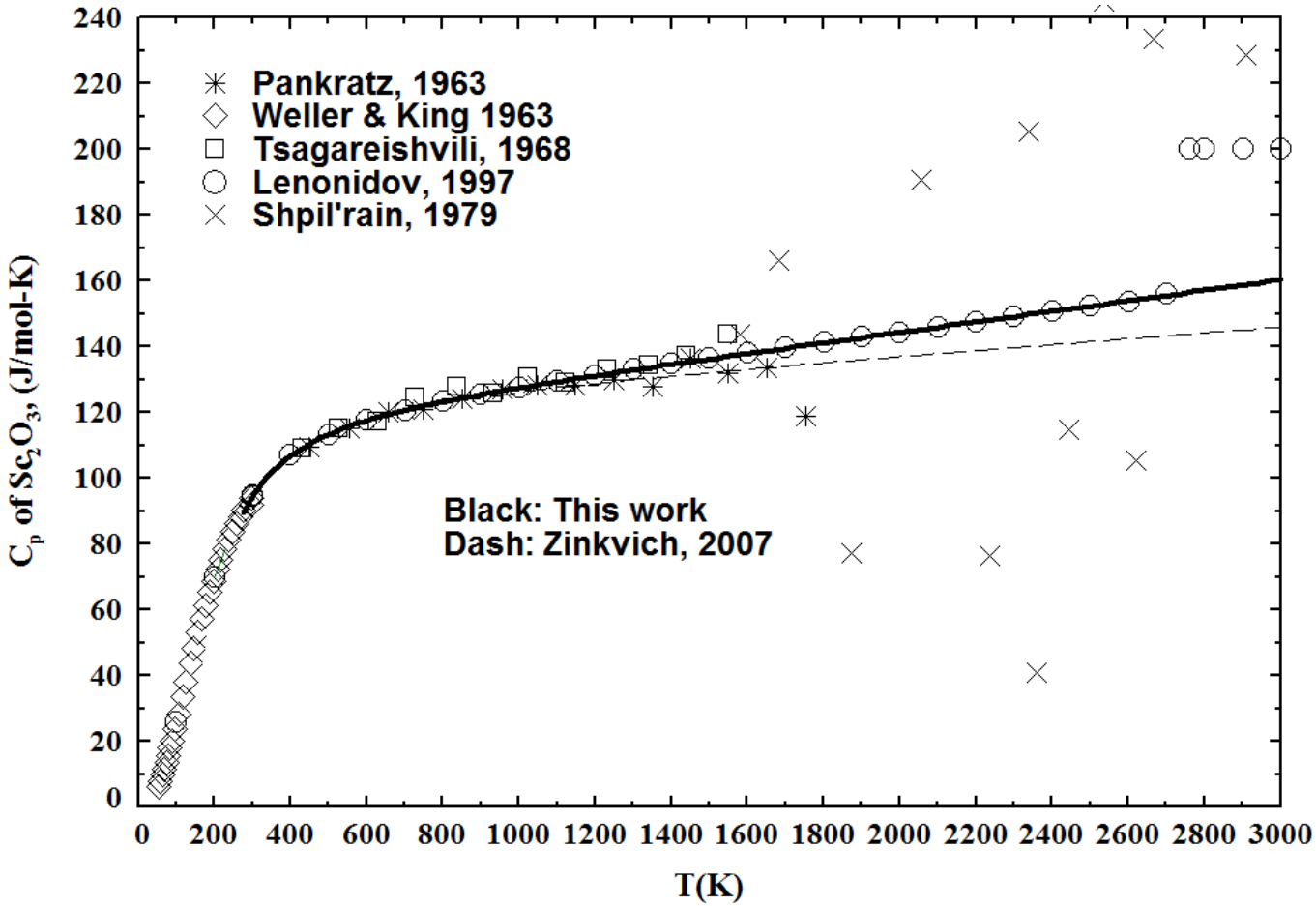

Figure 14 Optimized heat capacity of C – Sc_2O_3 along with experimental data

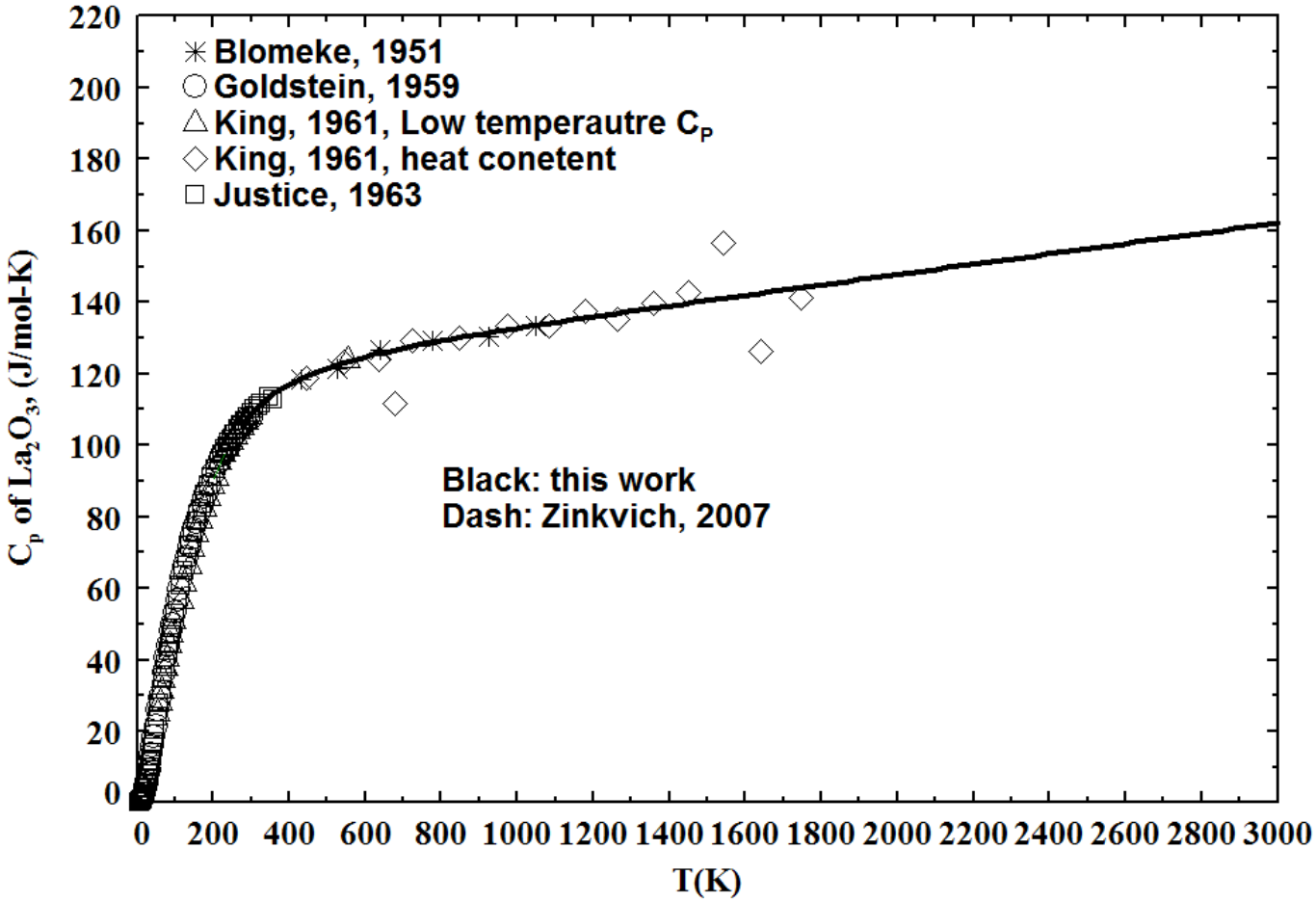

Figure 15 Optimized heat capacity of A – La_2O_3 along with experimental data

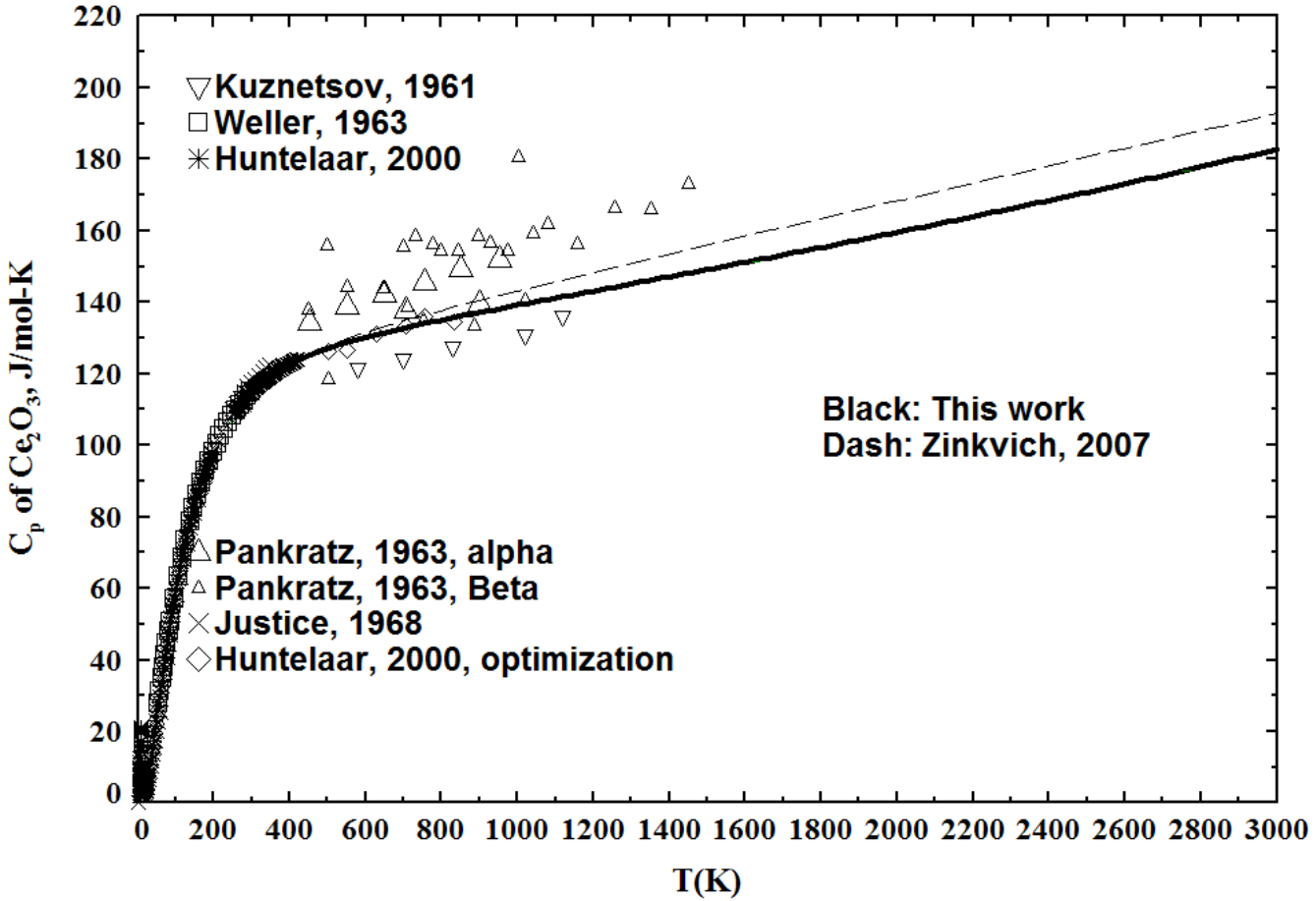

Figure 16 Optimized heat capacity of A – Ce_2O_3 along with experimental data

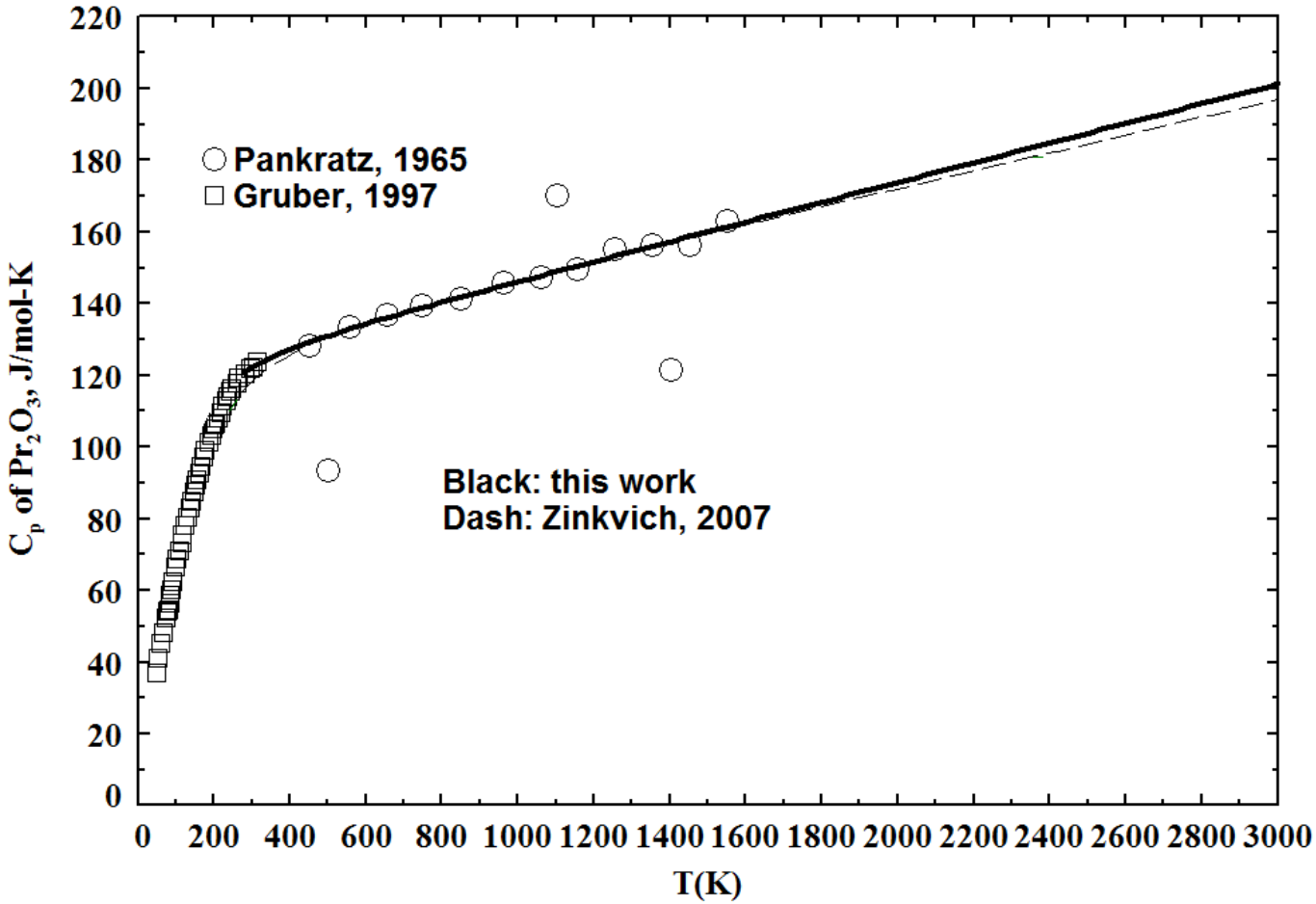

Figure 17 Optimized heat capacity of A – Pr_2O_3 along with experimental data

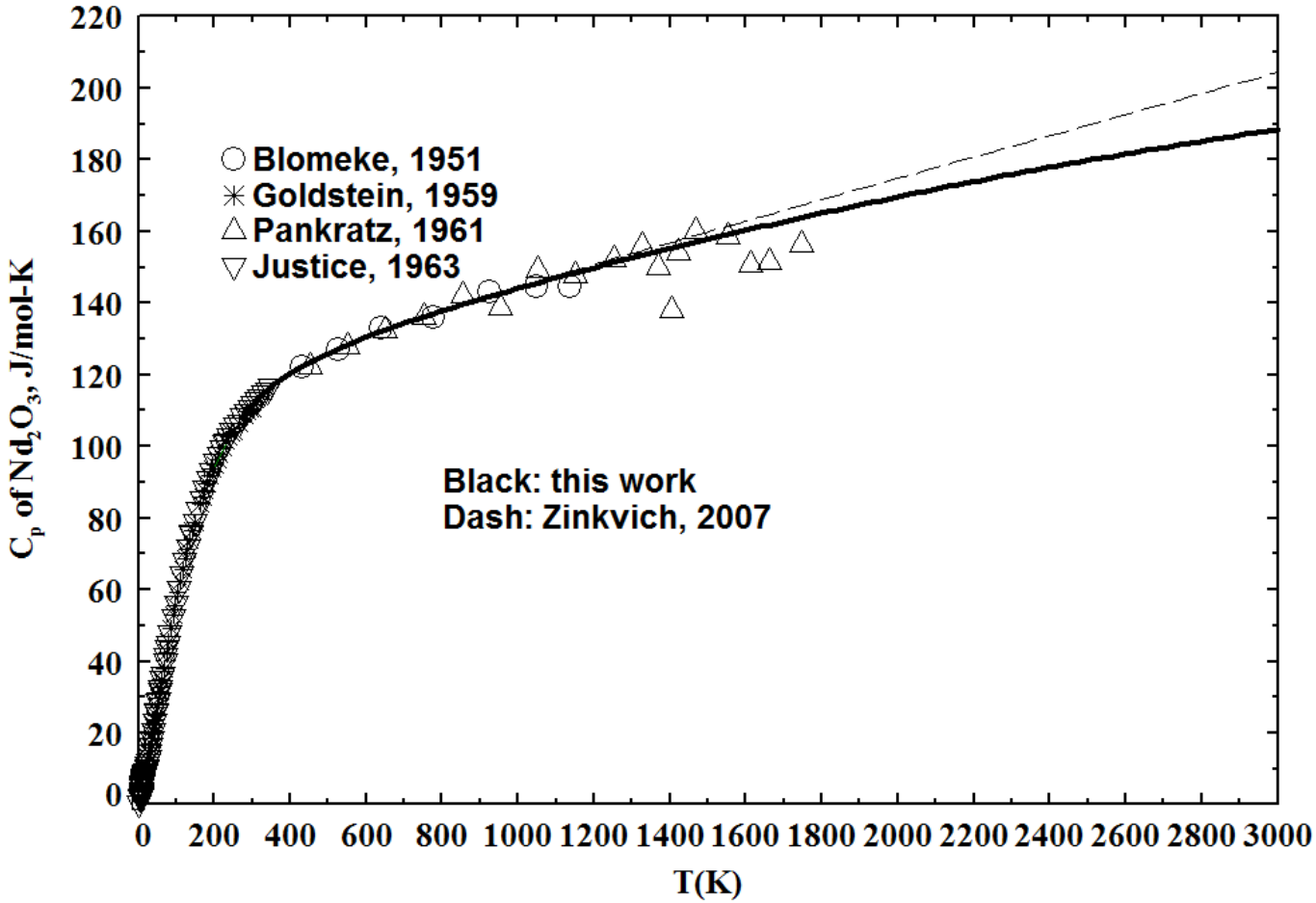

Figure 18 Optimized heat capacity of A – Nd_2O_3 along with experimental data

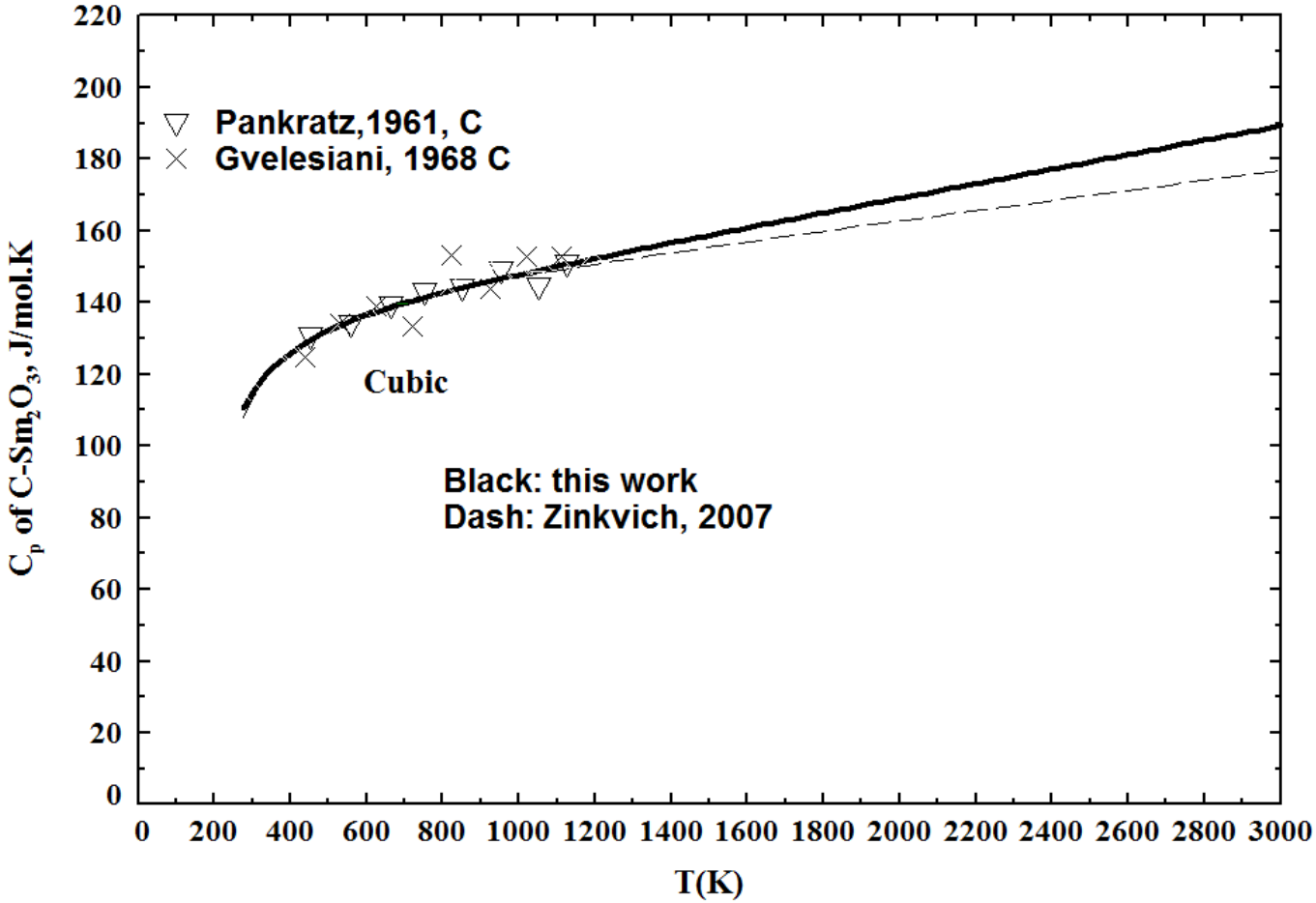

Figure 19 Optimized heat capacity of C – Sm_2O_3 along with experimental data

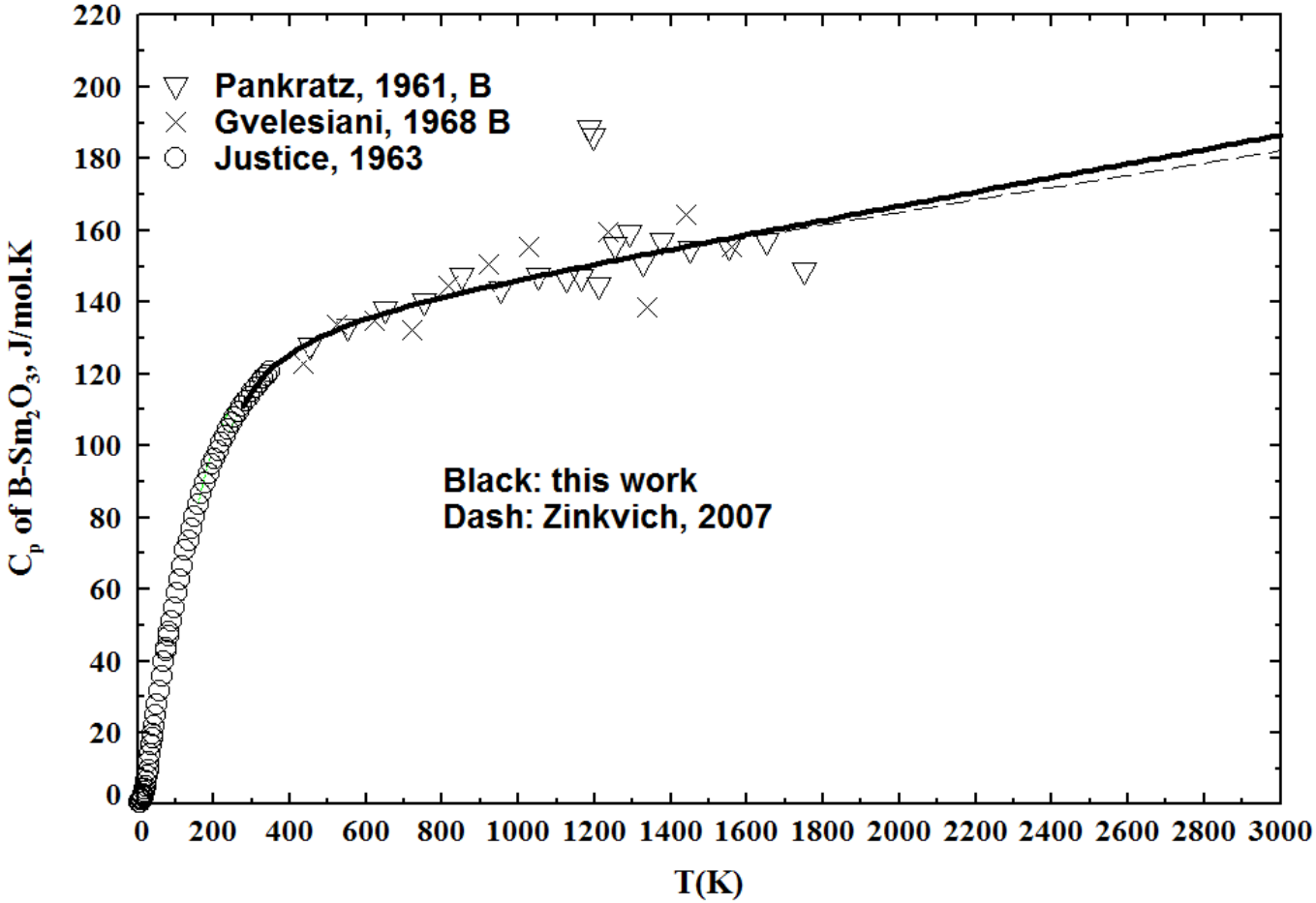

Figure 20 Optimized heat capacity of B – Sm_2O_3 along with experimental data

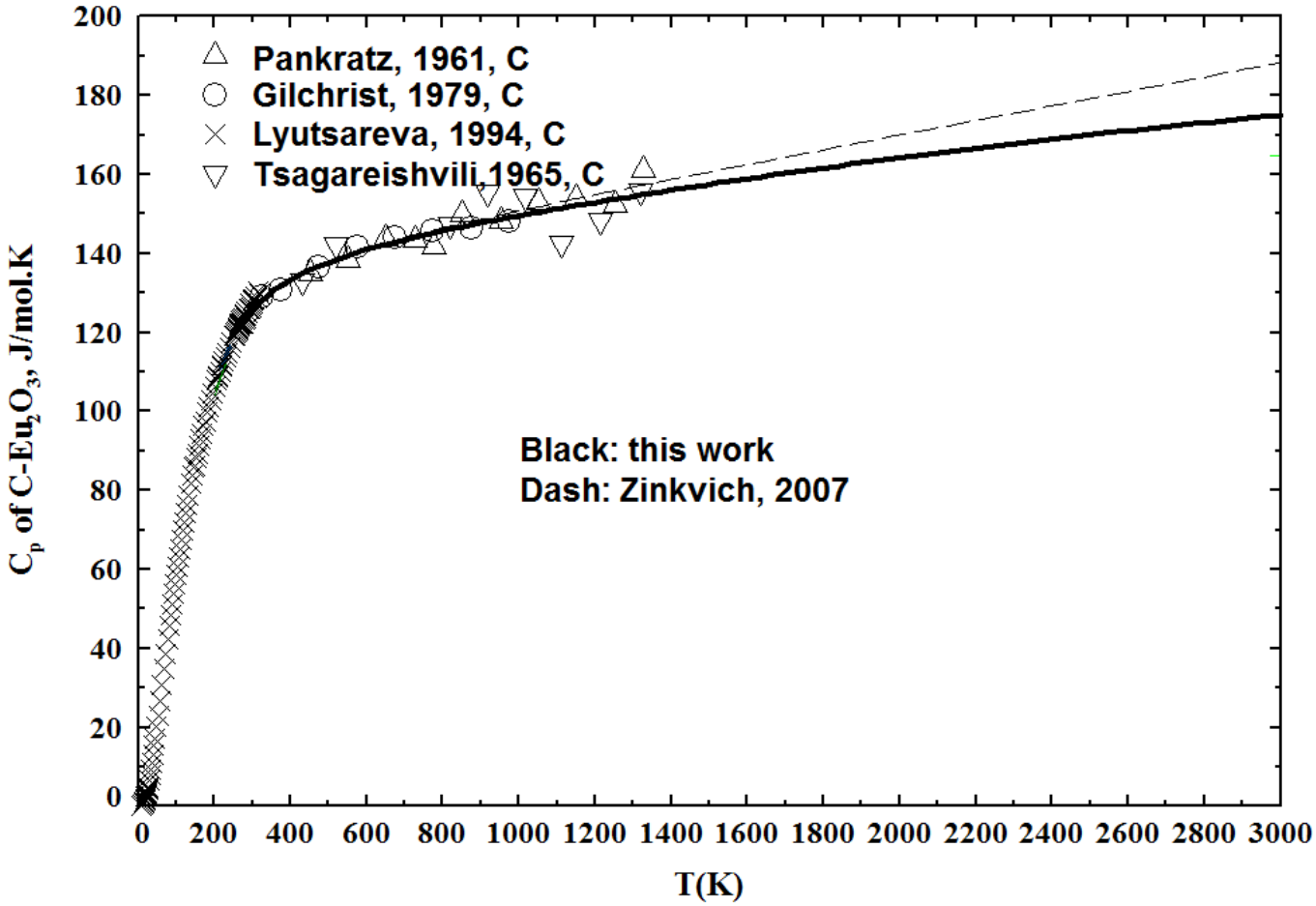

Figure 21 Optimized heat capacity of C – Eu_2O_3 along with experimental data

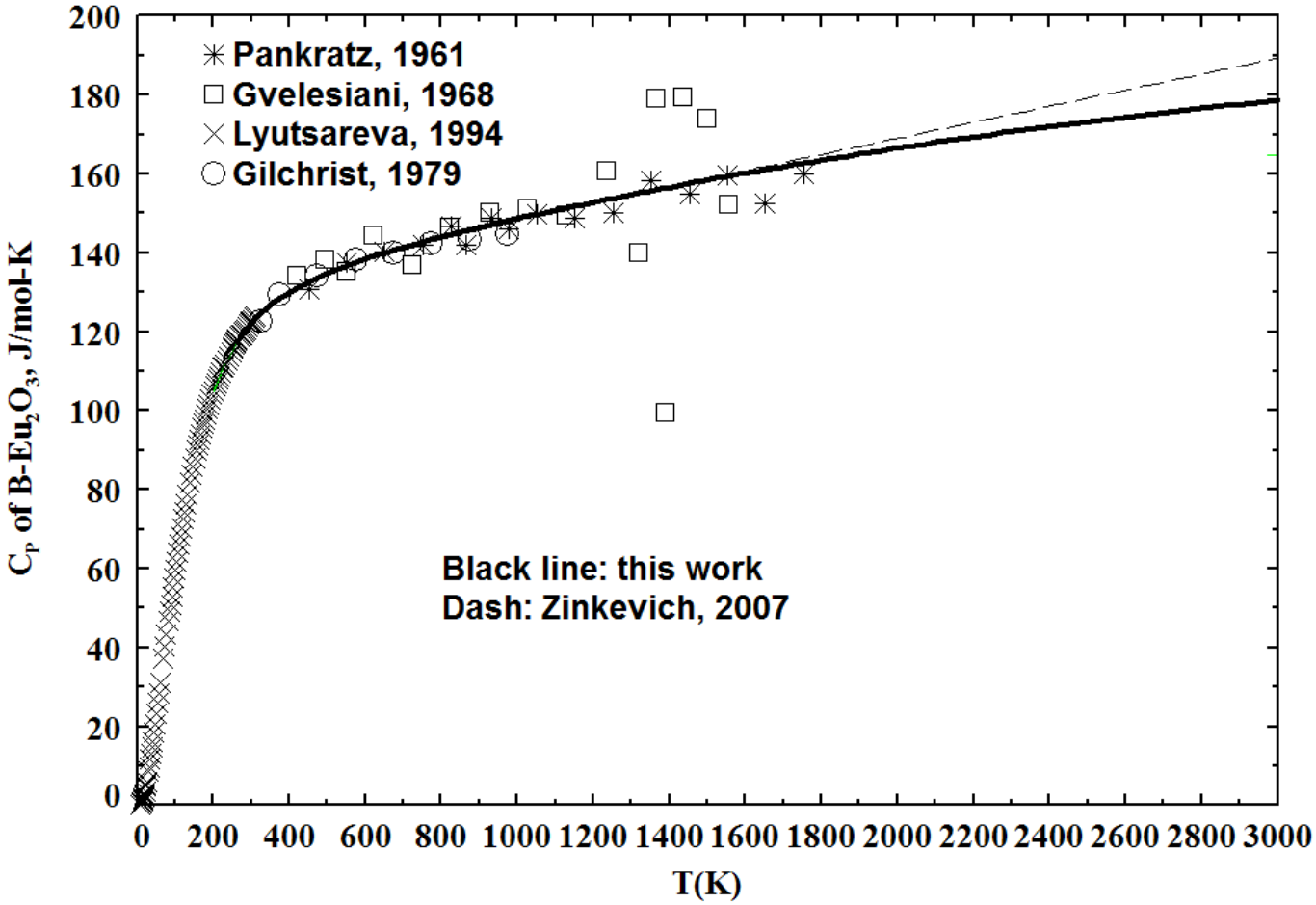

Figure 22 Optimized heat capacity of B – Eu_2O_3 along with experimental data

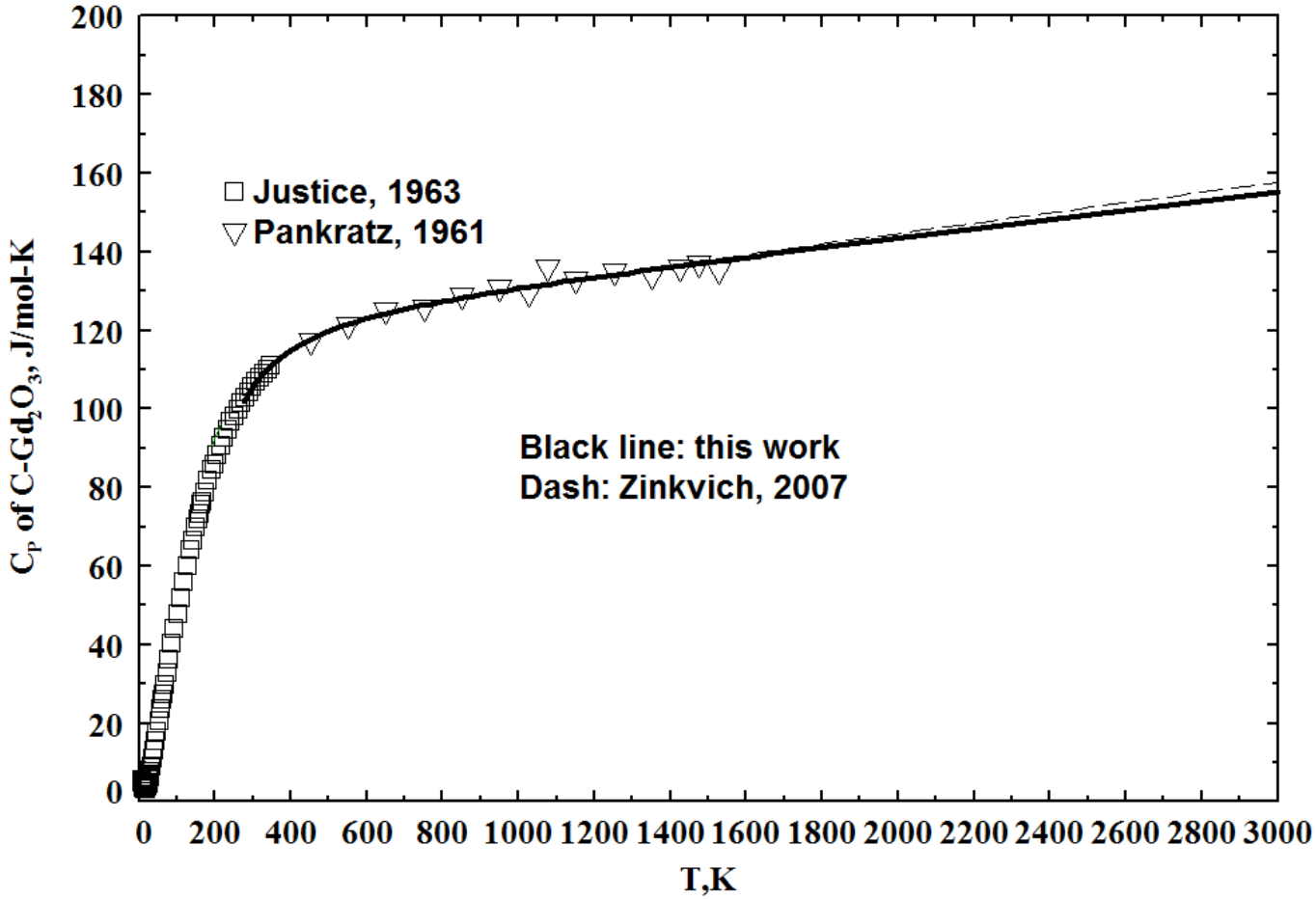

Figure 23 Optimized heat capacity of C – Gd_2O_3 along with experimental data

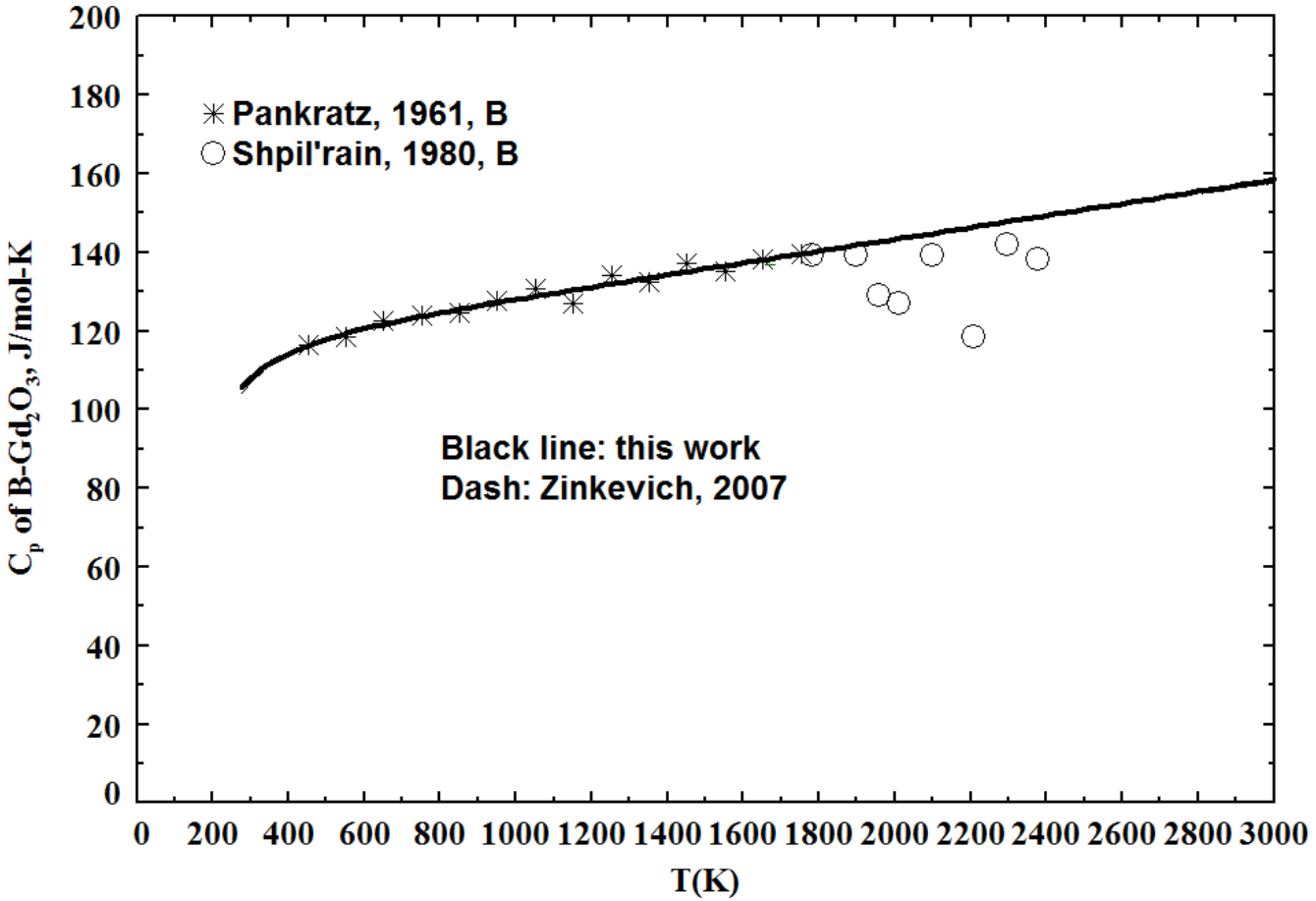

Figure 24 Optimized heat capacity of B – Gd_2O_3 along with experimental data

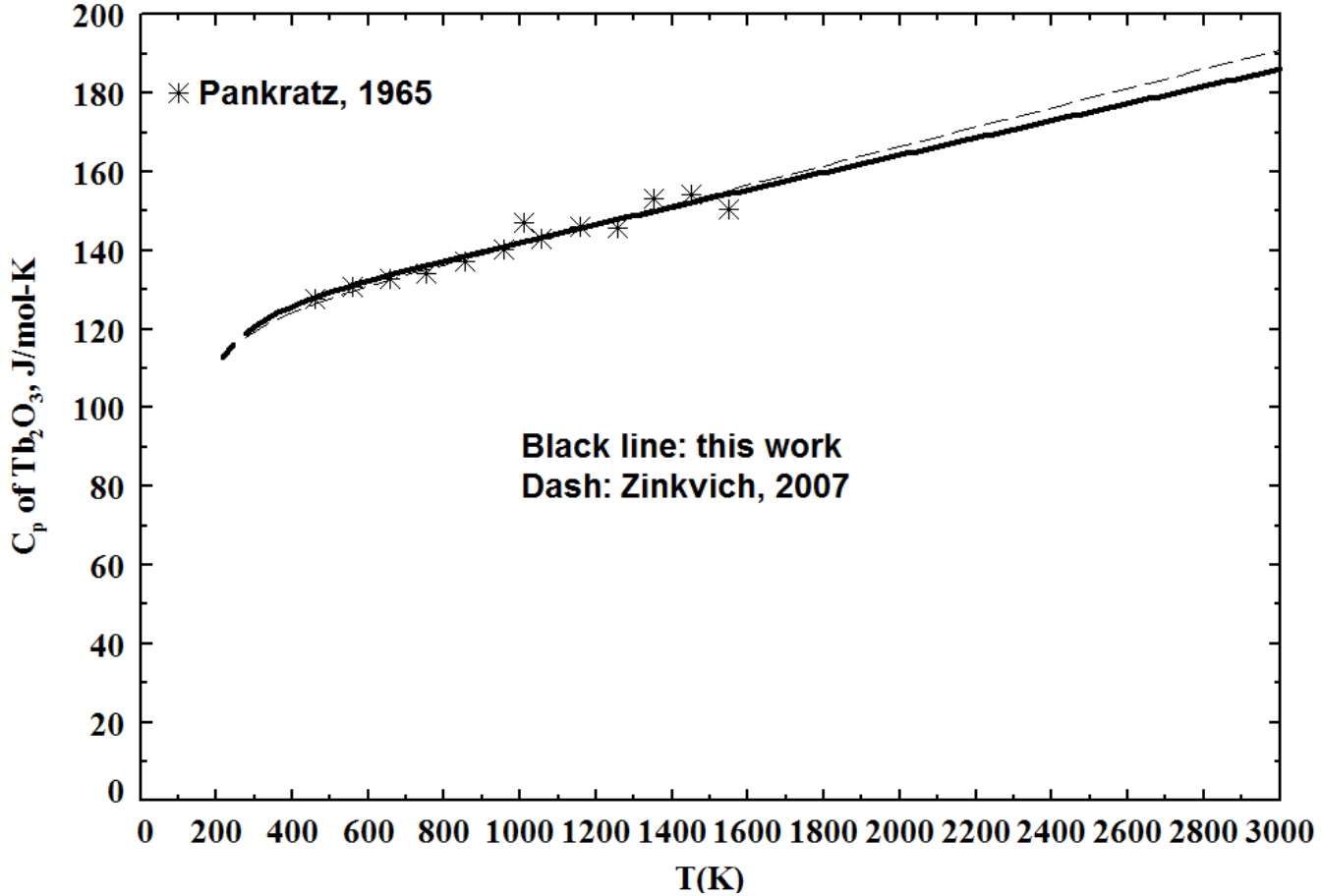

Figure 25 Optimized heat capacity of C – Tb_2O_3 along with experimental data

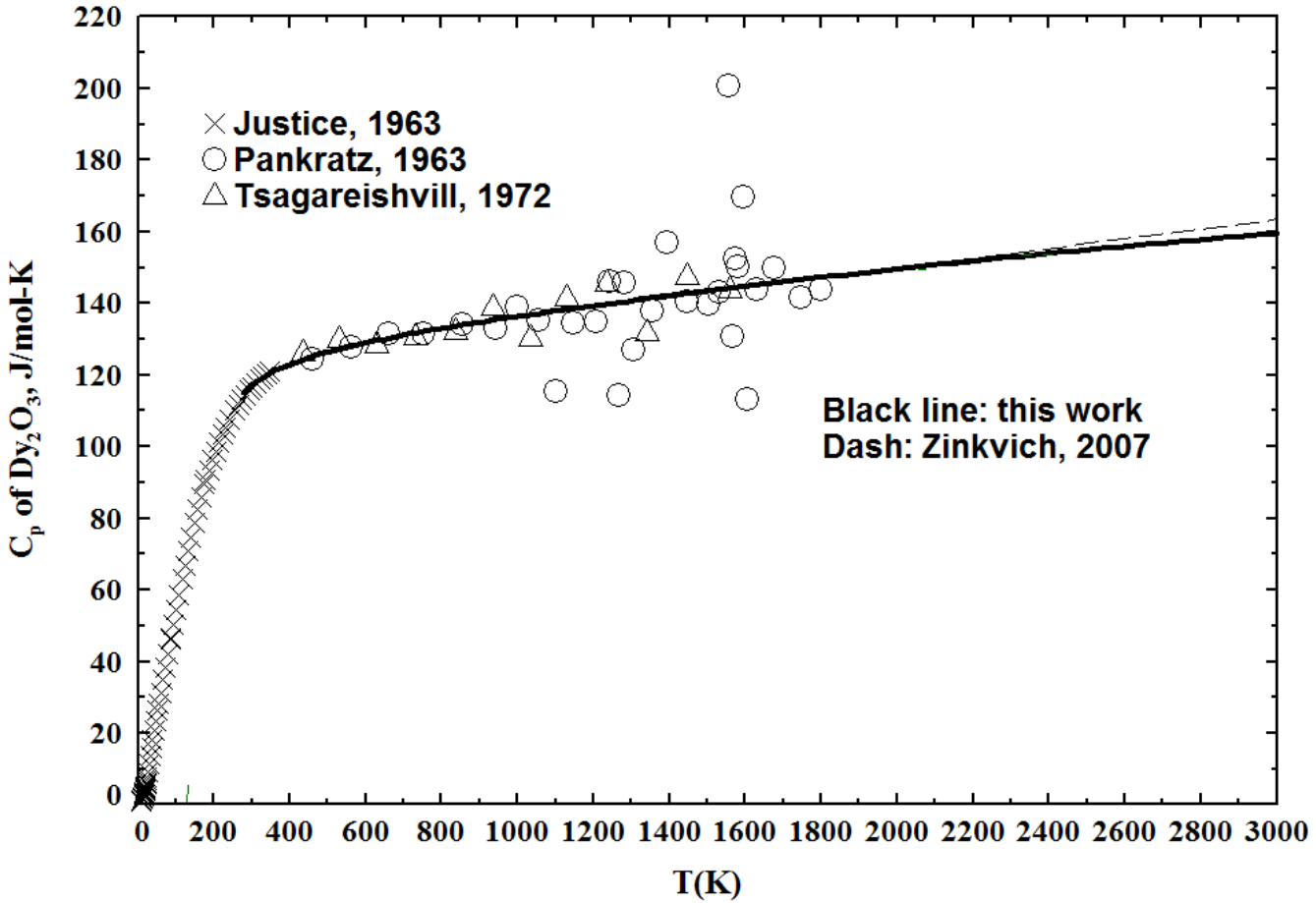

Figure 26 Optimized heat capacity of C – Dy_2O_3 along with experimental data

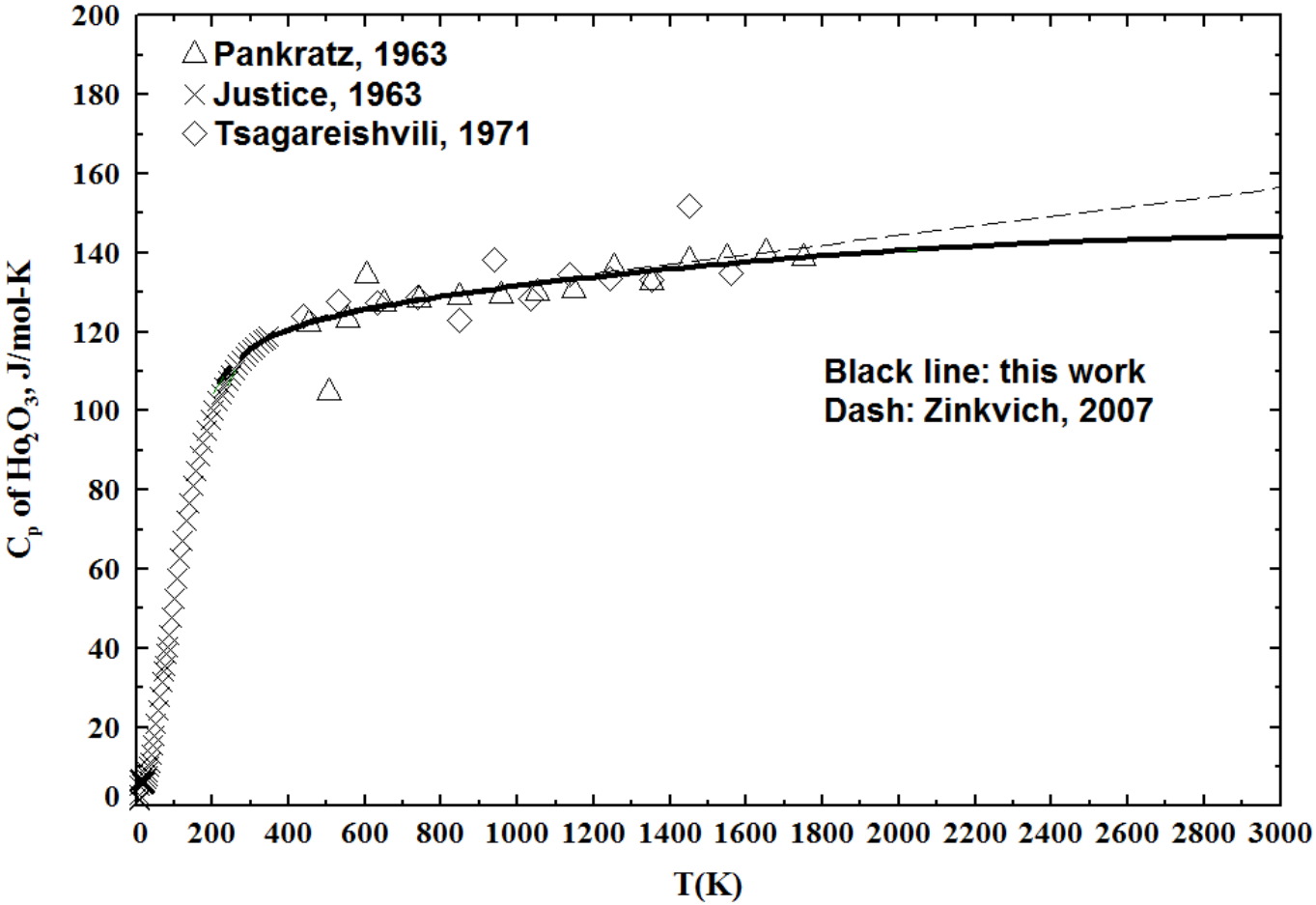

Figure 27 Optimized heat capacity of C – Ho_2O_3 along with experimental data

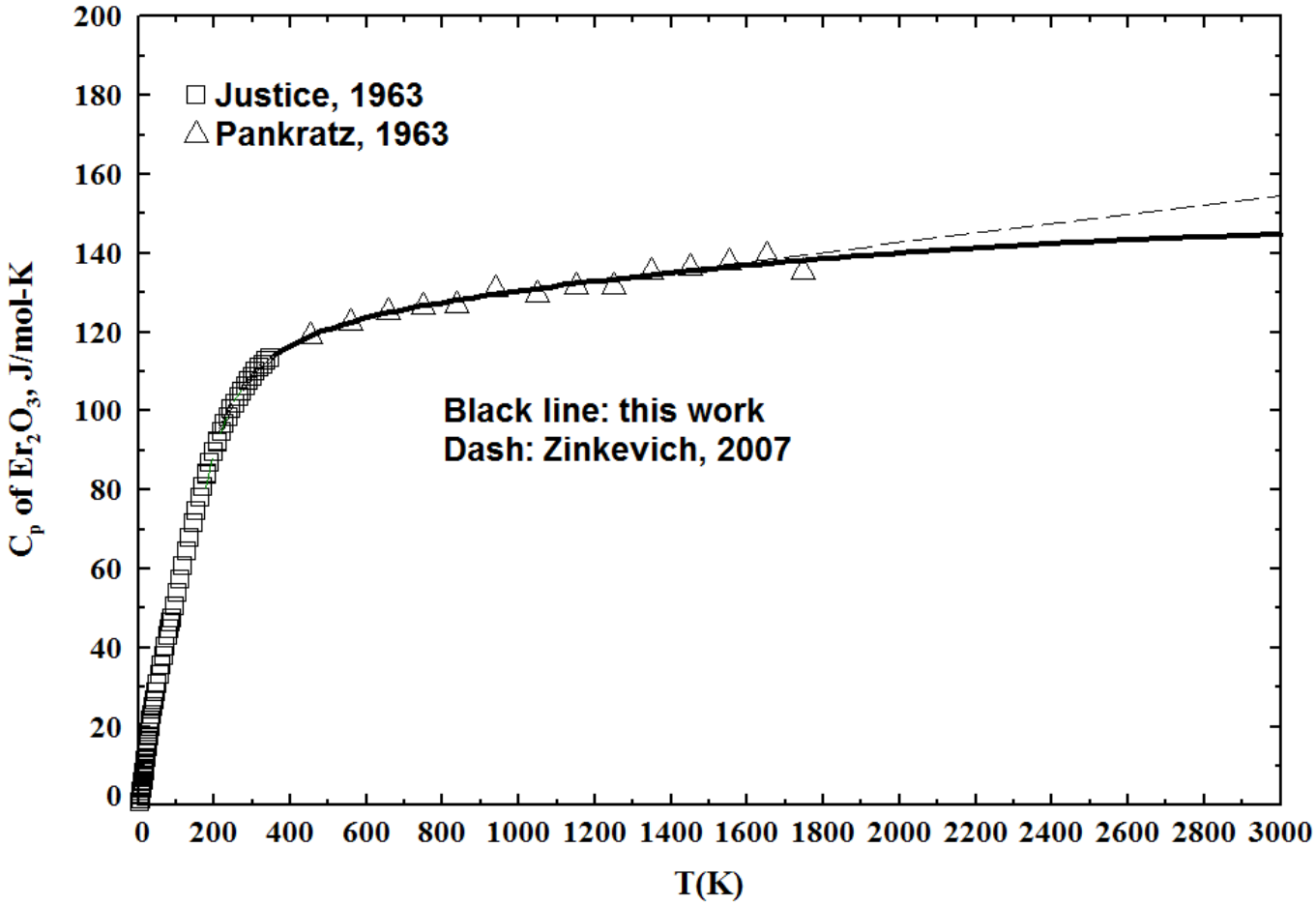

Figure 28 Optimized heat capacity of C – Er_2O_3 along with experimental data

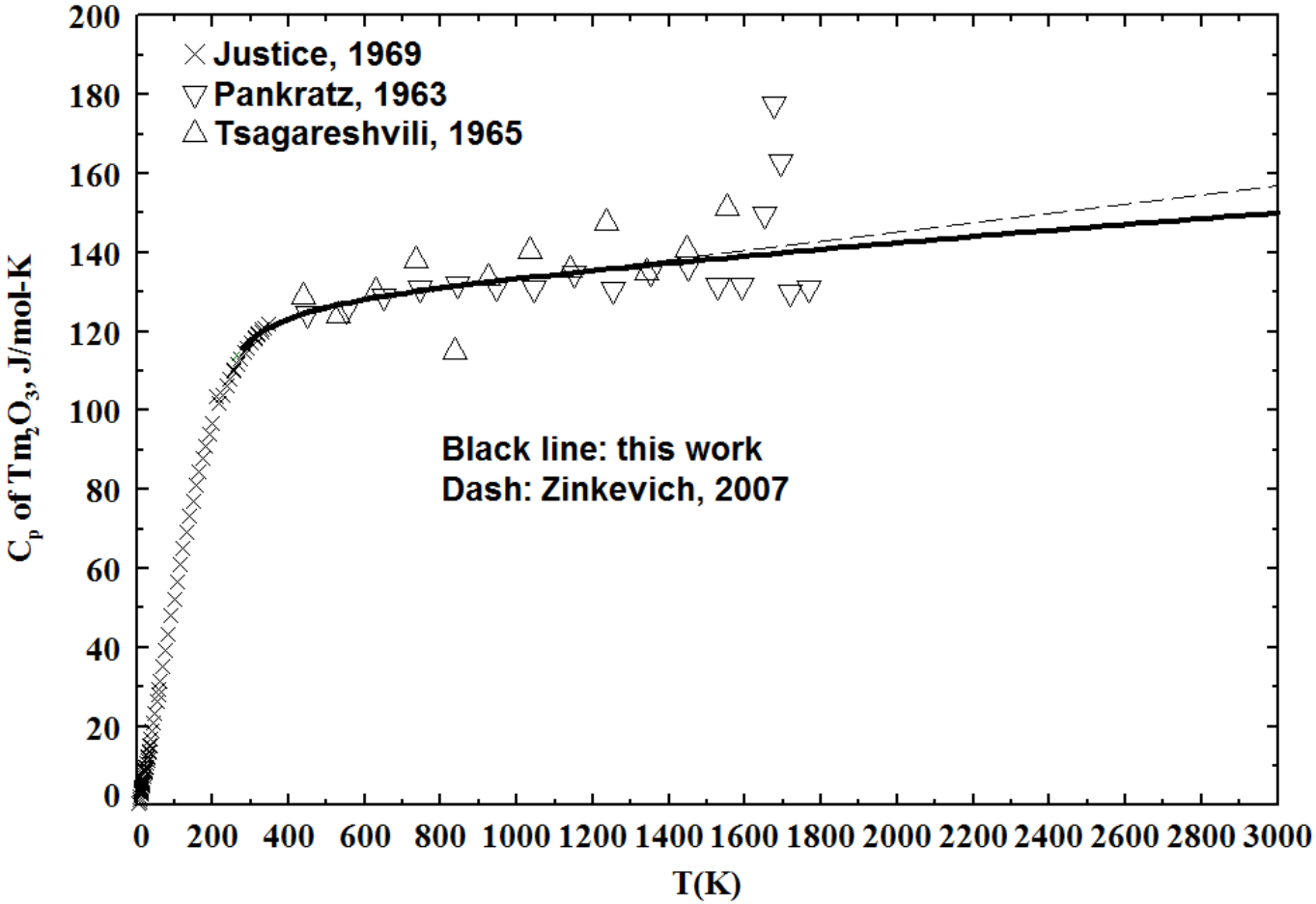

Figure 29 Optimized heat capacity of C – Tm_2O_3 along with experimental data

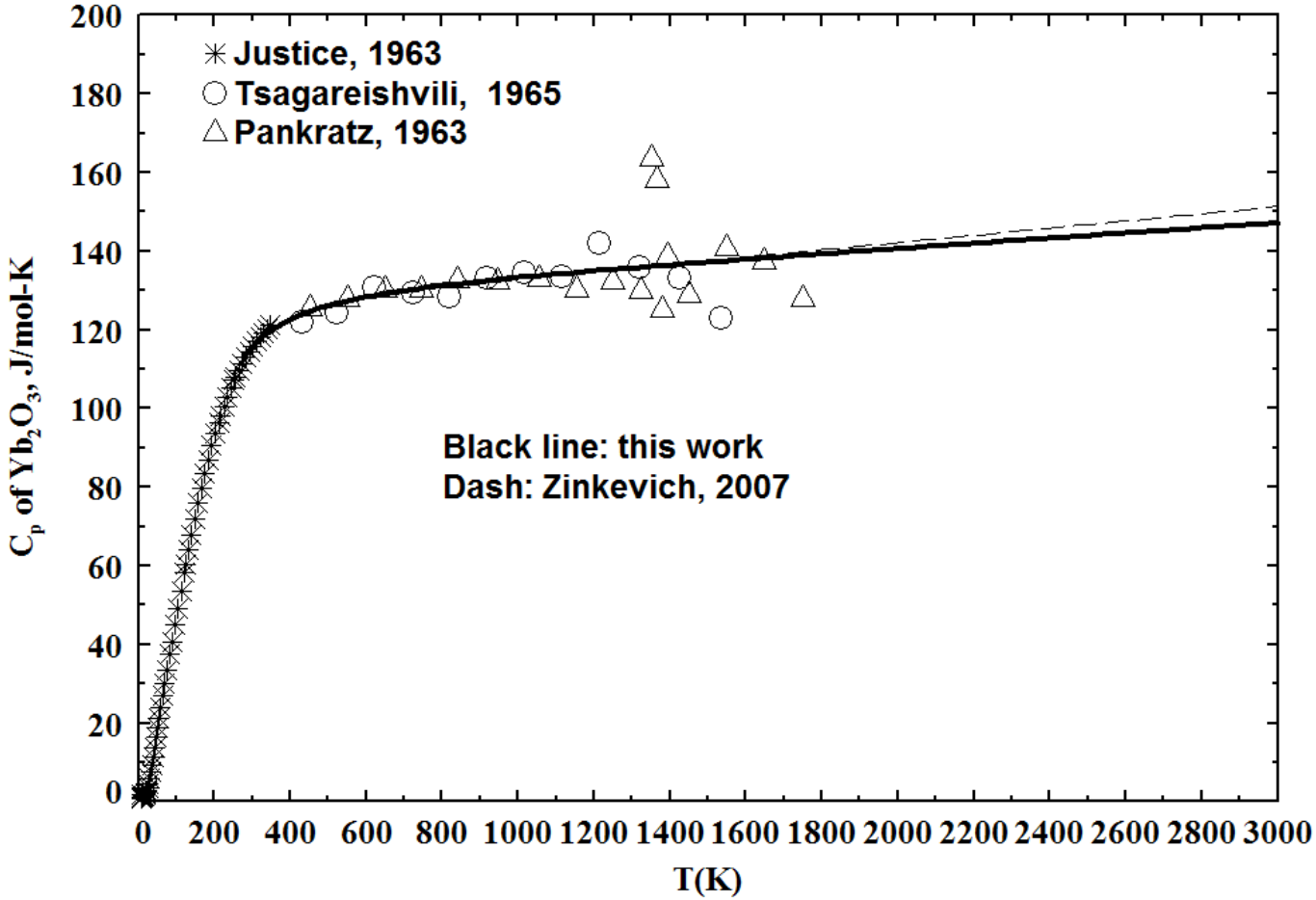

Figure 30 Optimized heat capacity of C – Yb_2O_3 along with experimental data

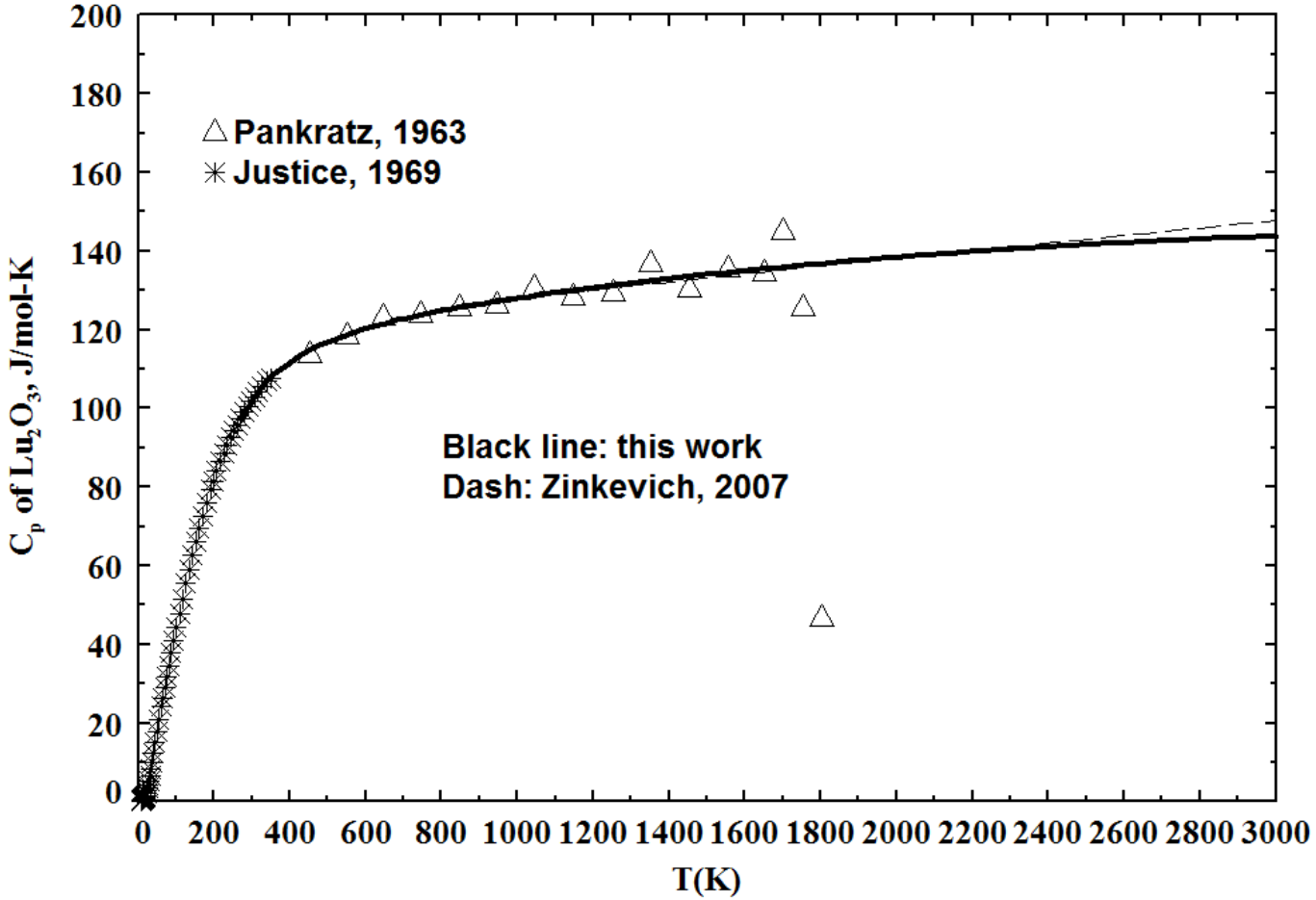

Figure 31 Optimized heat capacity of C – Lu_2O_3 along with experimental data

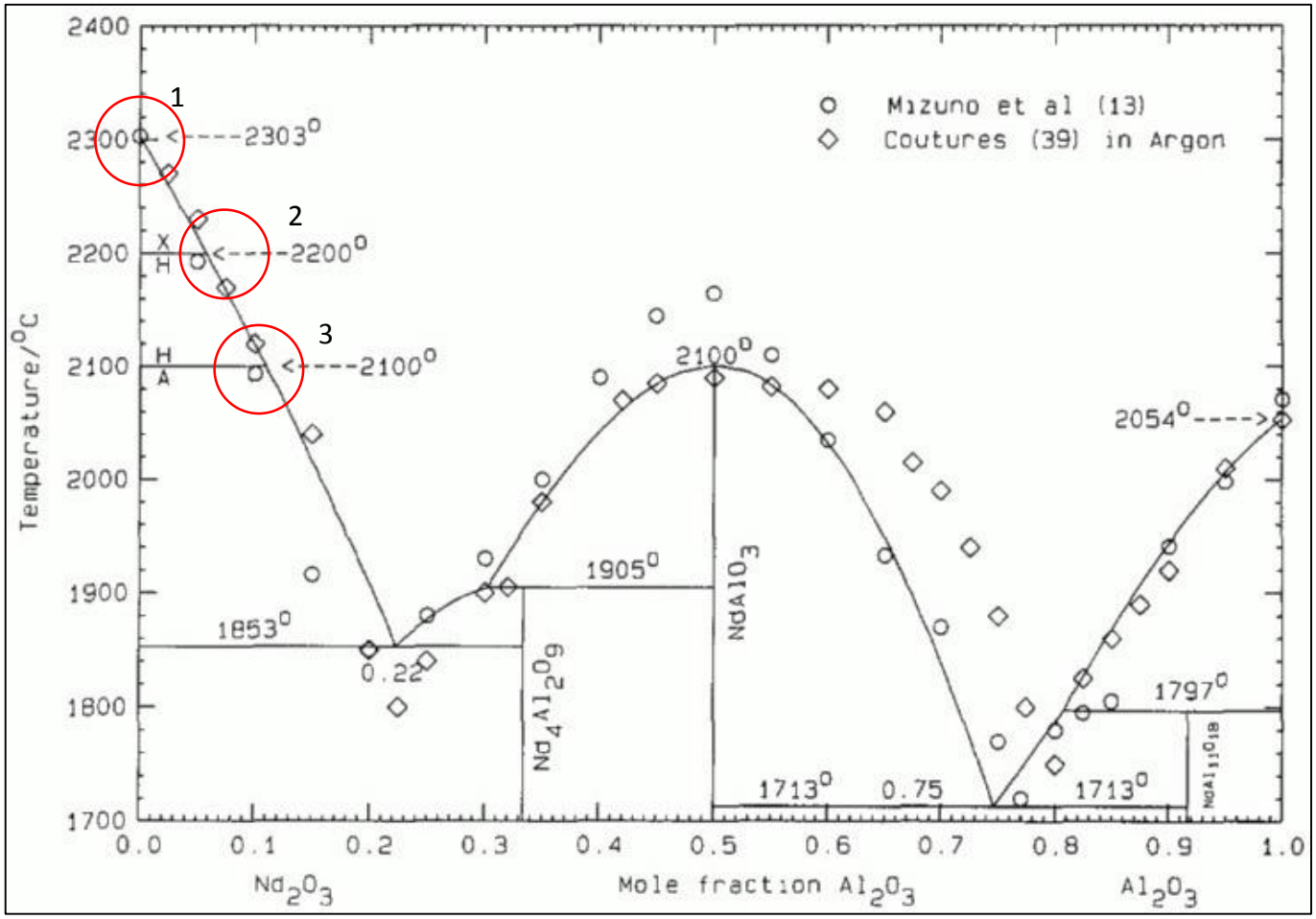

Figure 32 The optimized phase diagram of the Nd_2O_3 – Al_2O_3 [28] system along with expermental data by Mizuno et al., [26] and Coutures [147]

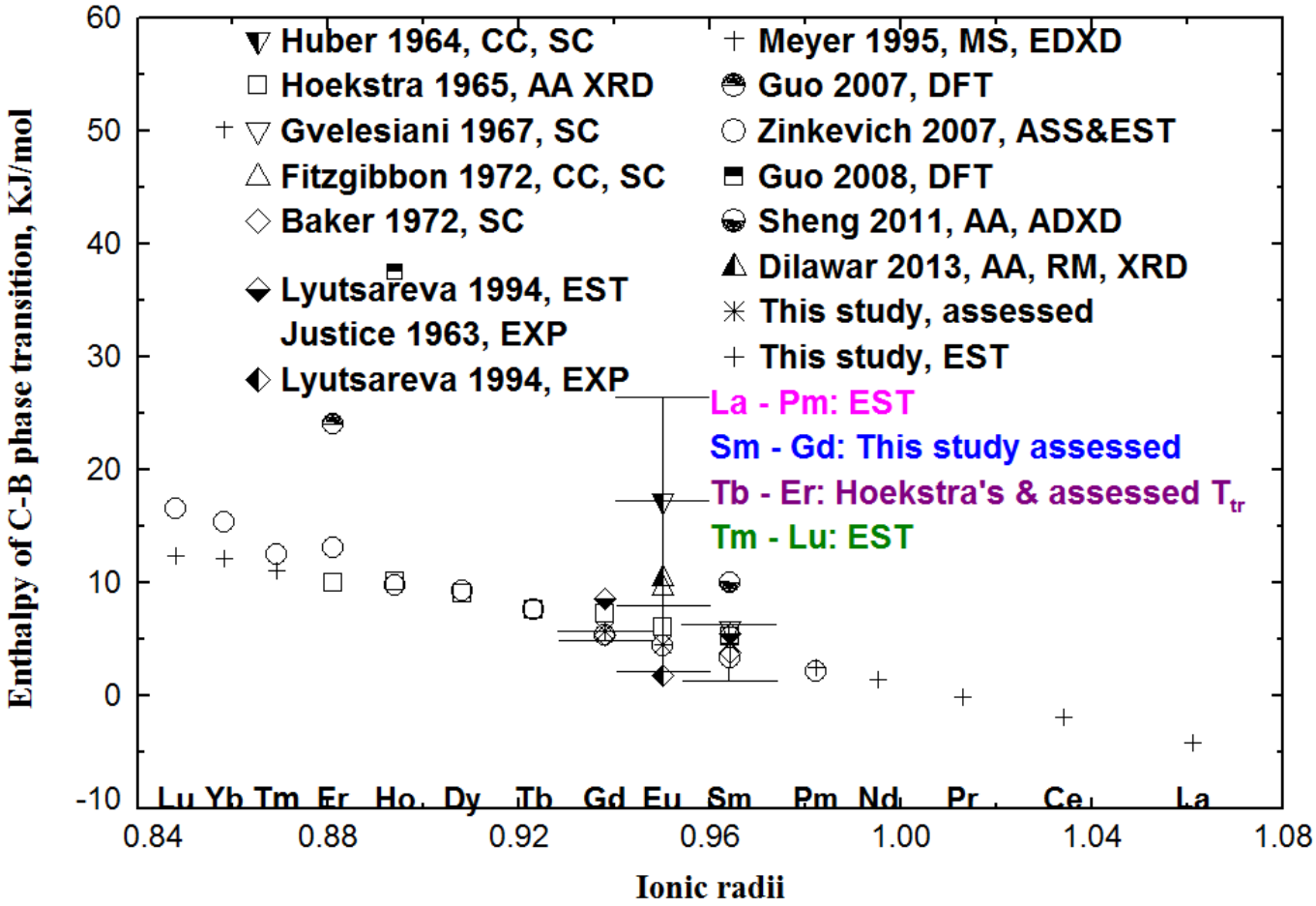

Figure 33 The summary of the enthalpies of C→B phase transition of RE_2O_3; AA: anvil apparatus; ADXD: angled dispersive X-ray diffraction; CC: combustion calorimetry; DFT: density functional theory; EDXD: energy dispersive X-ray diffraction; EST: estimation; MS: Mössbauer spectroscopy; RM: Raman; XRD: X-ray diffraction; SC: solution calorimetry; ionic radii in unit Å

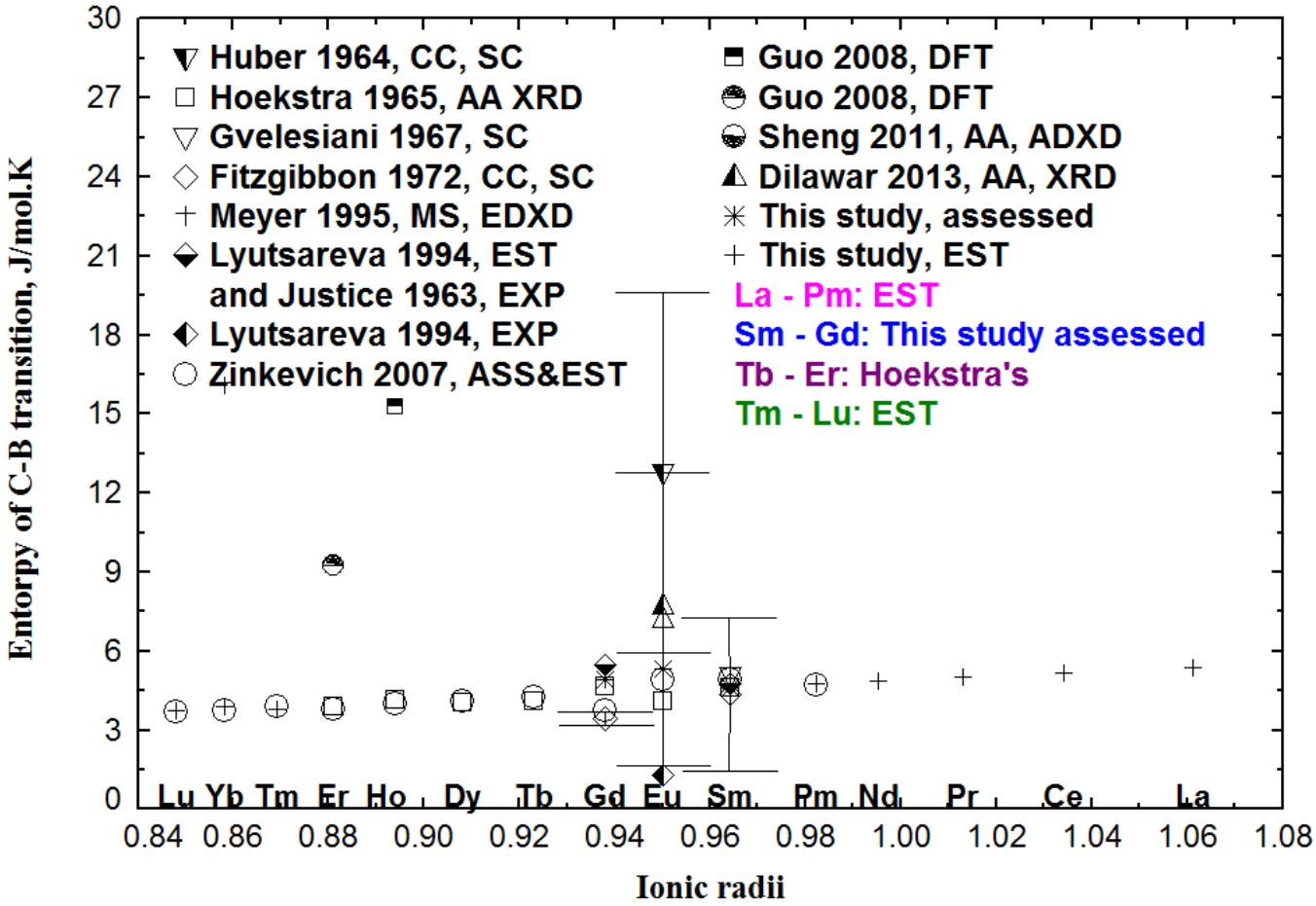

Figure 34 Summary of the entropies of C→B phase transition of RE_2O_3; AA: anvil apparatus; ADXD: angled dispersive X-ray diffraction; CC: combustion calorimetry; DFT: density functional theory; EDXD: energy dispersive X-ray diffraction; EST: estimation; XRD: X-ray diffraction; SC: solution calorimetry; ionic radii in unit Å

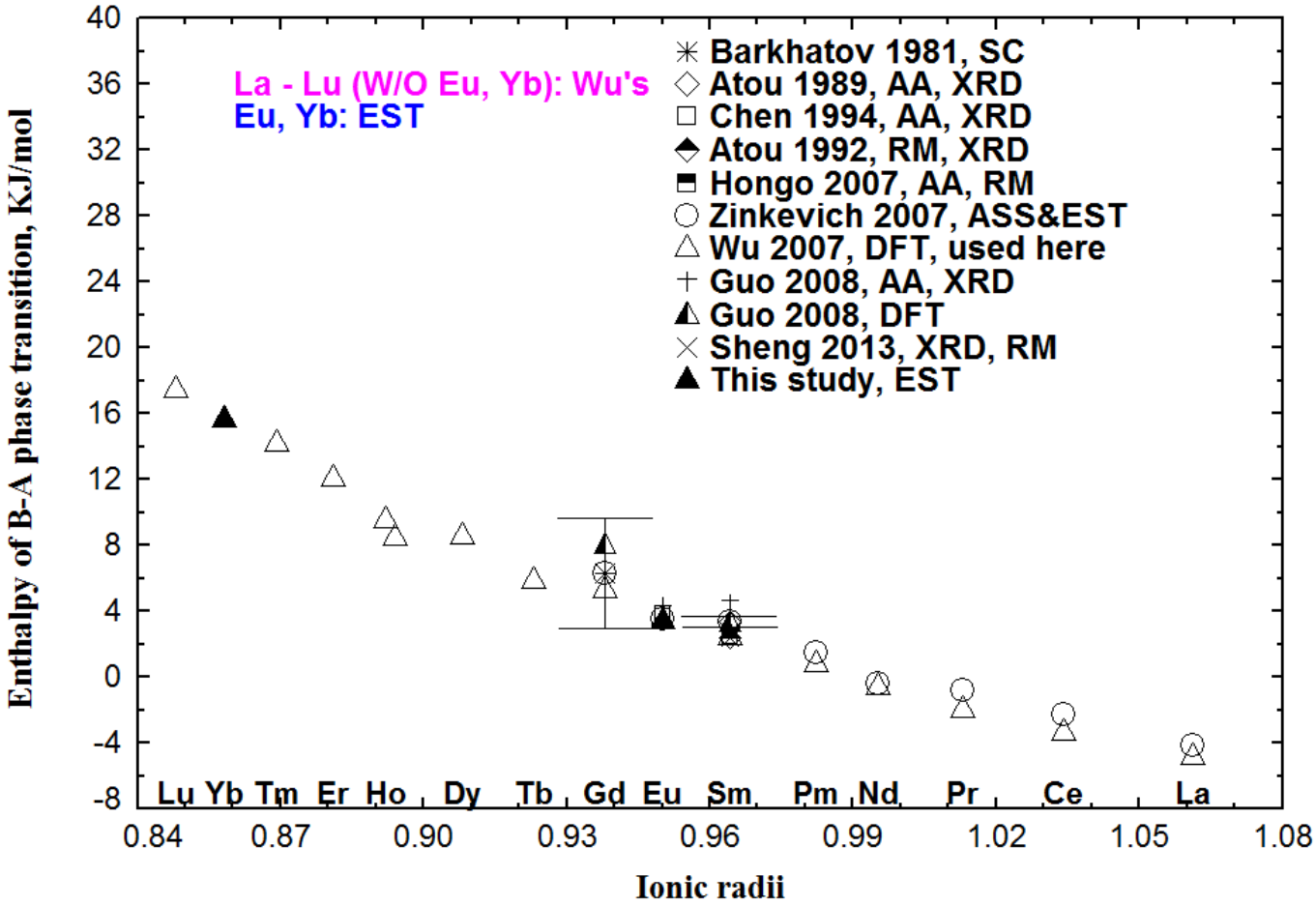

Figure 35 Summary of the enthalpies of B→A phase transition of RE_2O_3; AA: anvil apparatus; CC: combustion; DFT: density functional theory; EST: estimation; XRD: X-ray diffraction; SC: solution calorimetry; ionic radii in unit Å

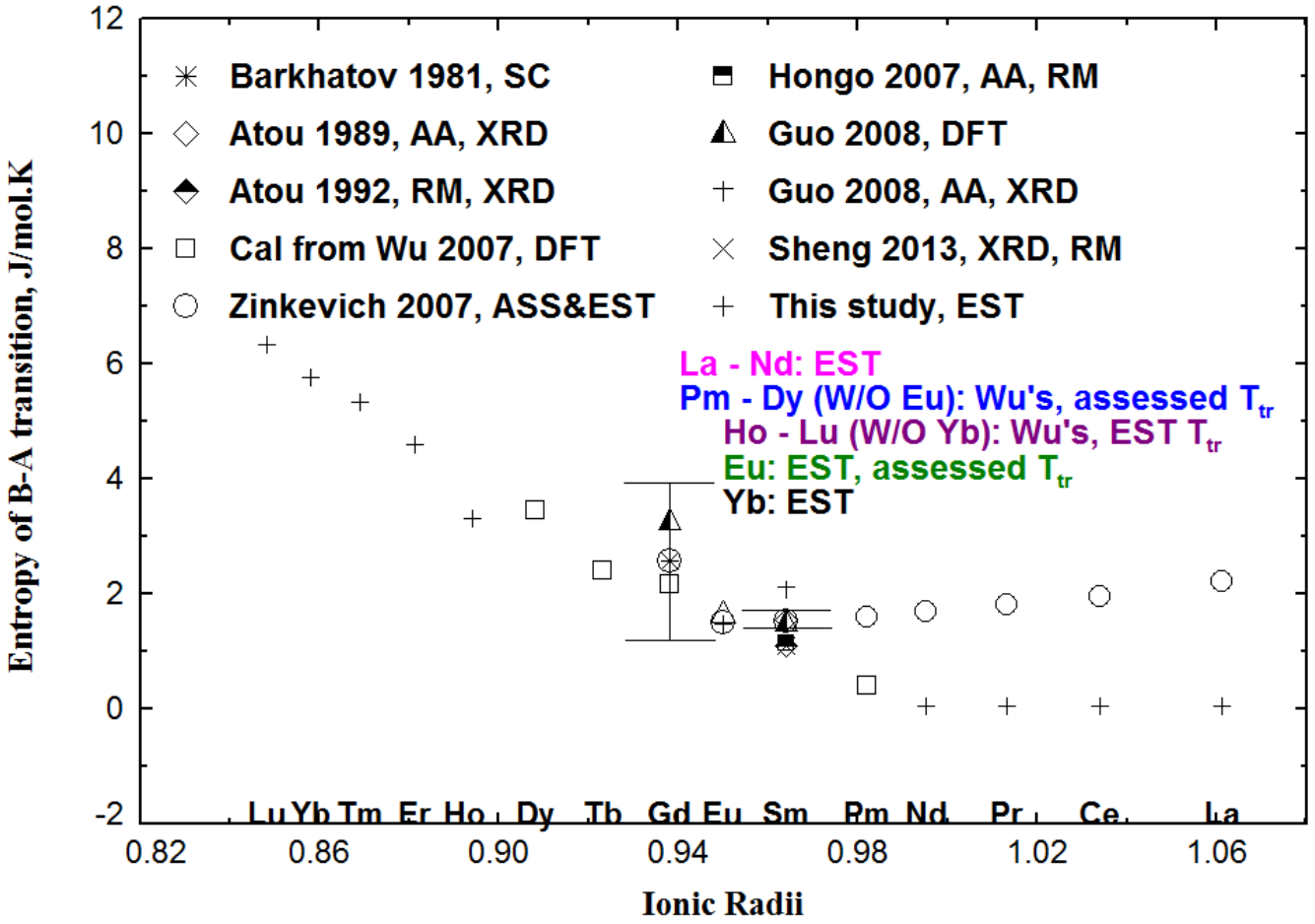

Figure 36 Summary of the enthalpies of B→A phase transition of RE_2O_3; AA: anvil apparatus; CC: combustion; DFT: density functional theory; EST: estimation; XRD: X-ray diffraction; SC: solution calorimetry; ionic radii in unit Å

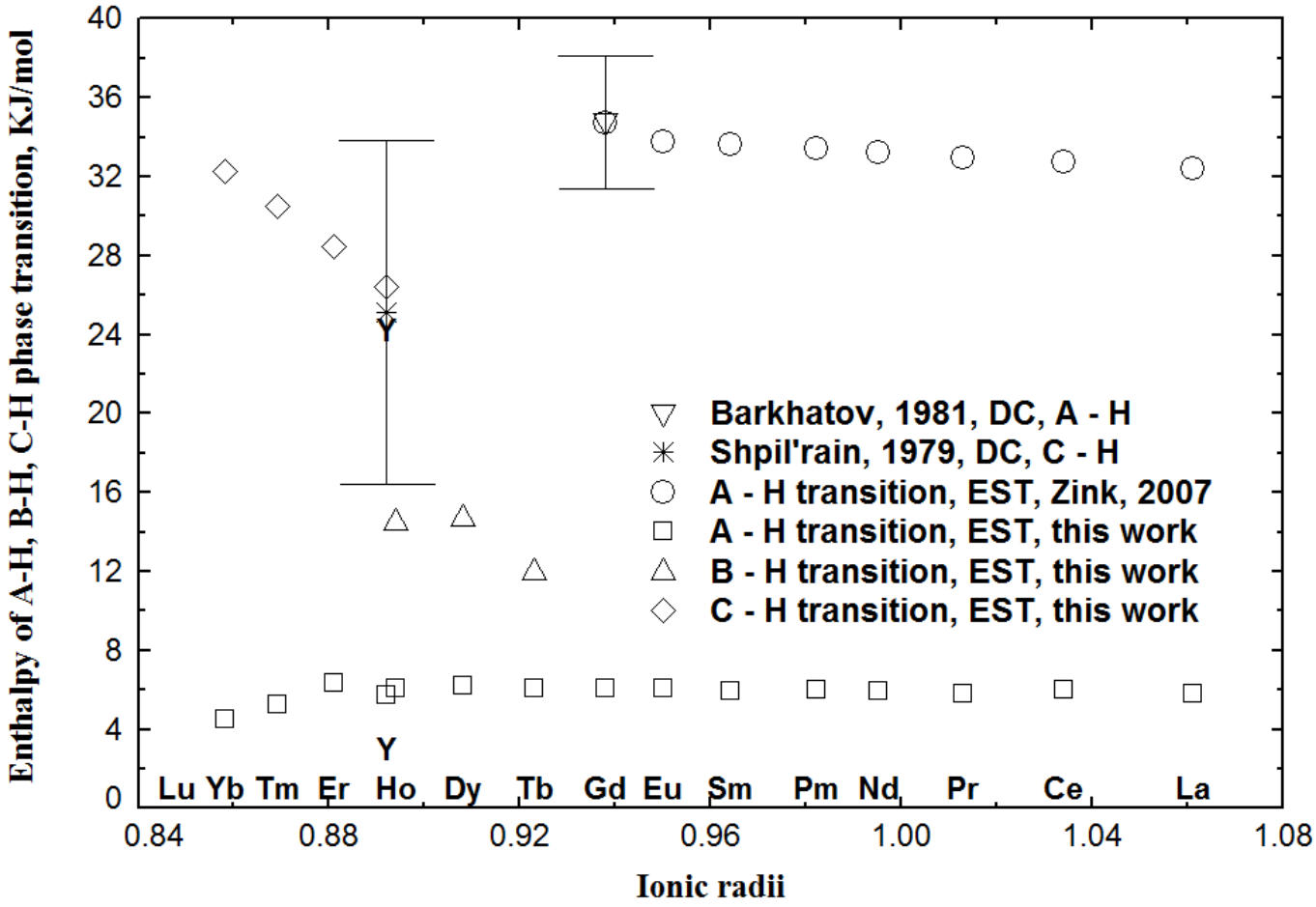

Figure 37 Optimized enthalpies of A→H, B→H and C→H transitions in this study in comparision to the optimized results by Zinkevich [2] and experimental data from Barkhatov et al., [20] and Shpil'rain et al. [21]; ionic radii in unit Å

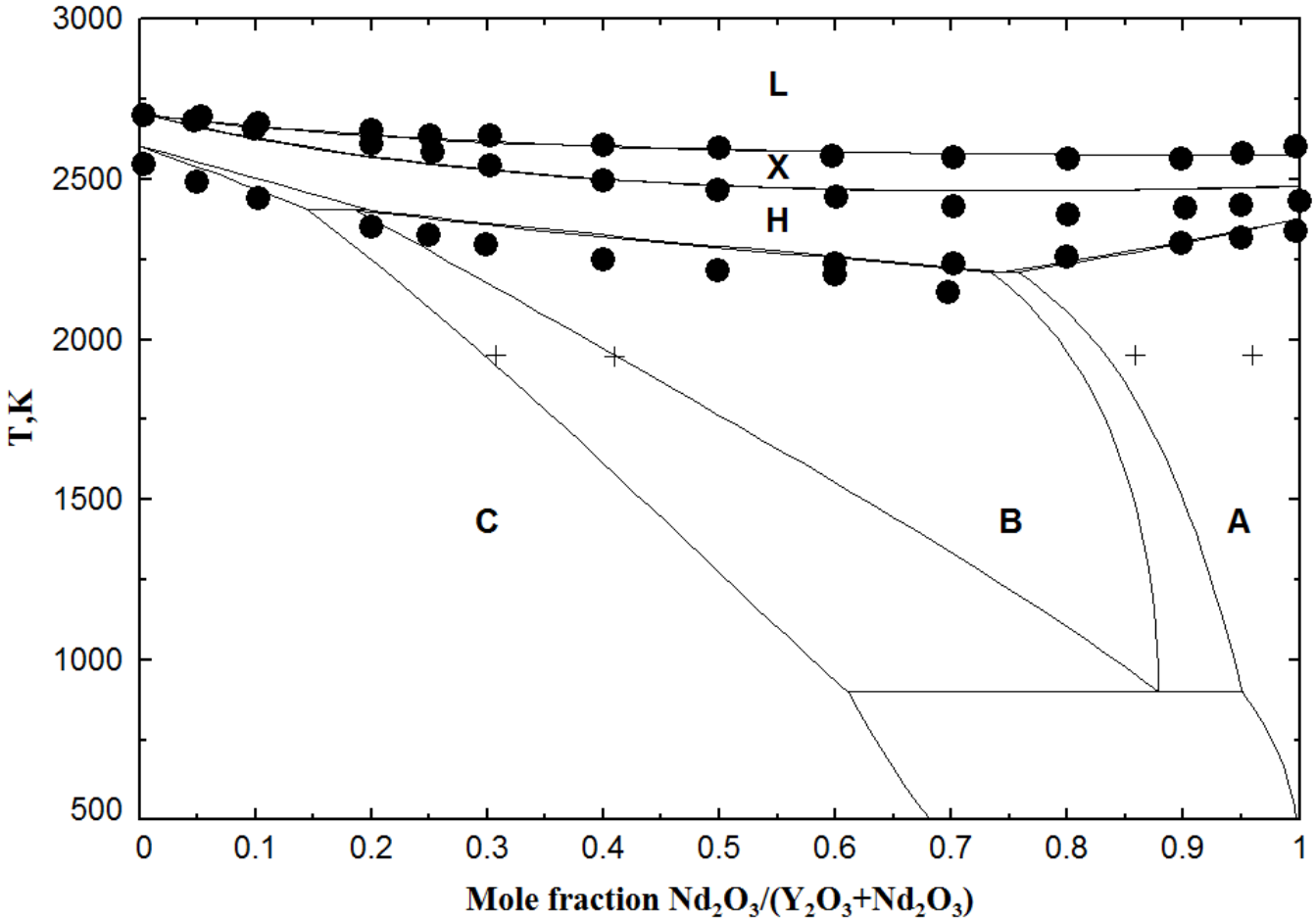

Figure 38 Calculated Y_2O_3 – Nd_2O_3 phase diagram along with experimental data; filled circle: DTA [137]; and cross: annealing [137]

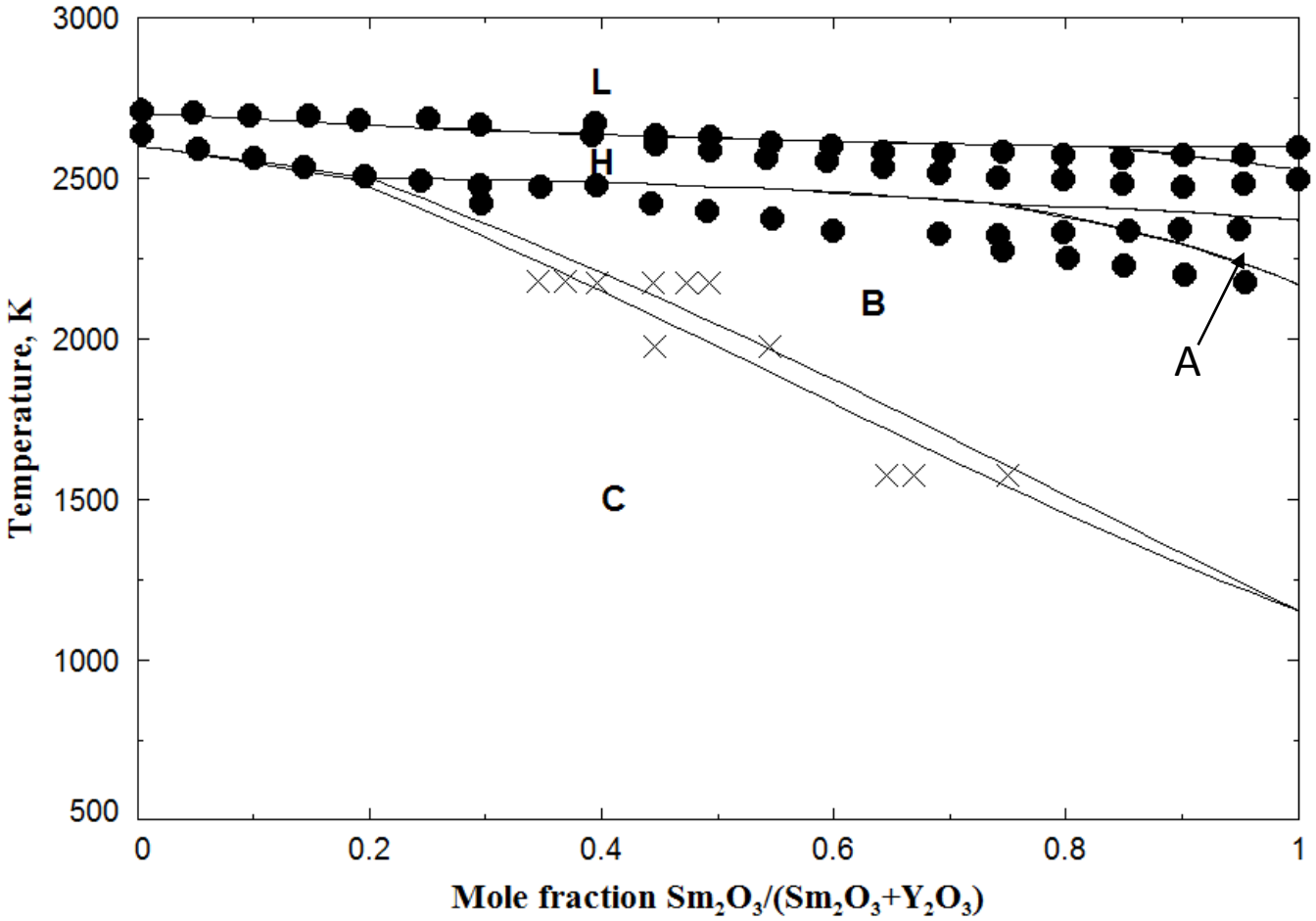

Figure 39 Calculated Y_2O_3 – Sm_2O_3 phase diagram with experimental data; filled circle: DTA [138]; X: annealing [138]

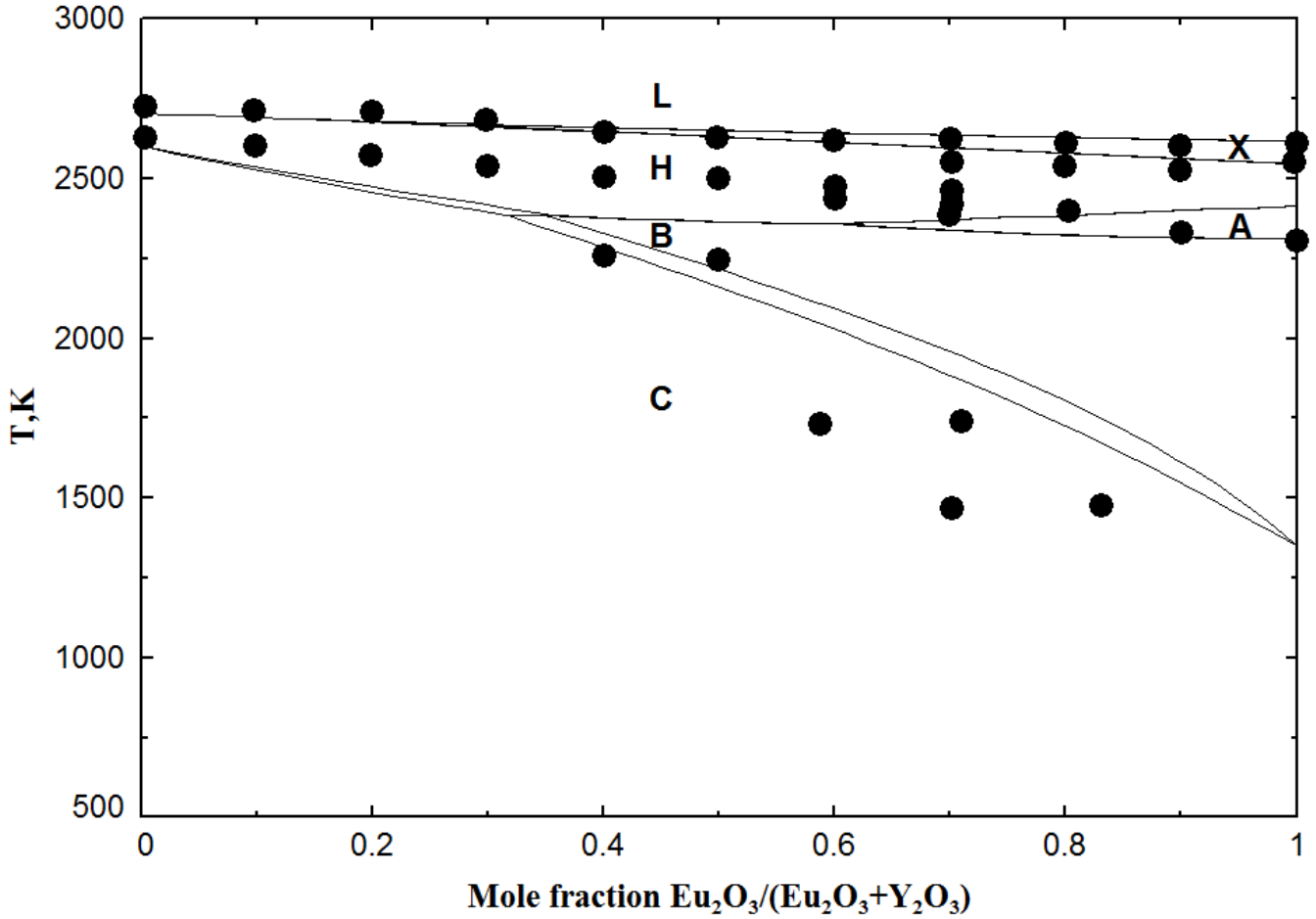

Figure 40 Calculated Y_2O_3 – Eu_2O_3 phase diagram with experimental data [139]

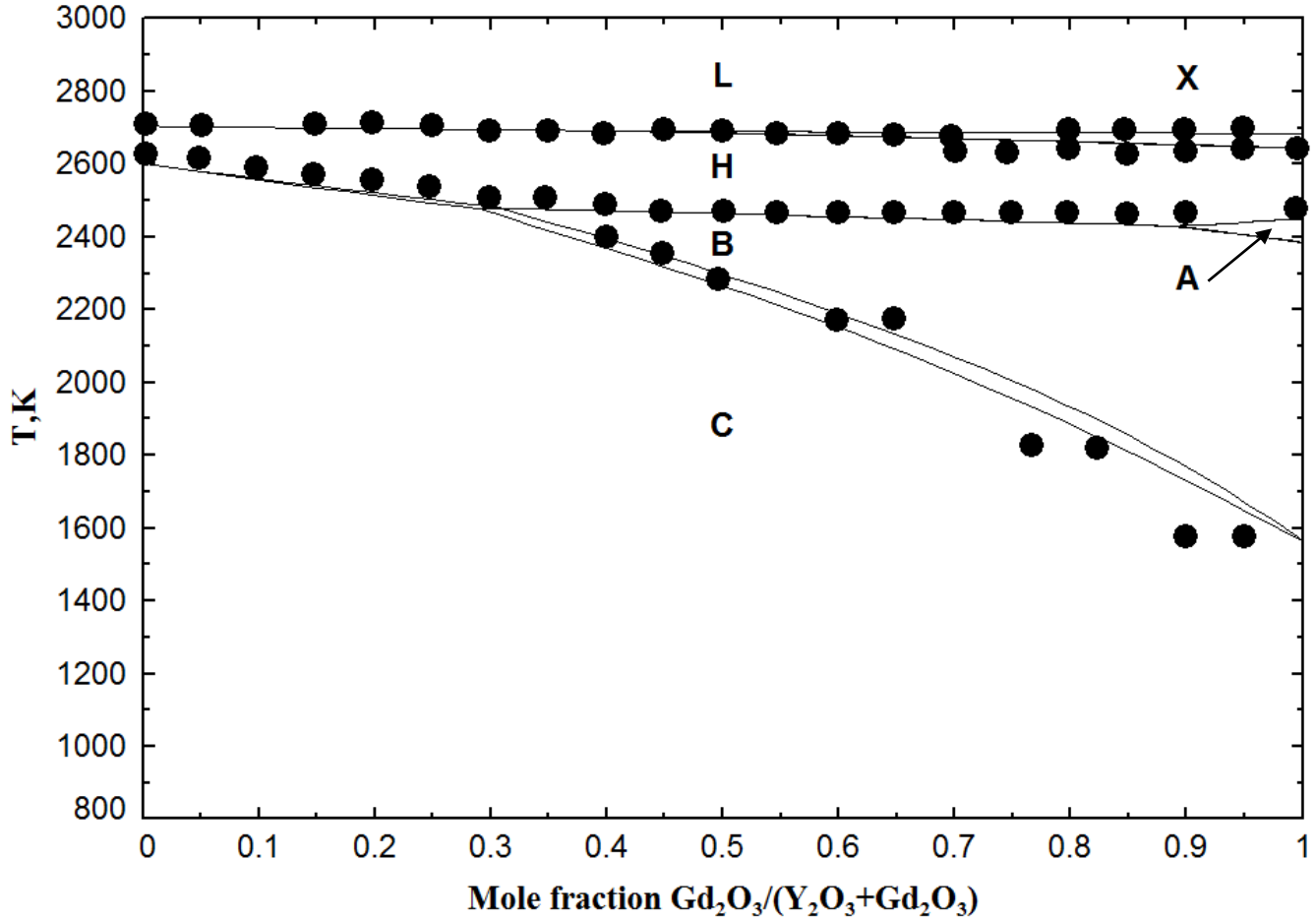

Figure 41 Calculated Y_2O_3 – Gd_2O_3 phase diagram with experimental data [139]

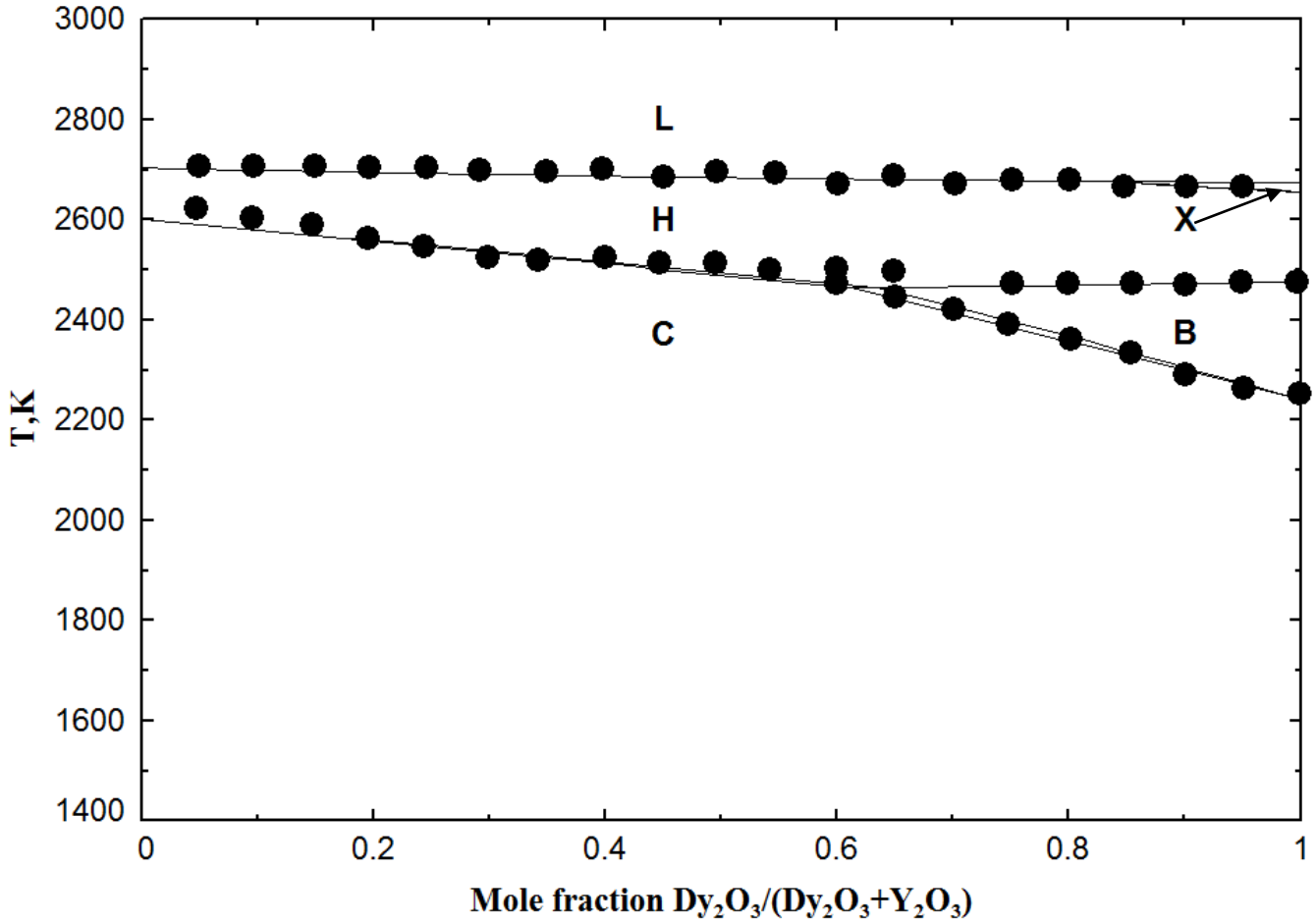

Figure 42 Calculated Y_2O_3 – Dy_2O_3 phase diagram with experimental data [140]

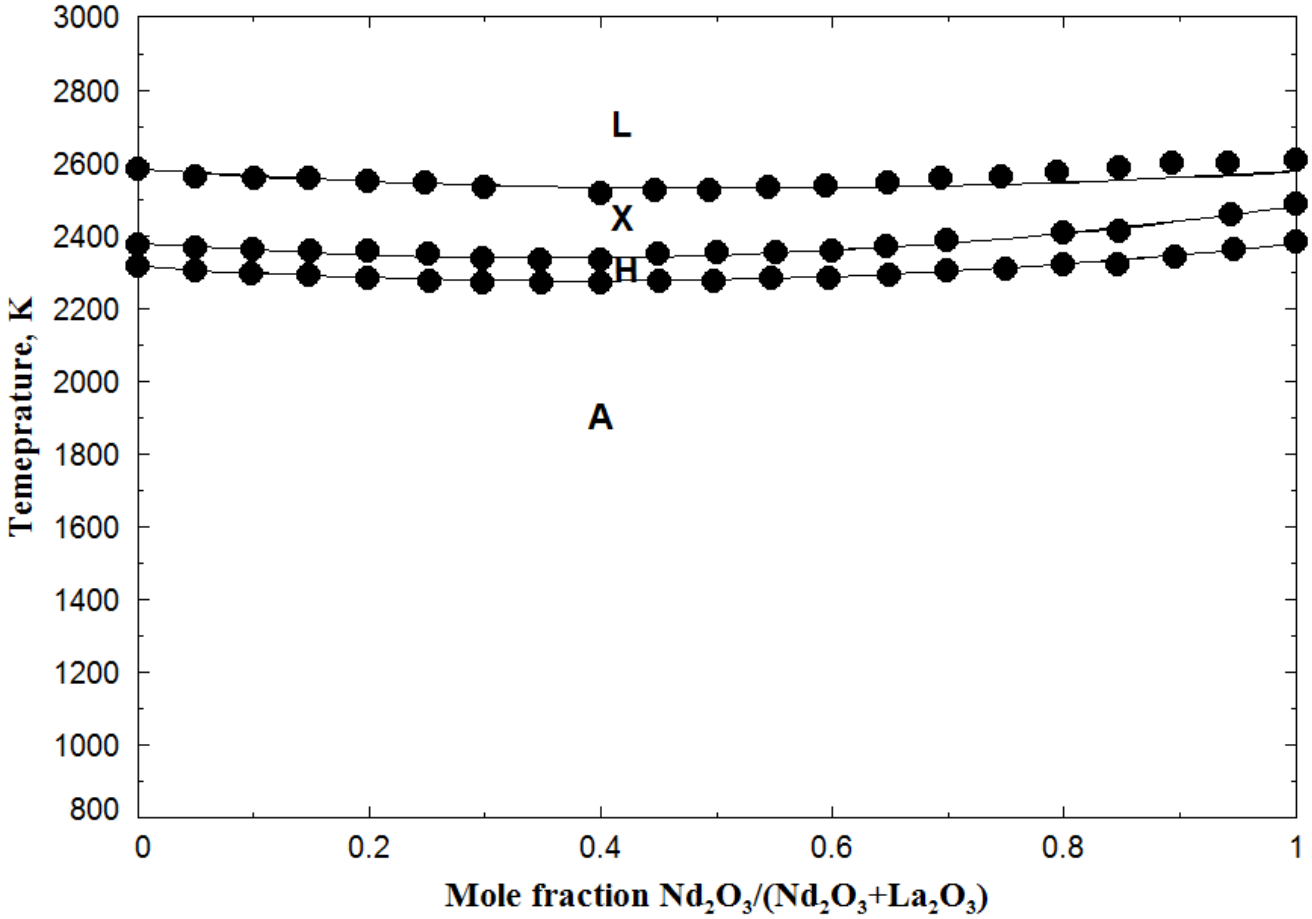

Figure 43 Calculated Nd_2O_3 – La_2O_3 phase diagram with experimental data [10]

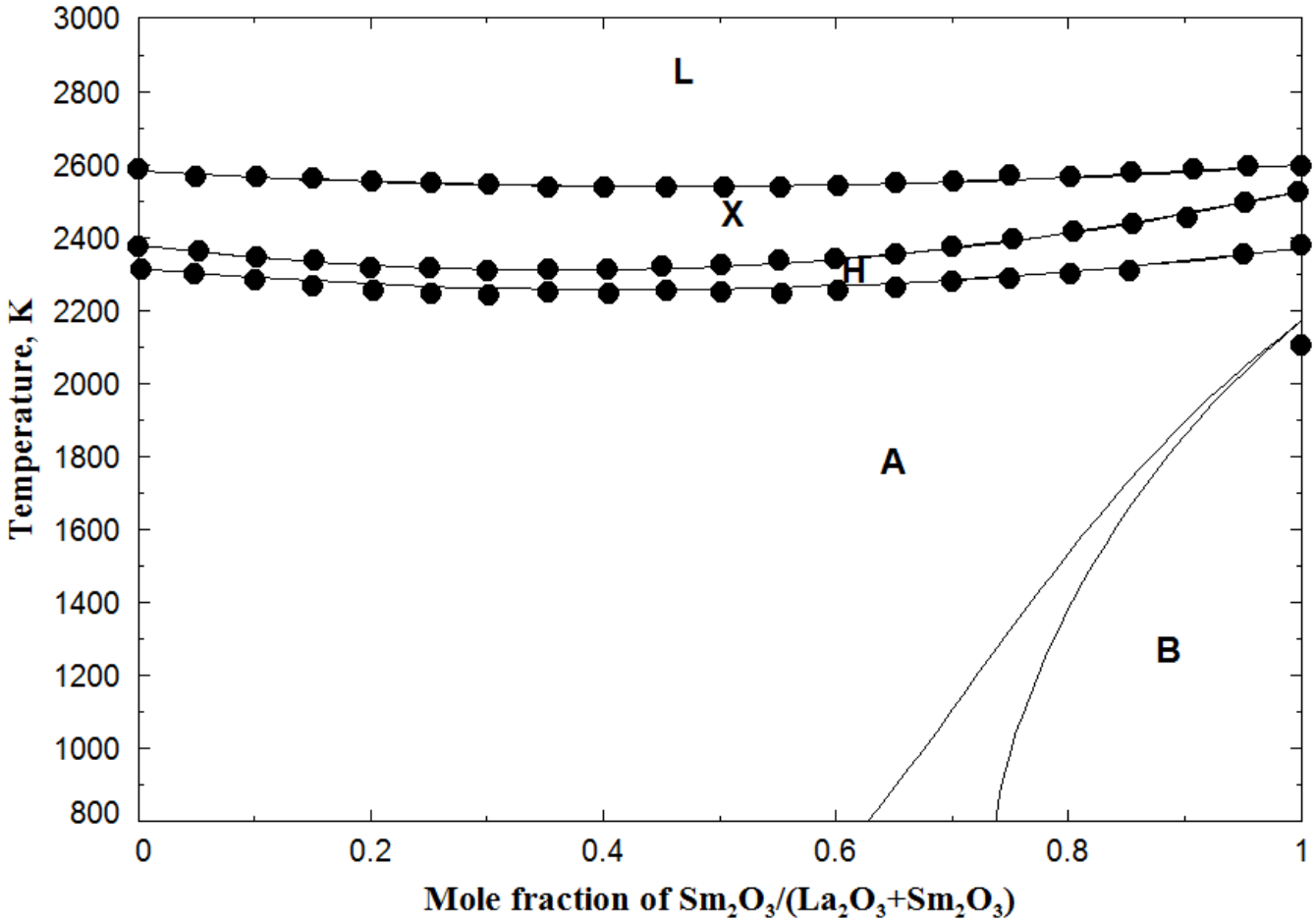

Figure 44 Calculated Sm_2O_3 – La_2O_3 phase diagram with experimental data [10]

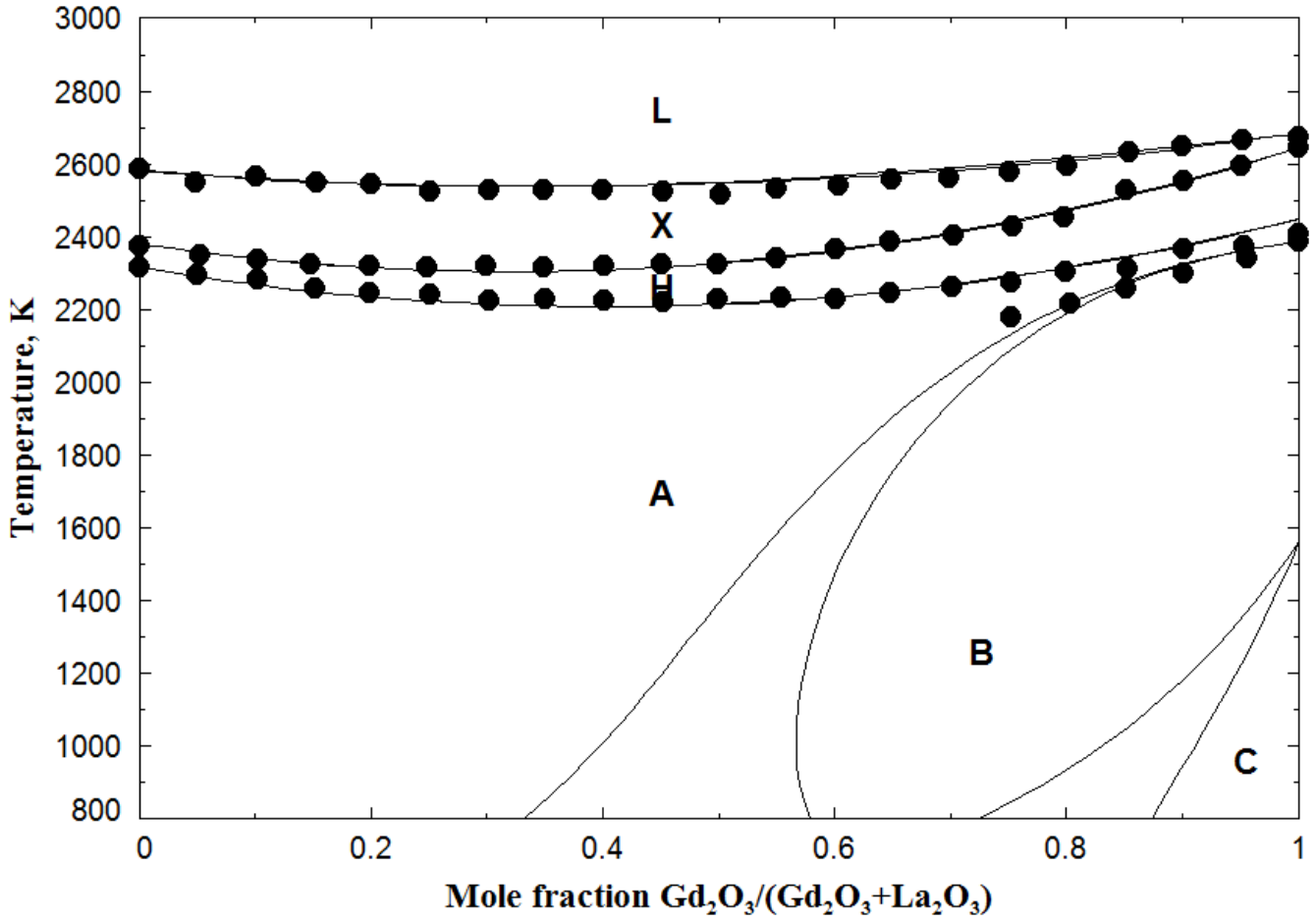

Figure 45 Calculated Gd_2O_3 – La_2O_3 phase diagram with experimental data [10]

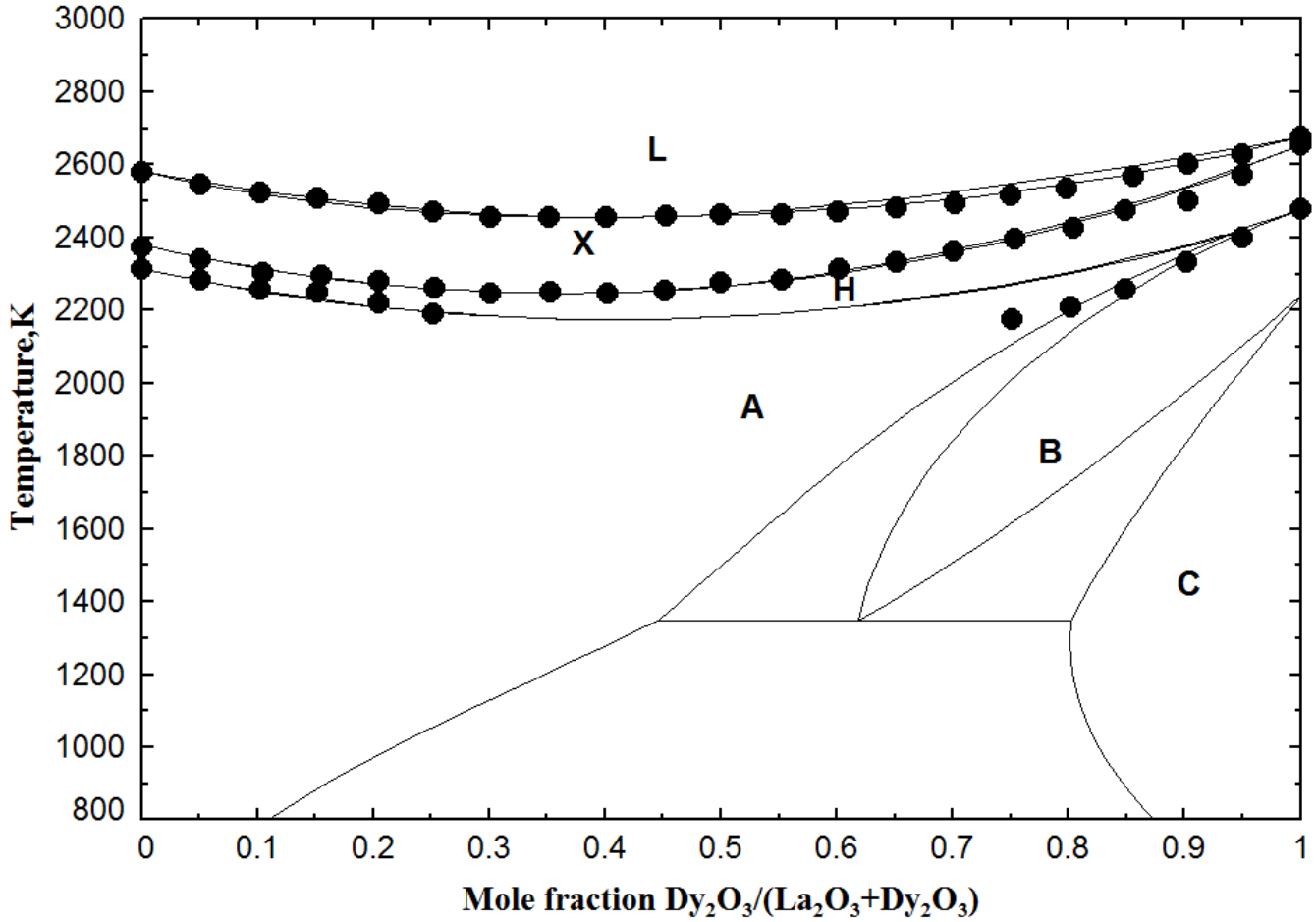

Figure 46 Calculated Dy_2O_3 – La_2O_3 phase diagram with experimental data [10]

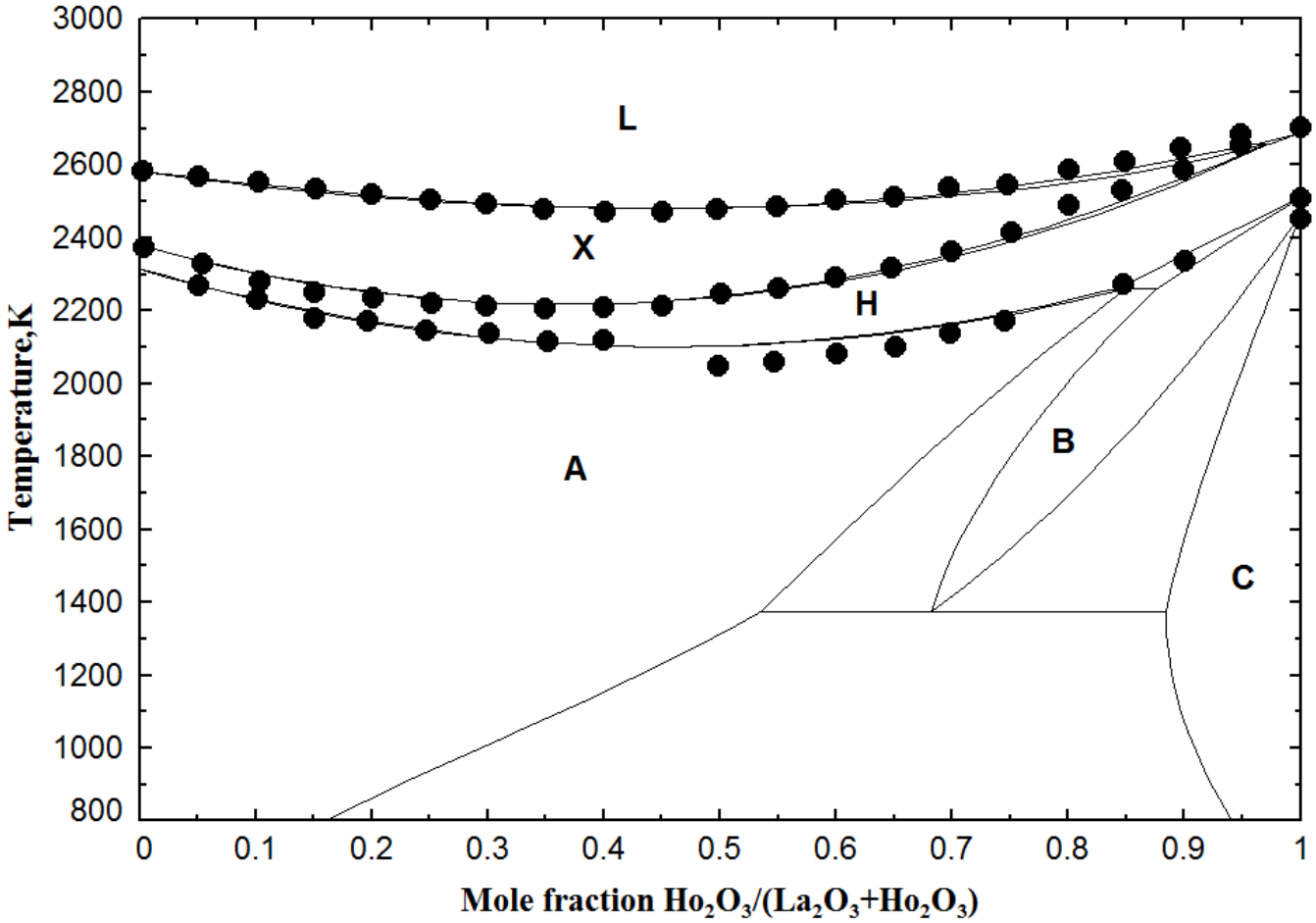

Figure 47 Calculated Ho_2O_3 – La_2O_3 phase diagram with experimental data [10]

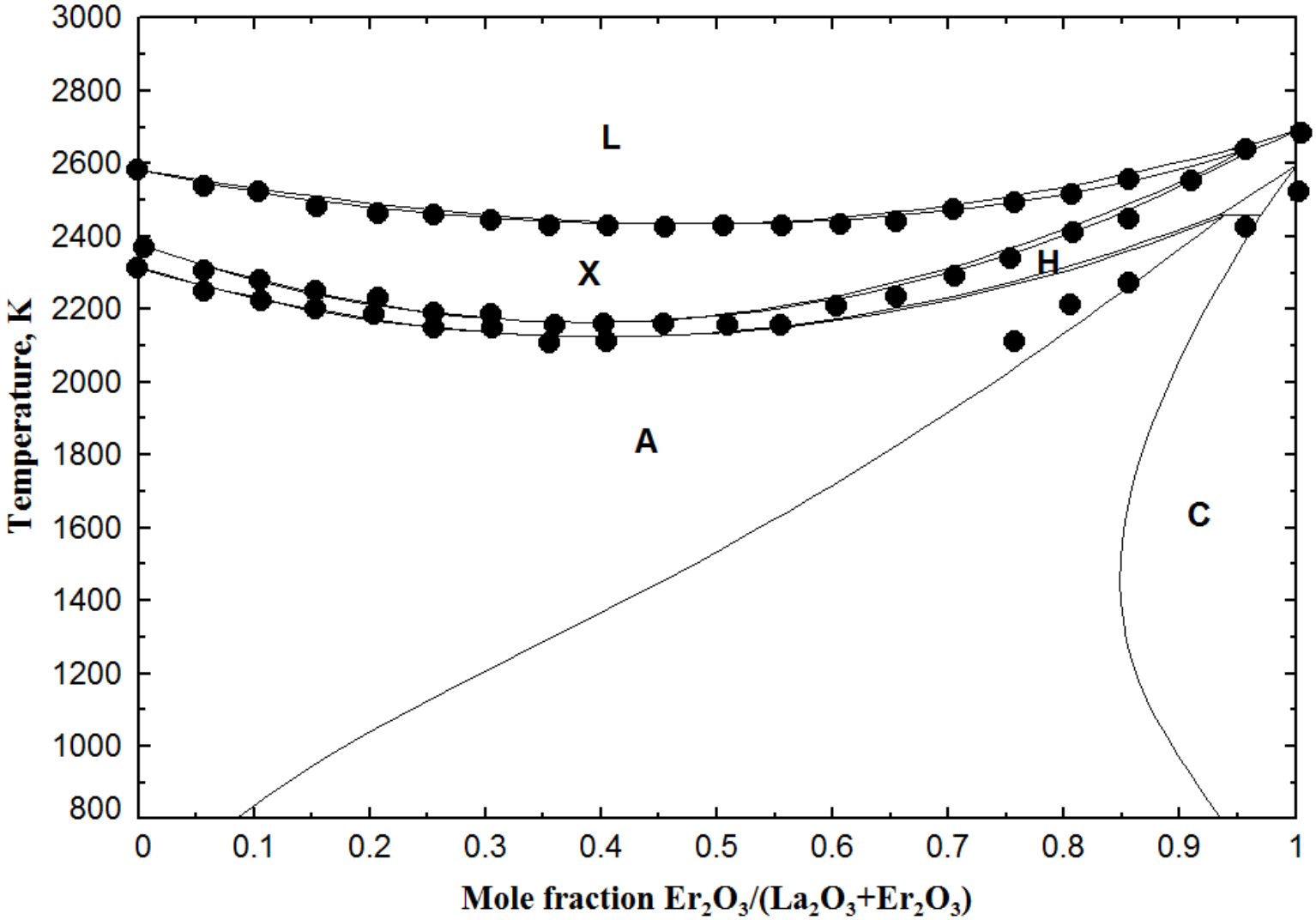

Figure 48 Calculated Er_2O_3 – La_2O_3 phase diagram with experimental data [10]

11. References

1. Wu, J., et al., *Low-Thermal-Conductivity Rare-Earth Zirconates for Potential Thermal Barrier Coating Applications.* J.Am.Ceram.Soc,. 2002. **85**(12): p. 3031-3035.
2. Zinkevich, M., *Thermodynamics of rare earth sesquioxides.* Progress in Materials Science, 2007. **52**(4): p. 597-647.
3. Foex, M. and J.P. Traverse, *Investigations about crystalline transformation in rare earths sesquioxides at high temperatures.* Rev. int. hautes temp. Refract., 1966. **3**: p. 429-453.
4. Aldebert, P. and J.P. Traverse, *Etude par diffraction neutronique des structures de haute temperature de La2O3 et Nd2O3.* Materials Research Bulletin, 1979. **14**: p. 303-323.
5. Shannon, R.D. and C.T. Prewitt, *Effective ionic radii in oxides and fluorides.* Acta Crystallographica Section B Structural Crystallography and Crystal Chemistry, 1969. **25**(5): p. 925-946.
6. Goldschmidt, V.M., T. Barth, and G. Lunde, *Geochemical distribution law of the elements. V. Isomorphy and polymorphy of the sesquioxides. The contraction of the "lanthanums" and its consequences.* Skrifter (Norske videnskaps-akademi. I--Mat.-naturv. klasse), 1925. **7**: p. 59-59.
7. Warshaw, I. and R. Roy, *Polymorphism of the Rare Earth Sesquioxides.* Journal of Physical Chemistry, 1961. **65**(11): p. 2048-2051.
8. Weigel, F. and V. Scherer, *Chemistry of promethium. II. Polymorphism of promethium-(III) oxide.* Radiochimica Acta, 1965. **4**(4): p. 197-202.
9. Tresvyatkii, S.G., et al., *Untersuchung des einflusses hochschmelzender oxide der elemente II. Gruppe des periodischen systems.* ÉTUDE DES TRANSFORMATIONS CRISTALLINES À HAUTE TEMPÉRATURE, 1971. **205**: p. 247-253.
10. Coutures, J.P. and M. Foex, *Etude a Haute TempCrature des Systsmes Formes par le Sesquioxyde de Lanthane et les Sesquioxydes de Lanthanides . I . Diagrammes de Phases (1400 °C < T < TLiquide).* Journal of solid state chemistry, 1976. **182**(17): p. 171-182.
11. Shevthenko, A.V. and L.M. Lopato, *Ta method applikation to the highest refractory oxide systems investigation.* Thermochimica Acta, 1985. **93**: p. 537-540.
12. Chikalla, T.D., C.E. McNeilly, and F.P. Roberts, *Polymorphic Modifications of Pm2O3.* Journal of the American Ceramic Society, 1972. **55**(8): p. 428-429.
13. Roth, R.S. and S.J. Schneider, *Phase Equilibria in Systems Involving the Rare-Earth Oxides . Part 1 . Polymorphism of the Oxides of the.* Journal of Research of the National Bureau of Standards-A.Physics and Chemistry, 1960. **64**(4): p. 309-316.
14. Curtis, C.E. and J.R. Johnson, *Ceramic Properties of Samarium Oxide and Gadolinium Oxide; X-Ray Studies of other rare-earth oxides and some compounds.* Journal of the American Ceramic Society, 1957. **40**(1): p. 15-19.
15. Curtis, C.E. and A.G. Tharp, *Ceramic Properties of Europium Oxide.* Journal of the American Ceramic Society, 1959. **42**(3): p. 151-151.
16. Fitzgibbon, G.C., E.J. Huber, and C.E. Holley, *Enthalpy of formation Europium sesquioxide.* Journal of chem Thermodynamics, 1972. **4**: p. 349-358.

17. Lyutsareva, N.S., G.A. Barezovskii, and I.E. Paukov, *Heat capacity of two Eu2O3 modifications in the temperature range 8-300K.* Russian Journal of Physical Chemistry, 1994. **68**(7): p. 1179-1182.
18. Kolitsch, U., *Hochtemperaturkalorimetrie und Phasenanalytik in SE2O3-Al2O3-SiO2-Systemem*. 1995.
19. Hoekstra, R., *Phase relationships in the rare earth sesquioxides at high pressure.* Inorganic chemistry, 1965. **5**(3): p. 754-757.
20. Barkhatov, L.S., et al., *Electric conductivity and heats of high-temperature phase transitions of gadolinia.* High temperatures-High pressures, 1981. **13**(1): p. 39-42.
21. Shpil'rain, E.E., et al., *Combined study of the thermophysical and eletrophysical properties of rare-earth sesquioxides in solid and liquid phases.* High temperatures-High pressures, 1979. **11**: p. 539-542.
22. Lambertson, W.A. and F.H. Gunzel, *Refractory oxide melting points, No. AECD-3465*. 1952.
23. Mizuno, M., et al., *Phase diagram of the system aluminum oxide-lanthanum oxide at elevated temperatures.* Yogyo Kyokaishi, 1974. **82**(12): p. 631-6.
24. Mizuno, M., T. Yamada, and T. Noguchi, *Phase diagram of the system aluminum oxide-samarium oxide at high temperatures.* Yogyo-Kyokai-Shi, 1977. **85**(8): p. 374-374.
25. Mizuno, M., T. Yamada, and T. Noguchi, *Phase diagrams of the system Al2O3-Eu2O3 and Al2O3-Gd2O3 at high temperatures.* Yogyo-Kyokai-Shi, 1977. **85**(11).
26. Mizuno, M., T. Yamada, and T. Noguchi, *Phase diagram of the system aluminum oxide-neodymium oxide at high temperatures.* Yogyo-Kyokai-Shi, 1977. **85**(2): p. 90-5.
27. Mizuno, M., T. Yamada, and T. Noguchi, *Phase diagram of the system aluminum oxide-praseodymium oxide at high temperatures.* Yogyo-Kyokai-Shi, 1977. **85**(1): p. 24-29.
28. Wu, P. and A.D. Pelton, *Coupled Thermodynamic Phase Diagram Assessment of the Rare Earth Oxide Aluminum Oxide Binary Systems.* Journal of Alloys and Compounds, 1992. **179**: p. 259-287.
29. Mizuno, M., T. Yamada, and T. Noguchi, *Phase diagram of the system aluminum oxide-dysprosium oxide at high temperatures.* Yogyo-Kyokai-Shi, 1978. **86**(8): p. 359-359.
30. Grobner, J., et al., *Re-assessment of the Y-O binary system.* Z.Metallkd, 1996. **87**: p. 88-91.
31. Navrotsky, A., *Direct calorimetric measurements of enthalpys of phase transitions at 2000-2400C in Yttria and Zirconia.* J Am Chem Soc, 2005. **88**(10): p. 2942-2944.
32. Shpil'rain, E.E., et al., *Measurement of the enthalpy of solid and liquid phases of yttria.* High temperatures-High pressures, 1976. **8**: p. 183-186.
33. Maister, I.M., et al., *Yttrium oxide-erbium oxide system.* Izvestiya Akademii Nauk SSSR, Neorganicheskie Materialy, 1984. **20**(3): p. 446-446.
34. Cordfunke, E.H.P. and R.J.M. Konings, *The enthalpies of formation of lanthanide compounds III. Ln2O3(cr).* Thermochimica Acta, 2001. **375**(1-2): p. 65-79.
35. Spedding, F.H., et al., *The separation of rare earths by ion exchange. I. cerium and yttrium.* Journal of the American Chemical Society, 1947. **69**(11): p. 2777-2781.
36. Cordfunke, E.H.P. and R.J.M. Konings, *The enthalpies of formation of lanthanide compounds II. Ln(3+) (aq)*. Vol. 375. 2001. 51-64.

37. Mah, A.D., *Heats and free energies of formation of Gallium sesquioxide and Scandium sesquioxide - report 5965.* US Bureau of Mines, 1962.
38. Huber, J.E. and C.E. Holley, *Experimental thermochemistry*, H.A. Skinner, Editor. 1962, Interscience Publishers, Inc.: N.Y. p. 89-89.
39. Huber, J.E., et al., *The heat of formation of Scandium oxide.* 1963. **2**(1): p. 1731-1733.
40. Leonidov, V.Y., et al., *The system of the key thermodynamic values for scandium and its compounds*. 1997: Moscow.
41. Huber, J.E. and C.E. Holley, *The heat of combustion of Yttrium.* Journal of phys chem, 1957. **61**: p. 497-497.
42. Lavut, E.G. and N.V. Chelovskaya, *Enthalpy of formation of diyttrium trioxide.* Journal of chem Thermodynamics, 1990. **22**: p. 817-820.
43. Wang, X.Y., et al., *Thermodynamics of lanthanide elements IV. Molar enthalpies of formation of Y3+(aq), YCl3(cr), YBr3(cr), and YI3(cr).* The Journal of Chemical Thermodynamics, 1988. **20**(10): p. 1195-1202.
44. Morss, R.L., et al., *Standard molar enthalpies of fomation of Y2O3, Ho2O3, and Er2O3 at the temperature 298.15K.* Journal of chem Thermodynamics, 1993. **25**: p. 415-422.
45. Huber, J.E. and C.E. Holley, *The heat of combustion of lanthanum.* Journal of Am. Chem. Soc, 1953. **75**: p. 3594-3595.
46. Fitzgibbon, G.C. and C.E. Holley, *The heat of formation of Lanthanum oxide.* Journal of phys chem, 1965. **69**(7): p. 2464-2466.
47. Gvelesiani, G.G. and T.S. Yashvili, *Standard heats of formation of lanthanum and samarium sesquioxides.* Zhurnal Neorganicheskoi Khimii, 1967. **12**(12): p. 3233-3236.
48. Merli, B.L., F. Rorif, and J. Fuger, *The Enthalpies of Solution of Lanthanide Metals in Hydrochloric Acid at Various Concentrations . Relevance to Nuclear Waste Long Term Storage.* Radiochimica Acta, 1998. **82**: p. 3-9.
49. Kuznetsov, F.A., T.N. Rezukhina, and A.N. Golubenko, *Determination of the heat of formation of Cerium (III) oxide by combustion in a bomb calorimeter.* Russian Journal of Physical Chemistry, 1960. **34**(9): p. 1010-1010.
50. Mah, A.D., *Technical report USBM-RI-5676.* US Bureau of Mines, 1961.
51. Baker, F.B. and C.E. Holley, *Enthalpy of formation of cerium sesquioxide.* Journal of Chemical & Engineering Data, 1968. **13**(3): p. 405-407.
52. Huber, J.E. and C.E. Holley, *The heat of combustion of Cerium.* J. Am. Chem. Soc, 1953. **75**: p. 5645-5645.
53. Huntelaar, M.E., et al., *The thermodynamic properties of Ce2O3(s) fromT→ 0 K to 1500 K.* The Journal of Chemical Thermodynamics, 2000. **32**(4): p. 465-482.
54. Putnam, R.L., et al., *Thermodynamics of formation of two cerium aluminum oxides, CeAlO3(s) and CeAl12O19.918(s), and cerium sesquioxide,Ce2O3(s) at T= 298.15 K.* The Journal of Chemical Thermodynamics, 2000. **32**(7): p. 911-921.
55. Spedding, F.H. and C.F. Miller, *Thermochemistry of rare earths. I. Cerium and Neodymium.* Journal of Am. Chem. Soc, 1952. **74**: p. 4195-4198.
56. Stubblefield, C.T., H. Eick, and L. Eyring, *Praseodymium Oxides. III. The Heats of Formation of Several Oxides.* Journal of the American Chemical Society, 1956. **78**(13): p. 3018-3020.

57. Fitzgibbon, G.C., J.E. Huber, and C.E. Holley, *The enthalpies of formation of Pr2O3 (hexagonal), Pr2O3 (cubic), and PrO1.811 (*).* Revue de Chimie Minerale, 1973. **10**: p. 29-29.
58. Spedding, F.H. and J.P. Flynn, *Thermochemistry of the Rare Earths. II . Lanthanum, Praseodymium, Samarium, Gadolinium, Erbium, Ytterbium and Yttrium.* Journal of Am. Chem. Soc, 1954. **76**(7): p. 1474-1474.
59. Stubblefield, C.T., *A 200 ml Solution Calorimeter with Semiautomatic Adiabatic Control.* Review of Scientific Instruments, 1969. **40**(3): p. 456-456.
60. Huber, J.E. and C.E. Holley, *The heat of combustion of Neodymium.* J.Am.Chem.Soc, 1952. **74**: p. 5530-5530.
61. Spedding, F.H., R.E. Eberts, and A.W. Naumann, *The heats of combustion of some rare-earth metals ISC-934*. 1959.
62. Fitzgibbon, G.C., D. Pavone, and C.E. Holley, *Enthalpy Formation Nd2O3-Hexagonal.* Journal of Chemical & Engineering Data, 1968. **13**(4): p. 547-548.
63. Yashvili, T.S. and G.G. Gvelesiani, *Standard enthalpies of formation of europium, gadolinium, and neodymium sesquioxides.* Zhurnal Fizicheskoi Khimii, 1971. **45**(4): p. 983-983.
64. Morss, L.R. and C.M. Haar, *Standard molar enthslpy of neodymium hydroxide of formation.* Journal of chem Thermodynamics, 1989. **21**: p. 1079-1083.
65. Monaenkova, A.S., A.A. Popova, and A.L. Il'inskii, *Standard enthalpy of transition of hexagonal Nd2O3 into cubic modification.* Russian Journal of Physical Chemistry, 1996. **70**(12): p. 2150-2153.
66. Stuve, J.M., *Technical report USBM-RI-6697.* US Bureau of Mines, 1965.
67. Popova, A.N. and A.S. Manaenkova, *Standard heat of formation of hexagonal neodymium oxide.* Zhurnal Fizicheskoi Khimii, 1989. **63**(9): p. 2340-2343.
68. Baker, F.B. and D. Pavone, *Enthalpies of formation of Sm2O3 (monoclinic) and Sm2O3 (Cubic).* Journal of chem Thermodynamics, 1972. **4**: p. 621-636.
69. Huber, J.E., et al., *The Heat of Combustion of Samarium.* J. Am. Chem. Soc., 1955. **77**(24): p. 6493-6493.
70. Hennig, C. and H. Oppermann, *Thermische Zersetzung und Lösungskalorimetrie von Ammoniumsamariumchloriden (Thermal decomposition and solution calorimetry of Ammonium Samarium Chlorides).* Z. Naturforsch, 1997. **52b**: p. 1517-1517.
71. Huber, E.J., G.C. Fitzgibbon, and C.E. Holley, *The heat of formation of Europium Sesquioxide.* The Journal of Physical Chemistry, 1964. **68**(9): p. 2720-2722.
72. Hennig, C., H. Oppermann, and A. Blonska, *Thermische Zersetzung und Lösungskalorimetrie von Ammoniumeuropiumchloriden.* Z. Naturforsch, 1998. **53b**: p. 1169-1179.
73. Stuve, J.M., *Heat of formation of Europium sesquioxide and Europium Trichloride-report of investigation 6640.* US Bureau of Mines, 1965.
74. Stubblefield, C.T., J.L. Rutledge, and R. Phillips, *The heats of formation of Anhydrous Europium (II) Chloride and of the aqueous Europium (II) ion.* The Journal of Physical Chemistry, 1965. **69**(3): p. 991-991.
75. Huber, J.E. and C.E. Holley, *The Heat of Combustion of Gadolinium.* Journal of Am. Chem. Soc, 1955. **77**: p. 1444-1445.

76. Stubblefield, T. and H. Eick, *Terbium Oxides. II. The Heats of Formation of Several Oxides.* J.Am.Chem.Soc, 1956. **78**: p. 3877-3877.
77. Fitzgibbon, G.C. and C.E. Holley, *Enthalpies of Solution and of Formation of several Terbium oxides.* Journal of Chemical & Engineering Data, 1968. **13**(January): p. 63-65.
78. Huber, J.E., E.L. Head, and C.E. Holley, *The heats of combustion of Dysprosium and Ytterbium.* Journal of phys chem, 1956. **60**: p. 1457-1458.
79. Huber, J.E., G.C. Fitzgibbon, and C.E. Holley, *Enthalpy of formation of dysprosium sesquioxide.* Journal of chem Thermodynamics, 1971. **3**: p. 643-648.
80. Huber, J.E., E.L. Head, and C.E. Holley, *The heat of combustion of Holmium.* Journal of phys chem, 1957. **61**: p. 1021-1021.
81. Stuve, J.M., *Heats of formation of Holmium and Terbium Trichlorides, report of investigations - 7046.* US Bureau of Mines, 1967.
82. Bettonville, S., J. Goudiakas, and J. Fuger, *Thermodynamics III . Molar enthalpies Tb3+(aq), Ho3+(aq), Yb3+(aq), Yb2+(aq), TbBr3(cr), HoBr3(cr), and YbBr3(cr) at 298.15K.* Journal of chem Thermodynamics, 1987. **19**: p. 595-604.
83. Huber, J.E., E.L. Head, and C.E. Holley, *The heat of combustion of Erbium.* The Journal of Physical Chemistry, 1956. **60**(11): p. 1582-1582.
84. Montgomery, R.L. and J.M. Stuve, *Technical report USBM-RI-5892.* US Bureau of Mines, 1961.
85. Bommer, H. and E. Hohmann, *Zur Thermochemie der seltenen Erden. II. Die Losungs- und Bildungs-warmen der wasserfreien chloride der seltenen Erden. (On the Thermochemistry of the Rare Earths. II. The Heats of Solution and Formation of the Anhydrous Rare-earth Chlorides.).* Ztschr. anorg. allgem. chem, 1941. **248**: p. 373-382.
86. Fuger, J., L. Morss, and D. Brown, *Thermodynamics of Lanthanide Elements. Part 2. Enthalpies of Formation of Erbium Trichloride and of the Aqueous Erbium Ion.* Journal of the Chemical Society, Dalton Transactions: Inorganic Chemistry, 1980(7): p. 1076-1078.
87. Huber, J.E. and C.E. Holley, *The heat of combustion of thulium.* Journal of phys chem, 1960. **64**(3): p. 379-379.
88. Huber, J.E., E.L. Head, and C.E. Holley, *The heat of combustion of Lutetium.* Journal of phys chem, 1960. **64**: p. 1768-1769.
89. Nugent, L.J., J.L. Burnett, and L.R. Morss, *Correlation of some thermodynamic properties of the lanthanide and actinide metals.* The Journal of Chemical Thermodynamics, 1973. **5**(5): p. 665-678.
90. Justice, B.H. and E.F. Westrum, *Thermo physical Properties of the Lanthanide Oxides . V . Heat Capacity , Thermodynamic Properties , and Energy Levels of Cerium (III) Oxide.* Journal of phys chem, 1968. **7**(6): p. 10-13.
91. Justice, B.H. and J.E.F. Westrum, *Thermophyspcal properties of the Lanthanide oxides. II. Heat capacities, thermodynamics properties, and some energy elevels of Samarium (III), Gadolinium (III), and Ytterbium (III) oxides from 10-350K.* Journal of phys chem, 1963. **67**: p. 345-351.
92. Justice, B.H. and J.E.F. Westrum, *Thermophysical properties of the Lanthanide oxides. I. heat capacities, thermodynamic properties, and some energy levels of Lanthanum (III) and Neodymium (III) oxides from 5 to 350K.* Journal of phys chem, 1963. **67**: p. 339-345.

93. Justice, B.H. and J.E.F. Westrum, *Thermophysical properties of the Lanthanide oxides. III. heat capacities, thermodynamic properties, and some energy levels of Dysprosium (III), Holmium (III), and Erbium (III) oxides.* Journal of phys chem, 1963. **67**: p. 659-665.
94. Justice, B.H., et al., *Thermophysical Properties of the Lanthanide Oxides, IV. Heat capcities and thermodynamic properties of Thulium (III) and Lutetium (III) oxides. electronic energy levels of several Lanthanide (III) Ions.* The Journal of Physical Chemistry, 1969. **75**(333).
95. Hill, R.W., *The specific heats of Tb2O3 and Tb4O7 between 0.5 and 22K.* Journal of phys chem, solid state phys., 1986. **19**(673-682).
96. Goldstein, H.W., et al., *The heat capacities of Y2O3, La2O3 and Nd2O3 from 16-300K.* Journal of phys chem, 1959. **63**: p. 1445-1449.
97. Gavrichev, K.S., et al., *Heat capacity and thermodynamic properties of Y2O3 in the temperature interval 14-300K*. 1993. p. 1731-1733.
98. Weller, W.W. and E.G. King, *Low-temperature heat capacities and entropies at 298.15 degrees K of the sesquioxides of Scandium and Cerium No. 6245.* US Bureau of Mines, 1963: p. 1-6.
99. King, E.G., W.W. Weller, and L.B. Pankratz, *Thermodynamic data for Lanthanum sesquioxide, No. 5857.* US Bureau of Mines, 1961: p. 1-6.
100. Gruber, J.B., et al., *Revisiting the thermophysical properties of the A-type hexagonal lanthanide sesquioxides between temperatures of 5 K and 1000 K.* The Journal of Chemical Thermodynamics, 2002. **34**(4): p. 457-473.
101. Pankratz, L.B., *High temperature heat contents and entropies of two Praseodymium oxides and three Terbium oxides-report 6781*. 1965.
102. Brown, R.E. and W.M. Hubbard. *The magnetic susceptibility of rare earth oxides below 4.2K*.
103. Henry, W.E., *Antiferromagnetism of ytterbium sesquioxide at liquid-helium temperatures.* Physical Review, 1955. **98**: p. 226-226.
104. Pankratz, L.B. and K.K. Kelley, *Thermodynamic data for gallium and scandium sesquioxides, No. 6198.* US Bureau of Mines, 1963: p. 1-7.
105. Pankratz, L.B. and K.K. Kelley, *High temperature heat contents and entropies of sesquioxides of Lutetium, Dysprosium, and Cerium-report 6248*. 1963.
106. Pankratz, L.B. and K.K. Kelley, *High temperature heat contents and entropies of sesquioxides of Europium, Gadolinium, Neodymium, Samarium and Ytrrium - report 6033.* Bureau of Mines, 1961.
107. Pankratz, L.B. and E.G. King, *High temperature heat content and entropies of the sesquioxides of Erbium, Holmium, Thulium, and Ytterbium, No. 6175.* US Bureau of Mines, 1963: p. 1-8.
108. Pankratz, L.B., E.G. King, and K.K. Kelley, *High temperature heat contents and entropies of sesquioxides of europium, gadolium, neodymium, samarium and yttrium, report of investigations 6033.* US Bureau of Mines, 1962.
109. Tsagareishvili, D.S. and G.G. Gvelesiani, *Heat contents and heat capacities of oxides of europium, thulium, and ytterbium at high temperatures.* Tr. Gruzinsk. Inst. Met., 1965. **14**: p. 187-198.

110. Tsagareishvili, D.S., T.S. Yashvili, and G.G. Gvelesiani, *Enthalpy and heat capacity of Scandium sesquioxide at high temperatures.* Soobshcheniia Izvestiia Akademii Nauk Gruzinskoi SSR, 1968. **49**: p. 174-180.
111. Tsagareishvili, D.S., G.G. Gvelesiani, and T.S. Yashvili, *Enthalpy and Heat capacity of Gd Sesquioxide at high tmeperatures.* Russian Journal of Physical Chemistry, 1969. **43**(4): p. 487-489.
112. Tsagareishvili, D.S. and G.G. Gvelesiani, *Enthalpy and heat capacity of Ho2O3 at high temperatures.* Inorganic materials, 1971. **7**: p. 1679-1680.
113. Tsagareishvili, D.S. and G.G. Gvelesiani, *Enthalpy and thermal capacity of Dy2O3 and Beta-Ga2O3 at high temperatures.* Ogneupory, 1972. **9**(11): p. 1936-1939.
114. Landa, Y.A., et al., *Determination of the enthalpy and specific heat of yttrium oxide at 1300 —2100 K.* Ogneupory, 1974. **2**: p. 16-18.
115. Seminko, I.V., A.D. Krivorotenko, and E.N. Fomichev, *Thermodynamic properties of Yttrium oxide.* Ogneupory, 1983. **4**: p. 22-24.
116. Yashvili, T.S., D.S. Tsagareishvili, and G.G. Gvelesiani, *Therdonamic properties of CeO2 and Y2O3.* Soobshcheniia Izvestiia Akademii Nauk Gruzinskoi SSR, 1967. **46**(2): p. 409-409.
117. Curtis, C.E., *Properties Yttrium Ceramics.* Journal of the American Ceramic Society, 1957. **40**(1951): p. 274-278.
118. Blomeke, J.O. and W.T. Ziegler, *The heat content, specific heat and entropy of La2O3, Pr6O11 and Nd2O3 between 30 and 900 degree.* J Am Chem Soc, 1951. **73**: p. 5099-5203.
119. Kuznetsov, F.A. and T.N. Rezukhina, *The high-temperature heat capacity of Cerium sesquioxide.* Russian Journal of Physical Chemistry, 1961. **35**(4): p. 470-471.
120. Gvelesiani, G.G., D.S. Tsagareishvili, and T.S. Yashvili, *Enthalpy and heat capacity of samarium and europium sesquioxides at high temperatures.* Izvestiya Akademii Nauk SSSR, Neorganicheskie Materialy, 1968. **4**: p. 553-556.
121. Gilchrist, K.E. and S.D. Preston, *Thermophsical property measurements on some neutron absorbing materials.* High temperatures-High pressures, 1979. **11**: p. 643-651.
122. Shpil'rain, E.E., et al., *Thermophsical properties of gadolinium oxide in solid phase.* Rev. int. hautes temp. Refract., 1980. **17**: p. 134-136.
123. Wu, B., et al., *Ab initio study on structure and phase transition of A- and B-type rare-earth sesquioxides Ln2O3 (Ln=La-Lu, Y, and Sc) based on density function theory.* Journal of Solid State Chemistry, 2007. **180**(11): p. 3280-3287.
124. Atou, T., et al., *Reversible B-type-A-type transition of Sm2O3 under high pressure.* Mat. Res. Bull, 1989. **24**: p. 1171-1176.
125. Chen, G., J.R. Peterson, and K.E. Brister, *An energy dispersive x-ray diffraction study of monoclinic Eu2O3 under pressure.* Journal of solid, 1994. **111**: p. 437-439.
126. Atou, T., et al., *Pressure-induced phase transition in rare earth sesquioxides*. 1992. p. 469-469.
127. Hongo, T., et al., *High pressure Raman spectroscopic study of structural phase transition in samarium oxide.* Journal of Materials Science, 2007. **42**(8): p. 2582-2585.

128. Guo, Q., et al., *Phase transformation in Sm2O3 at high pressure: In situ synchrotron X-ray diffraction study and ab initio DFT calculation.* Solid State Communications, 2008. **145**(5-6): p. 250-254.
129. Jiang, S., et al., *High-pressure x-ray diffraction and Raman spectroscopy of phase transitions in Sm2O3.* Journal of Applied Physics, 2013. **113**: p. 502-502.
130. Roth, R.S. *Phase Diagrams for Ceramics, Vol XI*. Westville, OH.
131. Atou, T., et al., *Shock-induced phase transition of M2O3 (M = Sc, Y, Sm, Gd, and In)-type compounds.* Journal of Solid State Chemistry, 1990. **89**(2): p. 378-384.
132. Atou, T., et al., *Shock-induced phase transition of scandium sesquioxide: Geometric factor governing high pressure transitions on rare earth sesquioxides.* AIP Conference Proceddings, 1994. **309**: p. 331-334.
133. Meyer, C., J.P. Sanchez, and J.P. Itie, *Mossbauer and energy-dispersive x-ray diffraction studies of the pressure-induced crystallographic phase transition in C-type Yb2O3.* Physical Review B, 1995. **51**(18): p. 12187-12193.
134. Guo, Q., et al., *Pressure-induced cubic to monoclinic phase transformation in erbium sesquioxide Er2O3.* Inorganic Chemistry, 2007. **46**(15): p. 6164-6169.
135. Jiang, S., et al., *Phase transformation of Ho2O3 at high pressure.* Journal of Applied Physics, 2011. **110**(1): p. 013526-013526.
136. Sharma, N.D. and A.K. Bandyopadhyay, *Raman spectroscopic studies of the rare earth sesquioxides and related compounds under high pressures*. 2013. p. 259-296.
137. Adylov, G.T., G.V. Voronov, and L.M. Sigalov, *The neodymium sesquioxide-yttrium sesquioxide system.* Izvestiya Akademii Nauk SSSR, Neorganicheskie Materialy, 1987. **23**(11): p. 1867-1867.
138. Shevthenko, A.V., et al., *Interaction of samarium and gadolinium oxides with yttrium oxide.* Inorganic materials, 1986. **22**: p. 681-5.
139. Andrievskaya, E.R. and L.M. Lopato, *Phase transformations in the ternary systems HfO2(ZrO2)-Y2O3-Eu2O3.* Key Engineering Materials, 1997. **132-136**: p. 1782-1785.
140. Nigmanov, B.S., et al., *Reaction of dysprosium oxide with yttrium oxide.* Izvestiya Akademii Nauk SSSR, Neorganicheskie Materialy, 1986. **22**(5): p. 780-780.
141. Reid, A.F. and A.E. Ringwood, *High-pressure scandium oxide and its place in the molar volume relationships of dense structures of M2X3 and ABX3 type.* Journal of Geophysical Research, 1969. **74**(12): p. 3238-3252.
142. Ma, Y., et al., *Pressure - induced strucutre phase transition on Y2O3.* Nuclear Techniques, 核技术, 2002. **25**(10): p. 841-841.
143. Husson, E., et al., *Phase transitions in yttrium oxide at high pressure studied by Raman spectroscopy.* Materials Research Bulletin, 1999. **34**(12): p. 2085-2092.
144. Halevy, I., et al., *Pressure-induced structural phase transitions in Y2O3 sesquioxide.* Journal of Physics: Conference Series, 2010. **215**: p. 012003-012003.
145. Seck, H.A., F. Dachille, and R. Roy, *High-pressure polymorphism and reactions of Dysprosium sesquioxides.* Inorganic chemistry, 1969. **8**(1): p. 165-165.
146. Lin, C.-M., et al., *Phase transitions in under high pressure.* Solid State Communications, 2010. **150**(33-34): p. 1564-1569.

147. Coutures, J.P., *Etude a haute temperature des systems formes par le sesquioxyde de neodyme avec les sesquioxydes d'yttrium et d'ytterbium.* Mat. Res. Bull, 1974. **9**: p. 1603-1612.